Emma Horn

March 2025

Declaration

I, *Emma Jane Horn*, hereby declare that the work on which this dissertation/t
rk (exce ackno ise) rk
n, g, itted
ty. thesis/d itted le, nfirm

r. ce, ch,
er.

e: Signed by candidate

e:

Permission for inclusion of publications

nfirm wn's
tion(s) is, ed,
tion(s):

1. **E.J. Horn**, R. Huddy & D.G. Randall. 2023. Gr
tion. *Science of The Total Environment.* 895(165050):1-11. OI: https://doi.org/10.1016/j.scitotenv.2023.165050.
2. **E.J. Horn**, R. & D.G. all. 2024.
tion. *Science of The Total Environment.* 951(175652):1-9. DOI: https://d i.org/10.1016/j.scit v.2024.175652.
3. **E.J. Horn**, D. & D.G. all. *Submitted*.
esium, d,
ess.

e: Signed by candidate e: _____

e: _____ er: _____

“Study the science of art. Study the art of science. Develop your senses - especially learn how to see. Realise that everything connects to everything else.”

— Leonardo da Vinci

Abstract

This thesis investigates the production of bio-tiles using microbially induced calcium carbonate ($CaCO_3$) precipitation (MICP) a sustainable alternative to conventional ceramic and cement tiles. The construction industry, a significant contributor to global CO_2 emissions, requires innovative materials to reduce its environmental impact. Bio-materials are often made at atmospheric temperature and pressure and therefore can potentially have a much lower environmental impact than conventional fired building materials such as bricks or ceramic tiles. MICP is a biomineralisation process and can be harnessed to precipitate $CaCO_3$ to bond particles into solid bio-materials. Bio-materials here are materials synthesised from the bio-cementation process. While multiple MICP pathways exist, this research investigates urea hydrolysis facilitated by the ureolytic bacteria, *Sporosarcina pasteurii*, due to its high $CaCO_3$ precipitation efficiency. There are multiple techniques of producing bio-materials with MICP, however, these techniques have not been compared under controlled conditions and there is no literature on the production of bio-tiles, offering a ripe area for research. Three distinct production techniques were explored, namely submersion, pumping, and an automated system, to evaluate their effectiveness in producing bio-tiles with competitive mechanical properties. The study aimed to assess the feasibility of each technique to produce bio-tiles that meet the performance standards of traditional ceramic and cement tiles in terms of breaking strength and modulus of rupture.

The submersion technique involved immersing moulds containing sand inoculated with *S. pastuerii* in a well-mixed bio-reactor filled with cementation solution containing urea, calcium chloride, and supplementary magnesium. The objectives were to investigate how calcium and urea concentration, particle size distribution (PSD) of aggregate material, volume of cementation solution and supplementary magnesium concentration influenced the strength properties of the bio-tiles produced with the submersion technique.

The study found that the submersion technique was able to produce bio-tiles that met international standards for extruded ceramic tiles. It was determined that an equimolar concentration of calcium and urea of 0.3 M was adequate for achieving sufficient breaking strength, furthermore, increasing the cementation solution concentration also enhanced the strength. However, to minimise input costs, maintaining an equimolar concentration of 0.3 M for both calcium and urea is recommended. A PSD with a wide range and an average size of 469 µm resulted in bio-tiles with the highest breaking strength and modulus of rupture, although this did not meet the required industry strength standard. Increasing the volume of cementation solution, which reduced the overall calcium utilisation efficiency, was found to positively affect breaking strength despite leading to reagent waste. The ideal magnesium concentration was identified as 0.3 M, which achieved a breaking strength above the standard. This enhancement in strength is attributed to magnesium slowing down the reaction and favouring the formation of the aragonite polymorph of $CaCO_3$ instead of calcite. For the first time, it was demonstrated that a slower rate of $CaCO_3$ precipitation resulted in stronger bio-tiles grown using MICP and a submersion technique. When combining the most effective volume of cementation solution with a suitable magnesium concentration, the resulting bio-tiles surpassed the standards set for conventional manufacturing of tiles with a water absorption of greater than 10%. This suggests that submersion is a viable simple method for producing bio-tiles with satisfactory strength properties.

To offer an alternative production method to the submersion technique, the pumping method (Lambert & Randall, 2019) was adapted to bio-tiles and tested. The pumping technique involves the periodic circulation of cementation solution through a sealed mould. This approach forced the solution through the pore spaces, thereby enhancing the $CaCO_3$ precipitation homogeneity and minimising reagent wastage. The objectives of this study were to evaluate the influence of seeding with $CaCO_3$

crystals on the strength properties of bio-tiles produced with a pumping technique, as well as to investigate how the breaking strength was affected by the bacterial ureolytic activity and the retention time of each treatment cycle.

The pumping technique resulted in substantial improvements in the mechanical properties of the bio-tiles, successfully producing bio-tiles that met the international standards for breaking strength and modulus of rupture for two different water absorption categories. Breaking strength improved by up to 47.6% and modulus of rupture by up to 26.2% when using the pumping technique. We showed that the inoculum with the highest ureolytic activity resulted in the strongest bio-tiles when employing a pumping method. This study also showed that shorter treatment intervals led to stronger bio-tiles. The introduction of additional $CaCO_3$ seeds significantly enhanced the breaking strength of the bio-tiles by 21-82%, increasing with greater masses of seeds. A higher seed loading allowed bio-tile strength properties to align with international standards for extruded tiles with water absorption between 6-10%. In comparison, the use of a lower seed loading resulted in bio-tiles exceeding the standards for tiles with a water absorption of greater than 10%. This method's success demonstrates its potential for producing bio-tiles that meet or exceed the strength criteria of conventional tiles, however, further optimisation is needed to reduce labour intensity and improve scalability.

An automated production technique, a prototype for binder jet 3D printing, was designed, developed and tested to integrate the benefits of both the submersion and pumping methods. This technique offered a scalable solution for bio-tile manufacturing with minimal manual intervention. The process was automated to deposit cementation solution. Briefly, an actuator raised and lowered a platform that held the inoculated sand, where in the lowered position, the chamber was sealed and the reaction could proceed, and when raised, the solution could drain. The technique was designed to be modular, making it a more attractive option for large-scale production. The key objectives of this study were to develop and optimise an automated technique for growing bio-tiles and evaluate its impact on breaking strength of bio-tiles when additional nutrients in the form of a daily nutrient broth-enriched treatment were added, in the presence of $CaCO_3$ seeds and supplemental magnesium.

The design and operational processes were refined to produce bio-tiles that conform to international standards for breaking strength and modulus of rupture. This marks the first time bio-tiles have been created using an automated method with freeze-dried urease-active bio-slurry. The study found that a supplement of 0.3 M magnesium chloride significantly improved the breaking strength of bio-tiles produced with the automated technique. While additional seeding with $CaCO_3$ crystals had minimal effect on breaking strength, it was beneficial for enhancing the formation of bio-tiles at corners and edges. Daily treatment of the bio-tiles with a cementation solution supplemented with nutrient broth resulted in a decrease in their strength properties. Multiple bio-tiles produced through this automated process with supplemental magnesium exceeded international standards for tiles with water absorptions above 10%. The process's scalability makes it suitable for commercial applications, where large volumes of bio-tiles could theoretically be produced with reduced operational costs. However, the initial investment in automation technology and the complexity of setting up such a system present challenges that must be addressed to make this approach economically viable. The study suggests that the automated technique has the greatest potential for scaling up bio-tile production while maintaining high-quality standards, but it requires further development to optimise cost-efficiency and simplify the operational process.

The research concludes that while each production technique offers unique advantages and challenges, the choice of method should be guided by specific production goals and resource availability. The submersion technique would be most suitable for small-scale production or experimental applications where cost and simplicity are primary concerns. In contrast, the pumping

technique is likely better suited for medium-scale operations that require higher strength bio-tiles with more consistent internal properties, albeit with some manual intervention. The automated technique, despite its greater complexity, has the greatest potential for large-scale, commercial bio-tile production, however product consistency needs to be refined. Future work should focus on validating these preliminary conclusions and optimising these techniques to improve efficiency, reduce costs, and enhance the mechanical properties of bio-tiles to meet the stringent requirements of the construction industry. Additionally, further research is needed to explore the range of other tests and quality standards to fully establish their suitability as a sustainable alternative to conventional building materials.

This comprehensive investigation into MICP-based bio-tile production demonstrates the potential for innovative bio-materials to revolutionise the construction industry by offering sustainable, cost-effective, and high-performance alternatives to traditional materials. The findings provide a foundation for future research and development efforts aimed at optimising the production processes, enhancing the mechanical properties, and scaling up the manufacturing of bio-tiles for widespread commercial use.

Acknowledgements

First and foremost, the most heartfelt thanks to my supervisor, Prof Dyllon Randall, without which this thesis would not take the form it does, let alone being finished in four years. For always pushing, questioning, encouraging and maybe even micromanaging, you really helped to shape my thinking and stop looking for the expected answers. I can't begin to express my gratitude for your quick responses, feedback and general availability – you really are a role model supervisor and a gift to work with.

Njabulo Thela and Hector Mafungwa, your steady presences in the lab not only gave me strength and certainty, but also many a laugh. With the both of you, I avoided many a mishap and hold-up – and the value of that is inexpressible. I really enjoyed MacGyver-ing with the both of you.

Also, all the other fellow postgrad presences in the lab through the years, Joshua Matesun, Cornelius Chen Chen, Jason Minnie, Daniel De Oliviera and Caitlin Courtney – to name some of the die-hards – you brightened my time in that smelly lab beyond measure.

I can't be sure I would have made it through this degree without the technical and emotional support of Ziba Rajan. All the coffees, all the dinners, all the late night couch conversations and tears shared – you helped me put all manner of things into perspective and always left me with a feeling of optimism that we can change the world, that we can find a way and it would all be worth it.

The rest of my friends, from home and through UCT, and beyond - your support of this crazy endeavour of mine, and the effort spent trying to understand some of the deepest technicalities with me has me, even now, beaming with joy and love for you. Even those who were around only at the beginning, or the special one beside me at the end and motivating me over the finish line – every thought, ponder, engagement was galactic to me.

Ten years with UCT Tai Chi Club and I'm perhaps a step closer to equanimity. Perhaps. For all the lessons, hours, activities and philosophising, I can easily say I wouldn't be who I am today without the club, the practice, weaved through my fibre biweekly – but most of all, because of the community and love created by our late coach, Peter Williamson, I am more and I am further along the path than I ever could have dreamed. May he rest in peace.

My mom, sister, stepdad and grandmother – you may not understand my crazy desire to dig this deep into academia, but your support, love and bragging helped me believe in myself. For that, there are no words, only incredible insanity that I may actually be able to push on to greater wonders.

I would like to recognise the technical input of the UCT Analytical Lab, for particle size distributions, Clear Design for the custom moulds and bio-reactors, as well as a huge thanks to the UCT Concrete Materials and Structural Integrity Research Unit (CoMSIRU), for the use of the strength-measuring equipment and all the related assistance throughout these four years.

This research was financially supported by Anglo Gold Ashanti as well as CSIR-merSETA, the University of Cape Town, the Water Research Commission (WADER) and the Oppenheimer Memorial Trust, and without whom, *none* of this document could have taken form, let alone begun. The world needs more of this kind of generosity to help people explore their curiosities and I am so honoured to have received a slice.

Table of contents

List of tables

List of figures

Abbreviations

Less common abbreviations and acronyms:

DIC	Dissolved inorganic carbon
EII	Energy-intensive industry
EICP	Enzyme induced calcium carbonate precipitation
EPS	Extracellular polymeric substances
FCFM	Full contact flexible mould
GDA	Gallery Discrete Analyser
ISO	International Organisation of Standards
MICP	Microbially induced calcium carbonate precipitation
MOR	Modulus of rupture
PSD	Particle size distribution
SANS	South African National Standards
SEM	Scanning electron microscope
SI	Saturation index
UCS	Unconfined compressive strength
UCT	University of Cape Town
XRD	X-ray diffraction

1 Introduction

The rapid expansion of global infrastructure presents both an opportunity and a challenge. As cities grow and populations swell, the demand for construction materials continues to surge. Approximately 20% of all buildings projected to exist by 2050 have not yet been built (Blanco *et al.*, 2021), highlighting the scale of future development. Infrastructure development influences approximately 70% of the 169 Sustainable Development Goals targets (Thacker *et al.*, 2019), underscoring its significance in shaping sustainable futures. However, the construction industry's heavy reliance on natural resources, coupled with escalating urbanisation—from 4.4 billion urban residents in 2023 to a projected 6.9 billion by 2050 (UN, 2019; World Bank Group, 2023)—demands a re-evaluation of traditional building practices. Moreover, with an estimated USD 139 trillion investment needed globally to achieve net-zero infrastructure by 2050 (Müller & Ahmed, 2024), the urgency for sustainable solutions has never been greater.

Climate change remains one of the most pressing existential threats, driven largely by greenhouse gas emissions from human activities (Prüss-Ustün *et al.*, 2016). The construction industry is a major contributor, responsible for about 15% of global emissions (Edenhofer *et al.*, 2014; UNEP, 2022a). While raw materials extraction and their transport are significant contributors, production processes of specific construction materials can have an even more severe impact. Concrete production alone accounts for 9% of total CO_2 emissions (Miller & Moore, 2020), nearly two-thirds of the construction sector's total impact. Furthermore, the demolition of buildings has led to increasing land use for construction waste (Qiu *et al.*, 2014). In response, the need for alternative, sustainable building materials has become increasingly urgent for maintaining the delicate balance of nature and our way of life. The heightened awareness of natural resource depletion, waste production, and the tangible effects of climate change pose significant challenges for innovation and drives consumer demand for impactful materials.

A paradigm shift towards sustainable construction materials is imperative. Materials with lower embodied energy, reduced life-cycle costs, and comparable performance to conventional materials are critical to addressing environmental pressures. In this context, biotechnology presents a promising avenue, offering construction materials with reduced environmental impacts through the use of processes that can make use of renewable energy and have minimal energy and temperature requirements (Myhr *et al.*, 2019). Amongst these, bio-cementation has recently garnered significant attention. Bio-cementation is a microbiologically induced process that produces calcium carbonate ($CaCO_3$), which acts like a glue to bond particles or materials together. Numerous studies highlight the application of microbially induced $CaCO_3$ precipitation (MICP) to improve the mechanical properties of existing construction materials (De Muynck *et al.*, 2010; Rahman *et al.*, 2020; Seifan & Berenjian, 2018). In particular, MICP has been used to heal cracks in concrete (Shaheen *et al.*, 2019), to clog pores in concrete to reduce its porosity (Noeiaghaei *et al.*, 2017), and to treat the surface of concrete (Joshi *et al.*, 2019; Wong *et al.*, 2020). Beyond improving conventional materials, MICP has also been explored in the fabrication of novel bio-materials—materials synthesised from the bio-cementation reaction—like bio-bricks (Bu *et al.*, 2018; Cheng *et al.*, 2020; Lambert & Randall, 2019), and "zero emission" concrete and slabs (Myhr *et al.*, 2019). However, the application of MICP in producing bio-tiles—biologically grown floor and wall tiles formed through bio-cementation—remains unexplored in literature.

The environmental impact of conventional tiles is substantial. Ceramic tiles require kiln firing at temperatures between 1050°C and 1300°C, and cement tiles are made primarily of the binder clinker which is produced through calcination of limestone (removing CO_2 to form CaO) at temperatures of

1400-1450°C (Melethil & Thomas, 2023). These processes result in high embodied energy and significant carbon emissions. Similarly, bricks, which are fired at 900°C to 1200°C, contribute further to the industry's footprint. The scale of production amplifies these concerns, where South Africa alone produces 3.6 billion bricks annually (Swisscontact & CBA, 2017) compared to 59.6 million m^2 of ceramic tiles, with bricks about 10 times the volume of tiles (Maluleke, 2017). Globally, the ceramic tile market size was valued at USD 379.8 billion in 2022 (Straits Research, 2023) while cement tiles reached a market size of USD 22.9 billion in 2023 (Data Horizzon Research, 2024), about 16 times smaller. In contrast, the global brick market size was estimated at USD 1,685 billion in 2023 (Precedence Research, 2024). Market prices reinforce these distinctions, with bricks selling for between USD 0.11-0.27 each, while tiles sell for USD 5.44-124.53 per m^2 (CTM, 2022; Italtile, 2022), based on South African market prices. In 2017, ceramic wall and floor tiles contributed more to the South African GDP (USD 188.5) than building bricks (USD 108.2 million) (Maluleke, 2017). Given the likely pricing disparity between traditional and bio-cemented bricks (Myhr *et al.*, 2019), potential commercial uptake remains limited. However, bio-tiles present a viable alternative, also offering a potentially profitable market entry point for developing MICP technology in comparison to other bio-materials (Rajasekar *et al.*, 2017).

Despite advances in bio-cemented materials, large-scale adoption remains elusive. Several technical barriers persist, including limitations in mechanical strength, lengthy production times, and the need for sustainable, scalable processes (Myhr *et al.*, 2019). The MICP process relies on key material inputs — urea as a carbonate (CO_3^{2-}) source (Achal *et al.*, 2011a), calcium chloride dihydrate for calcium supply (Anbu *et al.*, 2016; DeJong *et al.*, 2006) to form $CaCO_3$ between loose particles, which are usually sand (Rahman *et al.*, 2020), which as a whole forms the bio-cemented bio-material. The sourcing and processing of these materials raise concerns about energy consumption, resource depletion, and environmental impact. Integrating waste streams as substitutes for high-grade synthetic chemicals or replacing riverbank sand with more sustainable alternatives could significantly enhance the circular economy within the construction industry.

A critical challenge preventing widespread adoption of bio-materials is their insufficient mechanical strength—usually compressive strength when looking at soil, columns or bricks—compared to conventional counterparts (Bu *et al.*, 2018; Cheng *et al.*, 2020; Lambert & Randall, 2019). Addressing this limitation is essential for achieving commercial viability. If bio-materials can be developed with enhanced strength while maintaining their environmental benefits, they could meet industry standards and gain market acceptance. Therefore, the current study will investigate the fundamental aspects of MICP to overcome the physical limitations of bio-materials, with a particular focus on improving strength. Additionally, the research will explore different techniques for producing bio-materials and their effect on mechanical strength, starting with simpler, more passive methods and progressing towards more involved, active fabrication techniques. Finally, thought is given to ways to maximise environmental benefits through the use of industrial by-products and optimising process efficiency. By tackling these challenges, the study aims to contribute to the broader goal of reducing the construction industry's environmental footprint while fostering innovation in sustainable building materials.

References

V. Achal, X. Pan & N. Özyurt. 2011. Improved strength and durability of fly ash-amended concrete by microbial calcite precipitation. *Ecological Engineering.* 37(4):554-559. DOI:10.1016/j.ecoleng.2010.11.009.

P. Anbu, C.H. Kang, Y.J. Shin & J.S. So. 2016. Formations of calcium carbonate minerals by bacteria and its multiple applications. *SpringerPlus.* 5:1-26. DOI:10.1186/s40064-016-1869-2.

J.L. Blanco, H. Engel, F. Imhorst, M.J. Ribeirinho & E. Sjödin. 2021. *Call for action: Seizing the decarbonization opportunity in construction*. McKinsey & Company. Available: https://www.mckinsey.com/industries/engineering-construction-and-building-materials/our-insights/call-for-action-seizing-the-decarbonization-opportunity-in-construction [2024, 8/8].

C. Bu, K. Wen, S. Liu, U. Ogbonnaya & L. Li. 2018. Development of bio-cemented constructional materials through microbial induced calcite precipitation. *Materials and Structures/Materiaux et Constructions.* 51(30):1-11. DOI:10.1617/s11527-018-1157-4.

L. Cheng, T. Kobayashi & M.A. Shahin. 2020. Microbially induced calcite precipitation for production of "bio-bricks" treated at partial saturation condition. *Construction and Building Materials.* 231(117095):1-9. DOI:10.1016/j.conbuildmat.2019.117095.

CTM. 2022. *Ceramic Tile Market, All Floor Tiles, Cement Look*. Available: https://www.ctm.co.za/floors/tiles-by-room/all-floor-tiles-category.html?tile_styles=133&zzz-Cement_Desk_Image [2022, 11 March].

Data Horizzon Research. 2024. *Chemicals and Materials - Cement tiles market research report. Report code: DHR3048*. Fort Collins, United States.

W. De Muynck, N. De Belie & W. Verstraete. 2010. Microbial carbonate precipitation in construction materials: A review. *Ecological Engineering.* 36(2):118-136. DOI:10.1016/j.ecoleng.2009.02.006.

J.T. DeJong, M.B. Fritzges & K. Nüsslein. 2006. Microbially induced cementation to control sand response to undrained shear. *Journal of Geotechnical and Geoenvironmental Engineering.* 132(11):1381-1392. DOI:10.1061/(ASCE)1090-0241(2006)132:11(1381).

O. Edenhofer, R. Pichs-Madruga & C. Intergovernmental Panel on Climate. 2014. *Working Group III Contribution to the Fifth Assessment Report of the Intergovernmental Panel on Climate Change*. (9781107058217).

Italtile. 2022. *Natural Stone Cladding, Outdoor Tiles*. Available: https://www.italtile.co.za/outdoor/cladding-category.html [2022, 11 March].

S. Joshi, S. Goyal, A. Mukherjee & M.S. Reddy. 2019. Protection of concrete structures under sulfate environments by using calcifying bacteria. *Construction & building materials.* 209:156-166. DOI:10.1016/j.conbuildmat.2019.03.079.

S.E. Lambert & D.G. Randall. 2019. Manufacturing bio-bricks using microbial induced calcium carbonate precipitation and human urine. *Water Research.* 160:158-166. DOI:10.1016/j.watres.2019.05.069.

R. Maluleke. 2017. *Manufacturing industry: Production, 2017*. (978-0-621-47925-6). Pretoria, South Africa. Available: www.statssa.gov.za.

K. Melethil & B. Thomas. 2023. 7 - Photocatalytic applications of ceramics. In *Ceramic Catalysts.* M. Kurian, S. Thankachan and S.S. Nair, Eds.: Elsevier. 169-204. DOI:https://doi.org/10.1016/B978-0-323-85746-8.00003-5.

S.A. Miller & F.C. Moore. 2020. Climate and health damages from global concrete production. *Nature climate change.* 10(5):439-443. DOI:10.1038/s41558-020-0733-0.

V. Müller & Z. Ahmed. 2024. *Sustainable infrastructure: a paradigm shift towards greener investments*. EY. Available: https://www.ey.com/en_lu/insights/infrastructure/sustainable-infrastructure-a-paradigm-shift-towards-greener-inv [2025, 2/2/2025].

A. Myhr, F. Royne, A.S. Brandtsegg, C. Bjerkseter, H. Throne-Holst, A. Borch, A. Wentzel & A. Royne. 2019. Towards a low CO2 emission building material employing bacterial metabolism (2/2): Prospects for global warming potential reduction in the concrete industry. *PLOS ONE.* 14(4):e0208643. DOI:10.1371/journal.pone.0208643.

T. Noeiaghaei, N. Dhami & A. Mukherjee. 2017. Nanoparticles surface treatment on cemented materials for inhibition of bacterial growth. *Construction & building materials.* 150:880-891. DOI:10.1016/j.conbuildmat.2017.06.046.

Precedence Research. 2024. *Bricks market size, share, and trends 2024 to 2034. Report Code: 3654*. Ottawa, Canada: P. Research.

A. Prüss-Ustün, J. Wolf, C. Corvalán, R. Bos & M. Neira. 2016. *Preventing disease through healthy environments: a global assessment of the burden of disease from environmental risks*. Geneva, Switzerland: W. Press.

J. Qiu, D.Q.S. Tng & E.-H. Yang. 2014. Surface treatment of recycled concrete aggregates through microbial carbonate precipitation. *Construction & building materials.* 57:144-150. DOI:10.1016/j.conbuildmat.2014.01.085.

M.M. Rahman, R.N. Hora, I. Ahenkorah, S. Beecham, M.R. Karim & A. Iqbal. 2020. State-of-the-art review of microbial-induced calcite precipitation and its sustainability in engineering applications. *Sustainability.* 12(15):6281-6281. DOI:10.3390/su12156281.

A. Rajasekar, C.K.S. Moy & S. Wilkinson. 2017. MICP and advances towards eco-friendly and economical applications. *IOP Conference Series: Earth and Environmental Science.* 78(1):012016-012016. DOI:10.1088/1755-1315/78/1/012016.

M. Seifan & A. Berenjian. 2018. Application of microbially induced calcium carbonate precipitation in designing bio self-healing concrete. *World Journal of Microbiology and Biotechnology.* 34:168-168. DOI:10.1007/s11274-018-2552-2.

N. Shaheen, R.A. Khushnood, W. Khaliq, H. Murtaza, R. Iqbal & M.H. Khan. 2019. Synthesis and characterization of bio-immobilized nano/micro inert and reactive additives for feasibility investigation in self-healing concrete. *Construction & building materials.* 226:492-506. DOI:10.1016/j.conbuildmat.2019.07.202.

Straits Research. 2023. *Ceramic tiles market size, growth & analysis by 2031. Report code: SRAM466DR.* Amanora Park Town, India.

Swisscontact & CBA. 2017. *Clay brick production survey, Southern African Development Community (SADC)*. Pretoria, South Africa. Available: www.swisscontact.org.

S. Thacker, D. Adshead, M. Fay, S. Hallegatte, M. Harvey, H. Meller, N. O'Regan, J. Rozenberg *et al.* 2019. Infrastructure for sustainable development. *Nature Sustainability.* 2(4):324-331. DOI:10.1038/s41893-019-0256-8.

UN. 2019. *World urbanization prospects: The 2018 revision*. New York: U. Nations.

UNEP. 2022. *2022 Global status report for buildings and construction: Towards a zero-emission, efficient and resilient buildings and construction sector*. Nairobi: G.A.f.B.a. Construction.

L.S. Wong, A.F.M. Oweida, S.Y. Kong, D.M. Iqbal & P. Regunathan. 2020. The surface coating mechanism of polluted concrete by Candida ethanolica induced calcium carbonate mineralization. *Construction & building materials.* 257:119482. DOI:10.1016/j.conbuildmat.2020.119482.

World Bank Group. 2023. *Urban Development, Overview*. Available: https://www.worldbank.org/en/topic/urbandevelopment/overview [2024, Aug 10].

2 Literature Review

2.1 Microbially induced calcium carbonate precipitation

Microbially induced calcium carbonate ($CaCO_3$) precipitation is a biomineralisation process wherein specific microorganisms enzymatically catalyse the precipitation of bio-cement in the form of $CaCO_3$. Inspired by the inherent ability of these microorganisms to cement together loose particles, coprecipitate metal ions and sequester CO_2, bio-cementation has been the subject of extensive research for various engineering applications. These applications include the prevention of soil erosion (Whiffin *et al.*, 2007), healing of concrete cracks (Jonkers *et al.*, 2010; Seifan & Berenjian, 2018), immobilisation of groundwater contaminants (Ferris *et al.*, 2004), enhancement of oil recovery (Cunningham *et al.*, 2009), control of fugitive dust (Hamdan & Kavazanjian, 2016), creation of subsurface barriers against pollutant spread (Cunningham *et al.*, 2011), reduction of soil hydraulic conductivity (Nemati & Voordouw, 2003) and the production of bio-materials (Dikshit *et al.*, 2022; Lambert & Randall, 2019).

This biological process is a ubiquitous phenomenon that plays a crucial role in the cementation of natural systems such as caves, aquifers, sediments, soils and open water areas (Song *et al.*, 2022). It has been noted that under suitable conditions, most bacteria are capable of inducing the precipitation of $CaCO_3$ (Boquet *et al.*, 1973). The prevalence of MICP is largely attributed to the diverse array of pathways through which it can be achieved. Regardless of the specific pathway, MICP is typically facilitated by enzymes[1]. For instance, enzymatic urea hydrolysis is catalysed by the enzyme urease or the interconversion of CO_2 to HCO_3^- by the enzyme carbonic anhydrase (Li *et al.*, 2013a). Each pathway leads to the precipitation of $CaCO_3$ as the solution becomes sufficiently saturated (De Muynck *et al.*, 2010).

2.1.1 *Pathways of microbially induced calcium carbonate precipitation*

The major metabolic pathways of MICP are the heterotrophic pathways involving the nitrogen cycle, the sulphur cycle and the utilisation of organic acids, as well as autotrophic pathways such as photosynthesis and methane oxidation (Rahman *et al.*, 2020; Zhu & Dittrich, 2016). A summary of some of these pathways is depicted in Figure 2.1.

There are three different pathways within the nitrogen cycle (De Muynck *et al.*, 2010):

1. Ammonification of amino acids in aerobiosis;
2. Denitrification of nitrate in anaerobiosis or microaerophily; and
3. Ureolysis of urea or uric acid in aerobiosis.

Myxococcus xanthus utilises the ammonification pathway and has been found to precipitate uranium as meta-autunite, thereby providing protection to concrete structures exposed to radioactive wastes (Turick & Berry, 2016). *Pseudomonas aeruginosa* and *Diaphorobacter nitroreducens* utilise the

[1] An enzyme is a protein produced by a living organism which acts as a catalyst to accelerate a specific biochemical reaction by lowering its activation energy. Enzymes are very specific to what substrates they bind to, through the possession of complementary substrate binding regions (Alberts *et al.*, 2002). For example, hydrolase enzymes catalyse hydrolysis reactions and in the human body, lactase breaks down lactose into glucose and galactose.

denitrification pathway, have demonstrated the ability to close microcracks in concrete of 200-250 µm when immobilised and combined with clay particles (Ersan *et al.*, 2015).

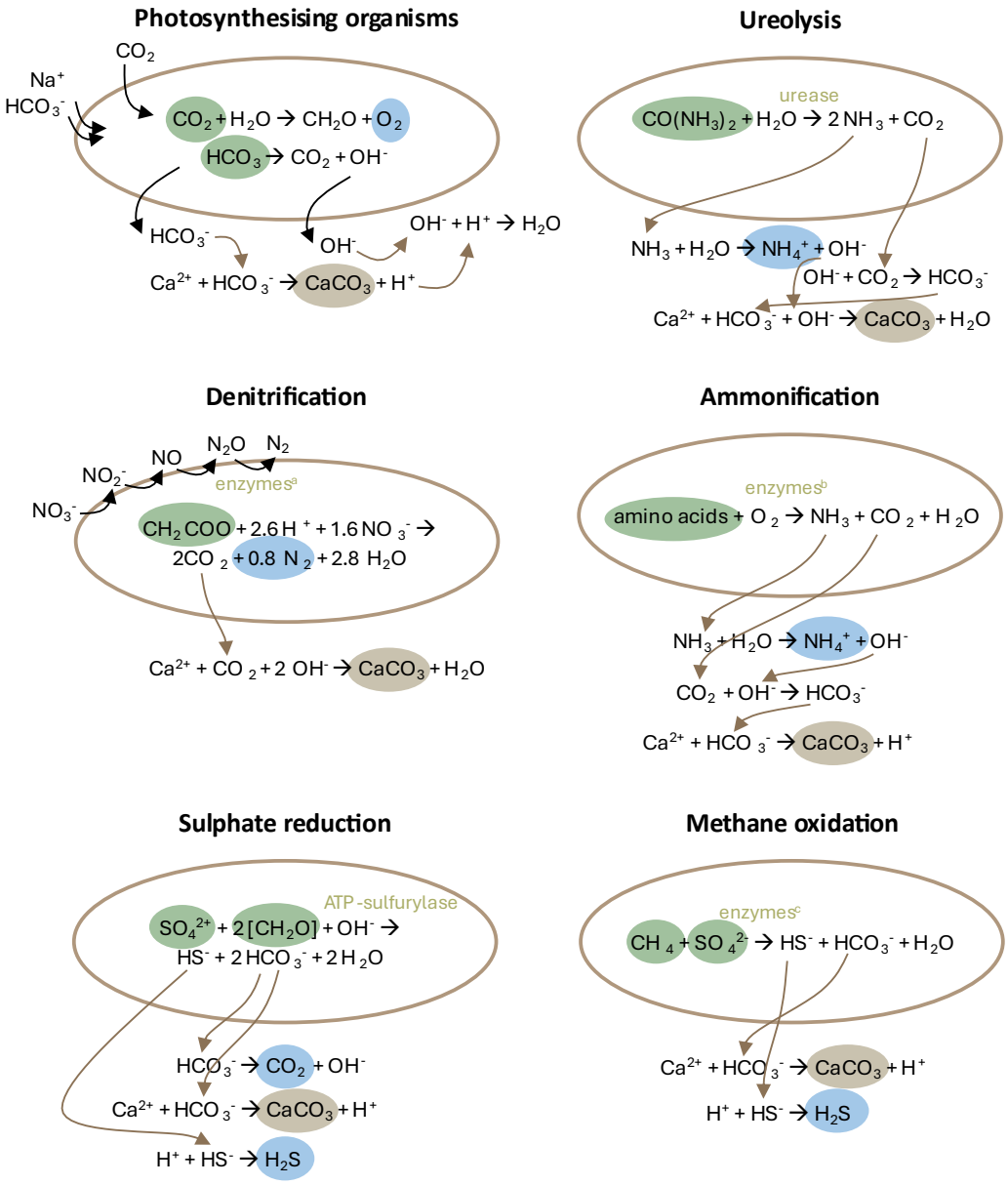

Figure 2.1: The biochemical reactions of the major pathways of MICP (Zhu & Dittrich, 2016). Ovals depict cell membranes. Green circles indicate substrates or inputs, brown, the desired $CaCO_3$ product, and blue, the pathway by-product. Black arrows indicate compounds crossing the cell membrane. Photosynthesis leads to the precipitation of $CaCO_3$ through the exchange of HCO_3^+/OH^- across the cell membrane using symporters and bicarbonate converted to CO_2 and OH^- by the CO_2 concentration mechanism, and then to organic matter. [a]For the denitrification pathway, the key enzymes involved include nitrate reductase, nitrite reductase, nitric oxide reductase and nitrous oxide reductase. [b]The ammonification pathway is catalysed by enzymes including proteinases, peptidases and deaminases. [c]Researchers are still investigating the enzymes responsible for the methane oxidation pathway.

The sulphur cycle pathway is utilised by sulphate reducing bacteria (SRB). Dissimilatory sulphate reduction occurs under anoxic conditions in organic substrate-rich environments, leading to the

formation of odorous and highly toxic H_2S gas (Hamdan *et al.*, 2017). Despite this drawback, SRB sourced from domestic acidic water have been added to concrete mixtures and resulted in a 61% increase in compressive strength (Tambunan *et al.*, 2019).

Cyanobacteria and microalgae are the primary microorganisms responsible for MICP with the photosynthesis pathway. However, their application faces the usual photosynthesis process challenges of supplying sunlight and CO_2 at scale (Seifan *et al.*, 2016). Methane oxidation is largely responsible for driving the change in concentration of CO_2 in marine and freshwater environments, and subsequently converts to CO_3^{2-} under certain conditions. As of 2019, there were no studies on the use of this mechanism in bio-materials and its development in bio-materials is unlikely given the high demand for methane as a resource (Castro-Alonso *et al.*, 2019).

Each pathway has its own drawbacks. For example, denitrification results in the build-up of byproducts that inhibit the bacteria (Hamdan *et al.*, 2017) and exhibits a slow rate of $CaCO_3$ precipitation (Pham *et al.*, 2018) despite being oxygen independent (Hamdan *et al.*, 2017). Amongst the various pathways, urea hydrolysis is considered less complex and has been demonstrated to have $CaCO_3$ precipitation masses 20-80% higher than other pathways (Castro-Alonso *et al.*, 2019), making it the most appropriate for commercial applications and the most studied MICP process (Achal *et al.*, 2011a; Anbu *et al.*, 2016).

2.1.2 *Urea hydrolysis pathway*

The hydrolysis of urea is induced through ureolytic microorganisms, which produce the enzyme that catalyses the reaction (Equation 1) to produce ammonia (NH_3) and carbamic acid (NH_2COOH) using the enzyme urease (urea amidohydrolase) (Mobley & Hausinger, 1989). This is followed by the spontaneous hydrolysis of carbamic acid to carbonic acid (H_2CO_3) and another mole of ammonia (Equation 2). Subsequently, bicarbonate ions (HCO_3^-) are produced from the carbonic acid (Equation 3). The ammonia from Equation 1 and 2 moves into equilibrium with ammonium (Equation 4). At neutral pH, the dominant species are ammonium and bicarbonate (Kim *et al.*, 2020). These reactions ultimately result in an increase in pH which promotes conditions that are favourable for the formation of carbonate ions from the bicarbonate by shifting the equilibrium of Equation 5 forward (Kumari *et al.*, 2016). Finally, when in the presence of free calcium ions or other divalent ions (M^{2+}), these reactions will result in the precipitation of $CaCO_3$ or MCO_3 at the surface of bacteria cells or other nucleation sites (Equation 6) (Gat *et al.*, 2014).

$$CO(NH_2)_2 + H_2O \xrightarrow{\text{urease}} NH_3 + NH_2COOH \quad (1)$$

$$NH_2COOH + H_2O \leftrightarrow H_2CO_3 + NH_3 \quad (2)$$

$$H_2CO_3 \leftrightarrow H^+ + HCO_3^- \quad (3)$$

$$2NH_3 + 2H_2O \leftrightarrow 2NH_4^+ + 2OH^- \quad (4)$$

$$HCO_3^- + H^+ + 2OH^- \leftrightarrow CO_3^{2-} + 2H_2O \quad (5)$$

$$Ca^{2+} + CO_3^{2-} \leftrightarrow CaCO_3\downarrow \quad (6)$$

The ammonia byproduct that ureolytic MICP produces is considered a major challenge (Choi *et al.*, 2017; De Muynck *et al.*, 2010). Technical approaches need to be employed to overcome its potential environmental impact (Song *et al.*, 2022). For example, ensuring the concentration of the ammonia

generating compound (urea) does not exceed that of the calcium source can decrease emissions (De Muynck *et al.*, 2010). Alternatively, an innovative approach is the production of fertiliser from the ammonium ions, either through the conversion of the ammonium ions into ammonium sulphate with sulphuric acid (Pradhan *et al.*, 2017) or concentration using reverse osmosis (RO) (Thörneby *et al.*, 1999).

Precipitation reactions occur throughout nature, usually at very slow rates (De Muynck *et al.*, 2010; Stocks-Fischer *et al.*, 1999). The use of a catalyst, such as urease, is crucial for the practical application of this process. A variety of urease-producing organisms have been identified (Anbu *et al.*, 2016), while those exhibiting high urease-activity are preferred for MICP processes. *Sporosarcina pasteurii* (formerly *Bacillus pasteurii*), an endospore-forming, non-pathogenic soil bacterium is commonly employed in MICP processes (Achal *et al.*, 2009).

As microorganisms perform enzymatic urea hydrolysis, they create an alkaline environment favourable for MICP conditions (Achal *et al.*, 2009). The bacteria themselves influence the precipitation of $CaCO_3$ by providing sites for calcium enrichment or nucleation sites for the precipitation of $CaCO_3$ (Ma *et al.*, 2020; Stocks-Fischer *et al.*, 1999) while producing localised concentration gradients (Henze & Randall, 2018). All of these factors collectively promote further $CaCO_3$ precipitation, enhancing the efficacy of the MICP process.

Other than the microorganisms, urea is a key ingredient of the ureolytic MICP process. Currently, the production of synthetic urea is inefficient, yielding low output and high CO_2 emissions (Kyriakou *et al.*, 2020). The source of urea chosen for this reaction may significantly enhance the sustainability of bio-materials grown with ureolytic MICP.

2.2 Sources of material inputs

The material inputs of the MICP process play a significant role in its overall environmental impact. These inputs can come from various sources, including virgin mineral deposits and high-energy synthetic chemicals. However, in some cases, human or industrial by-products may serve as more sustainable alternatives.

2.2.1 *Urea*

Conventionally, research into applications of MICP has relied on synthetic urea as the nitrogen source (Rahman *et al.*, 2020). A US-based company, BioMASON, has commercialised the production of bio-bricks and bio-tiles using synthetic urea in MICP (BioMASON, 2022), eliminating the need for high operating temperatures typically associated with clay-fired brick and ceramic tile manufacturing processes. However, synthetic urea is derived from ammonia, which is initially synthesised by the Haber-Bosch process primarily for fertiliser production. This process alone consumes approximately 2% of the world's energy due to the high demand for fertilisers (Pfromm, 2017), rendering the production of synthetic urea and, by extension, the bioMASON products energy intensive.

A more sustainable source of urea is human urine, either directly or as urea recovered from human urine. Urea contributes up to 90% of the nitrogen present in human urine (Lentner, 1981) and about 80% of the nitrogen in domestic wastewater, while constituting less than 1% of the total volume of wastewater (Höglund, 2001). Beyond the nitrogen, the urine fraction contains 56% of the phosphorous and 63% of the potassium in domestic wastewater (Höglund, 2001). Thus, recovering these nutrients

from this waste stream could partially close their usage cycle and potentially contribute to the world's circular economy.

However, most of the urea present in human urine degrades to other ions within 24 hours of collection, making MICP unfeasible without prompt utilisation (Udert *et al.*, 2003). To use urine for MICP, the enzymatic urea hydrolysis reaction needs to be delayed. This has been successfully achieved for bio-material production by increasing the pH to about 12.5 through the addition of calcium hydroxide ($Ca(OH)_2$) (Henze & Randall, 2018; Lambert & Randall, 2019; Randall *et al.*, 2016). Urine treated with $Ca(OH)_2$ can be stored for extended periods with minimal urea loss (Flanagan & Randall, 2018). This treatment precipitates out almost all the phosphorous present as a solid fertiliser, calcium phosphate, along with magnesium ions as $Mg(OH)_2$ (Flanagan & Randall, 2018; Randall *et al.*, 2016). However, the high operating pH's effect on the efficiency of MICP process, amongst other factors, must also be considered. As the use of urine for bio-material production has already been proven, synthetic urea offers beneficial process simplification for developing other proof of concepts.

2.2.2 *Calcium*

The most frequently used calcium source for MICP is calcium chloride ($CaCl_2$), as it allows higher urease activity and greater $CaCO_3$ production (Achal & Pan, 2014). Other calcium sources, such as calcium lactate, calcium acetate, calcium oxide and calcium nitrate, also facilitate MICP. However, the increase in pH and the number of bacteria cells are not as high as when $CaCl_2$ is used (Achal & Pan, 2014). These alternative calcium sources can promote different morphologies of $CaCO_3$ under the right conditions (Zehner *et al.*, 2021) and this will be discussed further in Section 2.6.1.

Calcium chloride is produced through three main techniques. The first is as a by-product from the Solvay process used to produce soda ash from limestone (mostly consisting of $CaCO_3$) and sodium chloride (NaCl) (Wang *et al.*, 2022a). The second is through the reaction of limestone with hydrochloric acid and subsequent purification with calcium hydroxide ($Ca(OH)_2$) to remove magnesium and concentrating through fluid bed dryers or flaking units (Delong & Liyan, 2014). The final technique of producing $CaCl_2$ is through the concentration and purification of naturally occurring brines from salt lakes and salt deposits, however this is only performed in the U.S. (Kiefer, 2002). As soda ash production decreased due to the abundance of caustic soda, alternative production methods for $CaCl_2$ through other means have become necessary. These other means require energy and resources and are best avoided to reduce the burden and requirement of virgin synthetic reagents.

Moreover, $CaCl_2$ is expensive and not environmentally friendly as the Cl^- ions react to form chloride salts that pollute water, and because of the energy that can be required in its production (Zehner *et al.*, 2021). Additionally, when MICP is used for steel reinforcement, the presence of Cl^- ions promotes corrosion of the reinforcements.

To lower the environmental impact of bio-materials, alternative calcium sources have been explored. Feasible sources for MICP include dairy waste (Kahani *et al.*, 2020), quarry limestone (Choi *et al.*, 2017), seawater (Ashraf *et al.*, 2021), bone meal (Gowthaman *et al.*, 2021), eggshell (Choi *et al.*, 2016) and wastewater from the food industry (Huang *et al.*, 2020).

2.2.3 *Loose particles*

Construction materials such as bricks and tiles may be produced from sand, however, clay has been used since about 8000 BC (Shubbar *et al.*, 2019). Bio-materials, on the other hand, are most commonly produced from forming bio-cement between sand grains until a solid is produced (Rahman *et al.*, 2020).

The term sand resources encompasses sand, clay, gravel, crushed rock and aggregate (UNEP, 2022b). Sand resources are the second most exploited raw resource in the world, second only to water (UNEP, 2019). At 4050 billion tons per year, their use has tripled in 20 years (UNEP, 2019). This is primarily due to the vast amounts of concrete used in construction, but sand resources are also utilised in asphalt and glass production, as well as for land reclamation and flood attenuation (UNEP, 2022b). Despite this immense demand and strategic importance, the sourcing and extraction of sand resources in many parts of the world remains ungoverned, potentially damaging riverine and marine ecosystems, some of which are already under threat (Bendixen *et al.*, 2021; UNEP, 2019). Current extraction rates exceed natural rates of replenishment from erosion (Hackney *et al.*, 2021). Therefore, it is necessary to consider additives to reduce the demand for sand resources or alternatives that can replace the input of sand resources entirely if we are to produce bio-materials without transgressing planetary boundaries. Potential waste materials that have been shown to benefit the properties of bio-cement or bio-mortar are shown in Table 2.1.

Table 2.1: The effect of various waste materials on the compressive strength of cement when they are treated with MICP and the percentage improvement that the MICP treatment offered over the use of each material directly without the preliminary MICP treatment (adapted from Song *et al*. (2022)).

Waste material	Ratio (%)	Compressive strength		References
		MICP (MPa)	Improvement (%)	
Fly ash	10	27.6	20	Dhami *et al.* (2012)
	30	14.9	27.9	Chahal *et al.* (2012)
Cr slag	73	0.36	N/A	Achal *et al.* (2013)
Recycled concrete aggregate	35	76.0	40.7	Wang *et al.* (2017)
Mixed recycled aggregate[a]	34	51.0	15.9	
Recycled fine aggregate	82	12.2	31.2	Zhan *et al.* (2020)
Recycled coarse aggregate	55	46.2	20.9	Sahoo *et al.* (2016)

[a]Mixed recycled aggregate consists of crushed concrete, masonry, glass, wood, etc. (Wang *et al.*, 2017)

Recycled concrete aggregates have been considered for reuse in concrete directly. However, their much higher water absorption (3.6-12.1%) compared to natural aggregates (<1%) typically results in reduced workability, increased slump and a significant reduction in compressive strength (Joseph *et al.*, 2015; Qiu *et al.*, 2014; Zhan *et al.*, 2020). Data in Table 2.1 shows that pre-treatment of recycled concrete aggregate with MICP is very promising in reducing water absorption and results in a cement that is 16-41% stronger than materials where no bio-mineralisation pre-treatment was performed. This indicates that recycled aggregates could also be effectively used to make bio-materials.

The use of effluents and waste materials may involve parameters that are not ideal, such as elevated pH, various particle size distributions (PSDs), unusual calcium sources and additives. These factors may influence the efficiency and effectiveness of $CaCO_3$ precipitation. Understanding their impact is essential for optimising the process and identifying ideal conditions for improved performance.

2.3 Factors affecting microbially induced calcium carbonate precipitation

Microbially induced $CaCO_3$ precipitation is a simple chemical process, however its control is complex. Biomineralisation processes are either biologically controlled or induced. The precipitation of $CaCO_3$ by bacteria is generally regarded as "induced" due to the dependence of the crystal formation and morphology on environmental conditions (Rivadeneyra *et al.*, 1993) rather than solely on the type of bacteria.

The precipitation of $CaCO_3$ is governed by the urease enzyme through four key factors (Achal *et al.*, 2009; Hammes & Verstraete, 2002):

1. The concentration of calcium;
2. The concentration of dissolved inorganic carbon (DIC);
3. The pH; and
4. The availability of nucleation sites.

Additionally, the type and concentration of bacteria, which is proportional to the availability of nucleation sites (Anbu *et al.*, 2016), and the ionic strength (Udert *et al.*, 2003) also contribute to the $CaCO_3$ precipitation dynamics. Retention time further influences the MICP process, with longer reaction times resulting in greater $CaCO_3$ deposition and bio-material strength (Zhao *et al.*, 2014b). The following sections describe the factors that have the most pronounced effects on $CaCO_3$ crystallisation.

2.3.1 *Bacteria and urease activity*

Being microbially induced, the bacteria that perform MICP and their excreted enzyme, urease, are crucial to the reactions and the formation and size of the $CaCO_3$ crystals. Bacteria serve two key roles in the formation of $CaCO_3$ crystals: providing nucleation sites and producing an organic matrix called extracellular polymeric substances (EPS).

First, the bacteria cells act as nucleation sites for the crystals, as they provide the required ionic components and alkaline environment that facilitates the formation of $CaCO_3$ (Achal *et al.*, 2009). In the case of *S. pasteurii*, the bacteria cells are structurally robust, allowing them to remain intact during the harsh mineralisation conditions, and the cell surface also has a highly negative charge which is good for binding positively charged calcium ions (Ma *et al.*, 2020). This contributes to the suitability of *S. pasteurii* for applications of MICP.

The second critical role of bacteria in MICP is the production of negatively charged EPS on the surface of bacterial cells, primarily consisting of proteins and polysaccharides (Chen *et al.*, 2022). Live bacterial cells and their concentration determine the quantity of EPS secreted (Chunxiang *et al.*, 2009). It has been confirmed that EPS is deeply involved in the formation of $CaCO_3$ particles and might provide surfaces for the supersaturation of calcium ions and serve as additional nucleation sites (Shao *et al.*, 2014; Zhu & Dittrich, 2016). Because of its viscosity and negative charge, EPS can incorporate metal cations, such as Ca^{2+}, Mg^{2+}, Fe^{3+} and Mn^{2+}, and induce the precipitation of $CaCO_3$ and accelerate its aggregation (Zhu & Dittrich, 2016). However, the precise impact of EPS constituents on crystal morphology, quantity and other precipitation characteristics remains unclear (Chen *et al.*, 2022).

Other than the bacteria themselves, the MICP process is dependent on the urease produced by the bacteria and the resultant ureolytic activity. Ureolytic activity is directly related to bacteria concentration. Of the many external environmental factors that impact the process, the bacteria or urease concentration has a profound effect on the crystallisation of $CaCO_3$ (Wen *et al.*, 2020). A higher bacterial density enhances nucleation rates and causes a compounded, non-linear increase in the number of $CaCO_3$ crystals. In a microfluidic chip reactor, a ninefold increase in bacterial cells per millilitre resulted in an 18.2-fold increase in crystal formation (Wang *et al.*, 2021). Higher ureolytic activity causes a greater excretion of EPS and a thicker deposit of $CaCO_3$ (Chunxiang *et al.*, 2009; Wen *et al.*, 2020). The initial ureolysis rate has also been found to influence $CaCO_3$ crystal size (Cheng *et al.*, 2017; Cuthbert *et al.*, 2012). Although direct use of the urease enzyme has been explored in the

enzyme-induced calcite precipitation (EICP) process, MICP remains preferable due to lower cost, better resistance to environmental conditions, and production of larger crystals (Murugan *et al.*, 2021).

Multiple species of urease-producing bacteria have been investigated in MICP research. Each species has different ureolysis rates and is able to produce different amounts of urease and $CaCO_3$ precipitation. A selection of urease-producing bacteria with particularly high urease activity is shown in Table 2.2. Each of the bacterial isolates in Table 2.2 were grown in nutrient broth medium with a 2% urea supplementation at 37°C and the crude culture tested for its urease activity using the phenol-hypochlorite assay method, and not necessarily tested for its MICP performance. Generally, *S. pasteurii* outdoes other bacteria by about double for the mass of $CaCO_3$ that is precipitated during MICP (Nayanthara *et al.*, 2019).

Table 2.2: Urease-producing bacteria and their respective sources and urease activity (adapted from Anbu *et al.* (2016)).

Bacteria	Isolation site	Urease activity (U/mL)	Reference
S. pasteurii	Wild strain MTCC 1761	425	Achal *et al.* (2009)
S. pasteurii	Phenotypic mutant strain	550	Achal *et al.* (2009)
Bacillus sp. CR2	Mine tailing soil, Urumqi, China	432	Achal and Pan (2014)
K. flava CR1	Mining ore soil, Urumqi, China	472	Achal *et al.* (2011b)
B. megaterium SS3	Calcareous soil, Andhra Pradesh, India	690	Dhami *et al.* (2013)
B. thuringiensis	Calcareous soil, Andhra Pradesh, India	620	Dhami *et al.* (2013)
S. pasteurii	Wild strain ATCC 11859	830	Grabarek *et al.* (2025)

U = µmol urea hydrolysed/min

2.3.2 *Physicochemical factors*

Several physicochemical conditions significantly influence $CaCO_3$ precipitation via urea hydrolysis, because the urease enzyme operates optimally under certain conditions. Key parameters include nucleation sites, ionic strength, temperature and pH (Anbu *et al.*, 2016). Nucleation sites will be discussed specifically in Section 2.3.5 due to the relation to seeding. Urea hydrolysis by urease-producing microorganisms causes an increase in pH through the production of ammonium ions (Equation 4) to approximately 9.2, crucial for $CaCO_3$ formation (Henze & Randall, 2018). This pH increase is due to the equilibrium state of the ammonia-ammonium ion pair and also provides the microorganisms a nitrogen and energy source (Achal *et al.*, 2009; Mobley & Hausinger, 1989).

Changing the pH affects the shape of the active site of the enzyme as well as its charge, which affects its ability to bind to and catalyse the reaction upon the substrate. While optimal growth of *S. pasteurii* occurs at pH 9.0 (Li *et al.*, 2013b), the extracellular urease enzyme activity peaks at pH 8.0, albeit with a wide active range (Gorospe *et al.*, 2013). This underscores the complexity of MICP, as elevated pH promotes $CaCO_3$ precipitation (Li *et al.*, 2013b), despite the optimal pH for urease being lower. Henze and Randall (2018) found that the upper pH threshold for *S. pasteurii* activity in treated synthetic urine was 11.2. The solution typically has a pH value above 12.0 so this indicated that treated urine may be used as a source of urea with minimal acid addition. Lambert and Randall (2019) successfully grew a bio-brick using treated human urine at an initial pH of 11.2. While pH has a large impact on the MICP process, many researchers do not regulate or note the pH values during experiments, as shown in

Table 2.3**Table *2.3***. Note that bio-material forms, such as the bio-columns and bio-bricks mentioned, will be discussed in Section 2.4, with the techniques for growing them.

Table 2.3: Comparison of MICP process parameters and resulting bio-column or bio-brick compressive strengths obtained.

pH	Calcium (M)	Urea (M)	Bacteria	Compressive strength (MPa)	Reference
n.d.[a]	0.05	0.05	*S. pasteurii*	0.35-1.3	Al Qabany and Soga (2013)
n.d.	1	1	*Bacillus sphaericus*	0.5-2.5	Cheng *et al.* (2013)
6.0	1.5	1.5	*S. pasteurii*	2.13	Zhao *et al.* (2014b)
7.0-7.5	0.3	0.3	*S pasteurii*	0.88-1.1	Choi *et al.* (2017)
11.2	0-0.2	0.3[b]	*S. pasteurii*	0.9	Henze and Randall (2018)
n.d.	0.5	0.5	*S. pasteurii*	0.39-0.46[d]	Bu *et al.* (2018)
11.2	0.09-0.13	0.3[c]	*S. pasteurii*	2.7[d]	Lambert and Randall (2019)
n.d.	1	1	*S. pasteurii*	4.0-5.8[d]	Cheng *et al.* (2020)
6.0-7.0	0.75	0.75	*S. pasteurii*	5-23	Nething *et al.* (2020)

[a] n.d. – no data
[b] synthetic urine was used
[c] urine was used
[d] bio-material in the form of bio-bricks, instead of bio-columns

Temperature also plays a vital role, affecting the activity of the urease enzyme and therefore, the urea hydrolysis rate (Ferris *et al.*, 2004; Stocks-Fischer *et al.*, 1999) as well as the reaction that forms the $CaCO_3$ (Equation 6) (Ferris *et al.*, 2004; Keykha *et al.*, 2017). The optimal temperature of the MICP process depends on the bacteria, *S. pasteurii* is usually cultivated at 30°C but has an optimal growth range of about 20-40°C (Chen *et al.*, 2022). These temperatures are fortunately very common in the natural environment.

Another factor that impacts the MICP process is the presence of other ions and salts in the aqueous medium. High concentrations can increase the osmotic pressure around bacteria cells and inhibit bacteria growth and urease activity (Kistiakowsky & Shaw, 1953; Yi *et al.*, 2021), and impede crystallisation (Udert *et al.*, 2003). High overall ionic strength and organic and inorganic complexing agents can inhibit crystal growth by blocking growing sites and significantly reduce the concentration of free lattice ions (Udert *et al.*, 2003).

The solubility of $CaCO_3$ is also a function of pH and the ionic strength (Stumm & Morgan, 1981). However, the solubility of $CaCO_3$ is so low ($K^0_{sp,\ apparent}$ ranges $3.9 \times 10^{-9} – 8.5 \times 10^{-8}$ for ionic strengths of 0.1-1000 mM) that it can be considered negligible in the MICP system (Yang *et al.*, 2024).

The utilisation of synthetic urea, or theoretically, urea recovered from urine by reverse osmosis (RO) and/or evaporation (Ray *et al.*, 2019), for MICP applications allows concentrations to be easily controlled and maximised as there are no other ions present increasing the ionic strength, as in the case of urine, for the microorganisms to withstand, apart from the required Ca^{2+} ions. Hence, synthetic urea, free of additional ions, is the most common nitrogen source researched for MICP and is typically used in concentrations of 0.5–-1.5 M (Table 2.3). Therefore, the high ionic strength of urine may be overcome, and stronger and more sustainable bio-materials may be manufactured.

2.3.3 *Reagent concentrations*

From Equations 1-6, it can be seen that one molecule of urea requires one molecule of calcium to form one molecule of $CaCO_3$. The aqueous solution fed to the bacteria containing the calcium and urea ions required for the MICP process is called a cementation solution and typically contains equimolar amounts of calcium and urea (Table 2.3). It has been shown that higher concentrations of calcium and urea ions in the cementation solution increase the amount of $CaCO_3$ precipitated (Zhao *et al.*, 2014b). A higher solution pH increases the concentration of carbonate ions present (Henze & Randall, 2018) also increasing the $CaCO_3$ precipitated, which generally increases the compressive strength of the bio-material (Whiffin *et al.*, 2007). However, it has been observed that calcium concentration has a more significant impact on the amount of $CaCO_3$ precipitated and the strength of the bio-materials compared to urea concentration (Okwadha & Li, 2010). While equimolar urea and calcium concentrations are often used, Yi *et al.* (2021) have shown that a ratio of 5:1 of urea to calcium results in an optimal mass of precipitated $CaCO_3$ and 25:4 for an optimal yield of $CaCO_3$ when using a urea concentration of 1 M. However, ionic strength of the cementation solution could also be influencing this finding (Lambert & Randall, 2019). Other studies have suggested differing concentrations for MICP, such as 0.5 and 0.25 M for urea and calcium, respectively, being best for calcite precipitation (De Muynck *et al.*, 2010).

Zhao *et al.* (2014b) found that an increase in the equimolar concentration of the cementation solution from 0.25 to 0.5 M caused the unconfined compressive strength (UCS) of their bio-columns to increase almost tenfold from 0.13 to 1.36 MPa. The UCS in this study increased, albeit more slowly, until a calcium concentration of 1.5 M. However, excessively high calcium concentrations can negatively affect urease activity (Gorospe *et al.*, 2013; Nemati *et al.*, 2005) and consequently, on the precipitation of $CaCO_3$.

The concentration of urea in urine ranges from 0.15 to 0.39 M (Putnam, 1971). Due to the inherent ionic strength of urine, the amount of additional calcium ions that may be added to the cementation solution is reduced for *S. pasteurii* to limit the total ionic strength of the solution. Henze and Randall (2018) used a calcium concentration of 0.11 M in their cementation solution. Therefore, diluting the urine or using more robust microbial catalysts capable of withstanding higher osmotic pressures is necessary to efficiently utilise the urea present.

2.3.4 *Particle size*

The particle size of the aggregate utilised and its distribution is another aspect that significantly affects the MICP reactions. Mortensen *et al.* (2011) identified that coarser and well graded sands have a faster $CaCO_3$ precipitation rate compared to finer and more poorly graded soils. Additionally, both very coarse and very fine soils take much longer to increase in shear wave velocity (Mortensen *et al.*, 2011), a parameter proportional to the mass of precipitated $CaCO_3$ (DeJong *et al.*, 2006). Based on the particle size distribution (PSD) of the particles, different crystal sizes are appropriate, where larger crystals are more suitable for cementing coarse particles and smaller crystals more suitable for fine particles (Xiao *et al.*, 2020; Zheng *et al.*, 2020).

Particle properties have been little studied for their effect on bio-materials (Rahman *et al.*, 2020). There have been some attempts to empirically model the strength of bio-cemented soils, and porosity and particle size have been included, along with $CaCO_3$ content and volume of cementation solution (Cheng & Cord-Ruwisch, 2014; Rahman *et al.*, 2020; Xiao *et al.*, 2019). These particle properties warrant further exploration. However, the D_{10} of the aggregate (the sieve through which only 10% of

the sample grains pass) has been shown to significantly affect the strength of bio-materials (De Oliveira *et al.*, 2021; Rahman & Hora, 2017). From the regression analysis performed by Rahman and Hora (2017), a D_{10} of 150-200 µm resulted in the greatest UCS (6 MPa) with a decreasing trend with increasing D_{10}.

2.3.5 *Calcium carbonate seeding*

In the field of crystallisation, seeding has been shown to have a significant effect on crystal precipitation (Parambil & Heng, 2017). Seeding, the process of adding pre-existing crystals to a reactor, significantly enhances crystal nucleation by increasing the availability of nucleation sites (Mullin, 2001). Crystal nucleation is the initial stage of crystallisation where, in the case of MICP, there is a phase transition from dissolved $CaCO_3$ to crystal nucleus or crystal growth as solid $CaCO_3$ continues to precipitate (Huang *et al.*, 2024). According to nucleation kinetics, this generally occurs spontaneously only when the solution system is in an oversaturated state (saturation index (SI) > 1). Two types of nucleation exist. Homogeneous nucleation, where crystals form from amongst bulk liquid, is rare. Heterogenous nucleation is where crystals form at a surface, at a solid-liquid or gas-liquid interface (Guichet *et al.*, 2019). Surfaces such as gas bubbles, granular particles, bacteria cells and $CaCO_3$ crystals all act as nucleation sites and contribute to the heterogeneous nucleation of $CaCO_3$ crystals, affecting the precipitation process (Zehner *et al.*, 2021).

Heterogenous nucleation lowers the activation energy for nucleation of a crystal and increases the rate of nucleation (Mullin, 2001). In particular, the presence of pre-existing $CaCO_3$ crystals, or seeds, lowers the supersaturation level required for nucleation (Lioliou *et al.*, 2007), where an SI of less than 1 can lead to nucleation. Nanoscale $CaCO_3$ crystals can form on the surface of *S. pasteurii* due to its particularly high negative cell surface charge (Ghosh *et al.*, 2019; Ma *et al.*, 2020). These nanoscale crystals contribute additional surfaces and seeds, and thereby enhance the overall effect of seeding. Although Zehner *et al.* (2021) demonstrated that seeding can affect the MICP process, further research is needed to understand its impact on the properties and strength of the resulting bio-materials.

2.4 Techniques for growing bio-materials with MICP

Microbially induced calcium carbonate precipitation has numerous applications, primarily focused on soil reinforcement and strengthening pre-existing structures rather than creating bio-materials directly. Despite this, MICP has the potential to form bio-materials of any shape by using calcium carbonate ($CaCO_3$) as a bio-cement to bind loose particles within a mould. The production of bio-materials via MICP is complex and influenced by various factors detailed in Section 2.3 and the impacts of the various aspects are neither yet fully understood nor optimised.

The technique used to grow bio-materials depends partly on the type of bio-material desired, which affects the factors and the course of the MICP reaction, ultimately influencing the properties, including the strength, of the bio-material. The type or shape of bio-material is usually selected based on the purpose of the structure, required scale or limitations of the study. Most research has focused on small bio-columns due to their ease of production and ability to measure soil permeability changes with minimal resources and time (Cheng *et al.*, 2013; Henze & Randall, 2018; Xu *et al.*, 2020). More recently, bio-bricks have become a research area of interest (Bu *et al.*, 2018; Cheng *et al.*, 2020; Lambert & Randall, 2019) beyond just the investigation of applying bio-cement to conventional bricks, for purposes such as repairing cracks in conventional bricks (Sarda *et al.*, 2009) and the strengthening of aged bricks (Raut *et al.*, 2014).

The treatment method directly influences the amount of $CaCO_3$ precipitated (Rahman *et al.*, 2020), its properties and distribution, and the scalability of the process.

2.4.1 *Injection technique*

Small bio-columns are typically produced using syringe tubes or other plastic tubes of appropriate size, with a series of injections of cementation solution at regular intervals (Cheng *et al.*, 2013). This technique, while straightforward, has significant drawbacks of needing each of the injections to be administered manually and clogging of pore volumes at the injection site often results in insufficient solidification throughout the material (Cheng & Cord-Ruwisch, 2014; Wang *et al.*, 2022b) and poor utilisation of reagents within (Whiffin et al., 2007).

2.4.2 *Submersion technique*

The submersion technique, developed by Zhao *et al.* (2014a) for bio-columns, offers significant potential for scaling up bio-material production. With this technique, the bio-material is submerged in a well-mixed bio-reactor containing cementation solution (Figure 2.2A). No additional bacteria or reagents are added during the experiment. The inoculated aggregate is packed into a mould, such that its shape and compaction is maintained when submerged. A full contact flexible mould (FCFM) made of permeable geotextile (Figure 2.2B) helps achieve more uniform $CaCO_3$ precipitation due to the large attachable area that prevents clogging (Zhao *et al.*, 2014a). The filled FCFMs are placed on a support shelf in a batch reactor, positioned above magnetic stirrers (Figure 2.2A).

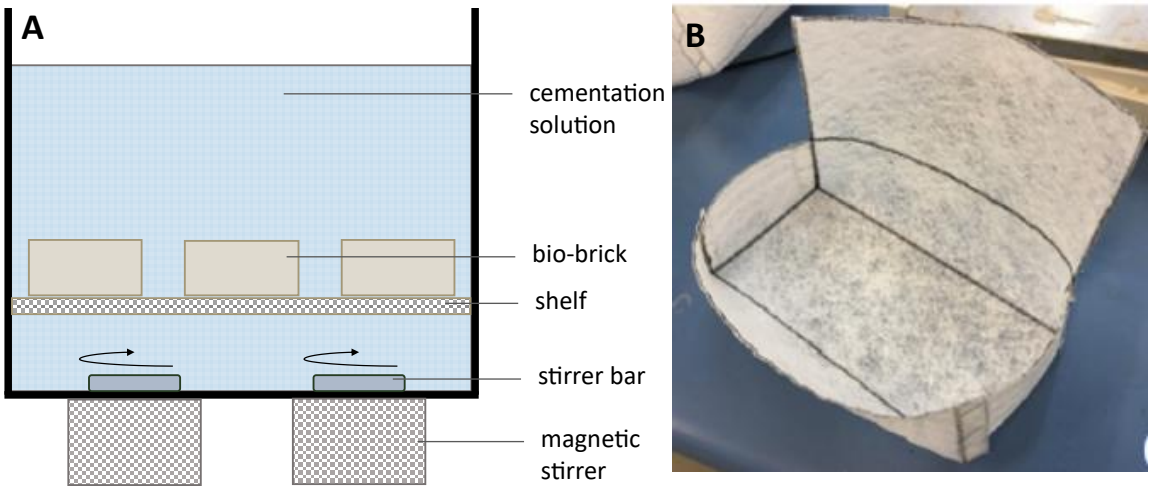

Figure 2.2: Submersion technique bio-reactor (A) and FCFM used to encapsulate the bio-bricks (B) (adapted from Cheng et al. (2020)).

This submersion technique was adapted by Cheng *et al.* (2020) to produce several bio-bricks simultaneously. The MICP reaction within the submerged bio-material is driven by chemical substance diffusion along concentration gradients and drives the cementation solution deeper into the bio-material (Cheng *et al.*, 2020; Zhao *et al.*, 2014b). This method was able to produce a bio-brick with a compressive strength of up to 5.9 MPa, though the centres were 0.8-1 MPa weaker than the sides. The sides have better contact with the cementation solution than the centres, confirming what Bu *et al.* (2018) had reported previously that the bio-material centres had a lower strength. Cheng *et al.* (2020) found that the efficacy of MICP decreased toward the centre of the bio-brick because the cementation solution was primarily consumed by bacteria at the outer edges, depositing $CaCO_3$ which clogs the pores and restricts the diffusion of urea and Ca^{2+} to the inner space. Hence, the manufacturing of a

bio-material that is thinner should allow for more consistent diffusion and compressive strength. This production technique is therefore ideal for a thin bio-material, such as a bio-tile, that would have a minimised inaccessible centre.

2.4.3 *Spraying technique*

The spraying technique essentially periodically sprays cementation solution over the inoculated bio-material and also faces fluid penetration challenges and reduced cementation towards the middle of the body as the volume to be cemented increases (Kim *et al.*, 2022). BioMASON has developed and commercialised a spraying method for producing full bio-bricks with MICP and synthetic urea (Dosier, 2016). They have found that an incremental layering method is advantageous to cementation consistency and strength performance (Dosier, 2016). Spraying is mainly referenced in literature for outdoor applications like soil stabilisation and hardening of unpaved roads (Cheng & Cord-Ruwisch, 2014; Kim *et al.*, 2022). Therefore, the advantages and disadvantages of a spraying technique for growing bio-materials can only be extrapolated. Use of a FCFM is likely as it would ensure the bio-tile maintains its shape and maximises surface area exposure. Periodic spraying of cementation solution could be automated, similar to the pumping technique.

2.4.4 *Pumping technique*

The pumping technique addresses fluid penetration and uneven cementation challenges by periodically pumping cementation solution through a sealed mould system instead of being manually injected. The mould is sealed to avoid ammonia volatilisation (Figure 2.3). An inoculated sand-Greywacke mixture is placed under slight compressive force from above and below using foam, allowing the incoming liquid to be dispersed evenly. This technique was used to grow the first bio-brick (222 x 106 x 73 mm) from human urine by Lambert and Randall (2019) and daily inversion of the bio-brick and swapping of inlet and outlet pipes ensured even cementation of the specimens. The pumping technique has also been used for studying soil reinforcement, where bio-columns are typically used as a proxy for the effect of MICP on soil (typically with a height of about 100 mm and diameter of 48 mm (De Oliveira *et al.*, 2021).

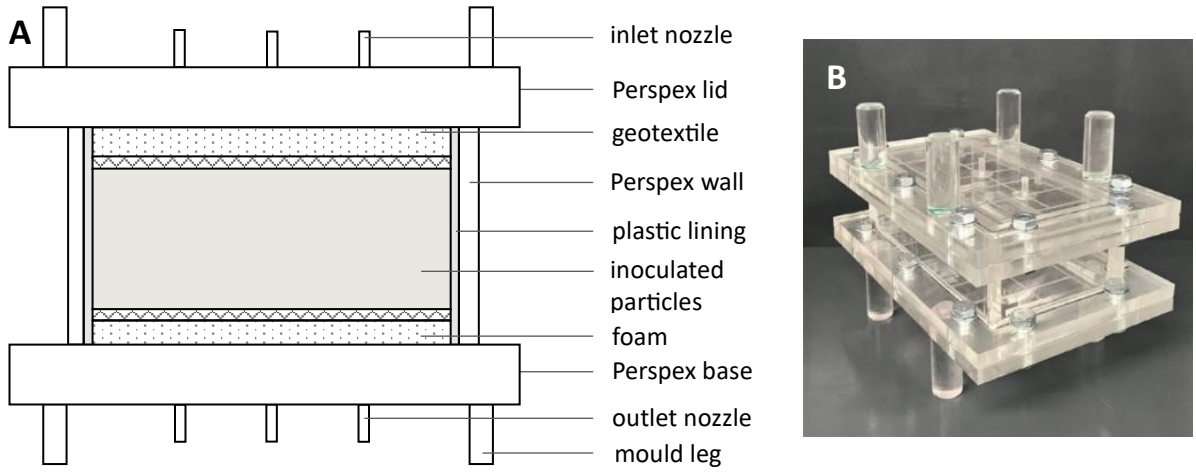

Figure 2.3: Diagram (A) and photo (B) of the Perspex bio-brick mould used by Lambert and Randall (2019). The top and bottom lids are identical and separable, sealed with an O-ring. A layer of geotextile ensured the influent and effluent nozzles were not clogged throughout the process.

Treatment cycles were programmed into an auto-dosing peristaltic pump where every two to four hours fresh cementation solution was pumped through the sealed mould such that the spent solution in the pore space is fully replaced (Lambert & Randall, 2019). As the solution is forced through the

pore space by the pump, it has good contact with the whole matrix of pores, even as precipitate builds up. Another advantage of this technique is that the precipitation is forced to occur inside the closed mould with none occurring externally during each treatment. Over the 4-day experiment duration, Lambert and Randall (2019) were able to achieve very high calcium utilisations of >97% for an influent calcium concentration ranging from 0.09 to 0.13 M and produced a bio-brick with a compressive strength (2.7 MPa) slightly below the minimum standard for non-facing bricks. While this is one of the highest strengths recorded to date (Table 2.3), they reported that the MICP process was inhibited by the inherent high ionic strength of human urine. Using the same system, de Oliveira and Fahn (2019) were able to produce a bio-brick of 16.1 MPa when utilising synthetic urea (0.3 M) and an equimolar amount of calcium, a solution with a much lower ionic strength than one where urine is the source of urea.

2.4.5 *Fully automated techniques*

An automated manufacturing process for MICP applications would offer considerable scalability potential where human intervention is significantly reduced. A fully automated process would add the required amount of sand, smooth and compact it and then solidify it into a bio-material through the addition of cementation solution.

Combining the automation and homogeneous cementation of the pumping technique with the submerging of the bio-material and simple operation of the submersion method, a 3D printing technique could offer a unique opportunity for making an optimised production process that draws on the benefits of each technique. Additive manufacturing technologies also have the potential to be modular and therefore highly scalable. They can also offer a layered approach that overcomes fluid penetration challenges and expands on the options for bio-materials that can be bio-cemented and therefore makes it a good option for an MICP technique to grow bio-materials. Commercialisation revolves around the ability to scale which extends to the ease of operation, to what extent a production process can be automated and ultimately, making the process more economical by increasing throughput. There has been little success with scaling up MICP and even fewer instances reported in literature (Rahman *et al.*, 2020).

Binder jet 3D printers are a type of additive manufacturing machine where a liquid binder (cementation solution in combination with bacteria) is added to loose particles (inoculated/pure sand) to form a solid material (bio-material). Nething *et al.* (2020) successfully automated the production of spatial bio-cemented structures, selectively depositing urease-active sand in a lattice-like pattern amongst pure sand to improve fluid penetration and increase the homogeneity of cementation. The pure sand was removable at the conclusion of the experiment, leaving only the geometrically stable 3D printed product. Small-scale bio-columns were also grown in 20 mL syringe tubes using an automated version of the injection method (Nething *et al.*, 2020) and resulted in compressive strengths of up to 23 MPa. Erdmann *et al.* (2022) instead used a pressurised (0.69 bar) dispensing unit for both bacteria and cementation solutions to prove that a layer of $CaCO_3$ could be printed. The sand was packed and the surface smoothed by hand, and therefore the process was not fully automated. Apart from these instances, the literature on 3D printing using MICP is scarce and there is none to the authors' knowledge on 3D printing construction bio-materials. Although the small bio-columns of Nething *et al.* (2020) are a start, the method does not account for fluid penetration challenges.

2.4.6 *Comparison of techniques*

Each bio-material production technique has potential applications in construction, however each requires refinement for the production of materials that meet international standards, especially when

considering scalability. The advantages and disadvantages of each of these techniques are given in Table 2.4.

Table 2.4: Advantages and disadvantages of the various methods of bio-material manufacturing with MICP.

Production method	Advantages	Disadvantages	Bio-material	Parameters investigated	References
Injection	• Fast (hours-days) • Low resource intensity	• Manual packing and unpacking • Inefficient fluid penetration • Manual	Bio-columns	0.01-0.5 M magnesium	Xu *et al.* (2020)
				Use of urine, pH 11.2	Henze and Randall (2018)
				20 & 100% saturation, fine & coarse sand, freeze-thaw, acid rain resistance	Cheng *et al.* (2013)
Pumping	• Partly automated • Solution forced through pores • Minimal reagent waste	• Manual packing and unpacking • Pipes disconnecting cause leaks • Pipe blockages and pump faults • Needs to be flipped daily	Bio-bricks	Retention time (1, 2, 4h), alternative bacteria nutrients	Lambert and Randall (2019)
			Bio-tiles	Ureolytic activity, retention time (1, 2, 4h), $CaCO_3$ seed mass	This study

Submersion	• Simple operation
	  ○ No leaks
	  ○ No programming
	• Many units in one reactor
		• Manual packing and unpacking
		• Precipitation occurs in the bulk
		• Good mixing crucial
		• Inefficient fluid penetration
			Bio-tiles	Ureolytic activity, particle size, 0.1-1 M calcium, 0.1-0.5 M magnesium, volume	This study

			Bio-bricks	Saturation (50%, 100%), retention time (4-16 days), salt attack, fire resistance	Cheng *et al.* (2020)
			Bio-columns/-bricks	Mould comparison, $CaCO_3$ %	Bu *et al.* (2018)
			Bio-columns	Mould comparison	Zhao *et al.* (2014a)
Spraying	• Partly automated • Simple operation	• Manual packing and unpacking • Inefficient fluid penetration	Bio-bricks/-tiles	-	BioMASON (2022)
			Bio-columns	Bacteria and chemical concentration	Kim *et al.* (2022)
3D printer	• Practically fully automated • Simple operation once running • Modular • Minimal reagent waste	• Specialised personnel required • Design restricted to no metal parts • Complex technology	$CaCO_3$ layer	3D printing technique	Erdmann *et al.* (2022)
			Spatial structure, bio-columns	Fluid penetration, 3D printing techniques	Nething *et al.* (2020)

2.5 Tiles as a choice of bio-material

Cheng *et al.* (2020) observed that the efficacy of MICP with a submersion technique decreases toward the centre of the bio-brick. This was because the cementation solution is primarily consumed by bacteria at the outer edges, clogging these pores with $CaCO_3$ which restricts the diffusion of urea and Ca^{2+} to the inner space. Consequently, the manufacturing of a thinner bio-material should mitigate the nutrient transfer challenges of smaller particles and poor mixing (De Oliveira *et al.*, 2021) because it minimises the inaccessible centre. This method requires significantly less energy compared to conventional tiles. The growth of bio-tiles would allow for the application of multiple MICP techniques more effectively due to their reduced thickness.

Commercial tiles must adhere to various different quality standards. Some of the important standards include maximum deviations in thickness, straightness of sides, rectangularity, surface flatness as well as minimum resistance to surface abrasion, household chemicals, staining, crazing and frost, and finally, maximum moisture expansion and minimum colour resistance to UV light (ISO, 2018). In addition to these specific dimensional and surface quality requirements, tiles are also required to meet certain strength properties.

2.5.1 *International strength standards for tile manufacture*

According to SANS 227 (2007), a conventional non-facing brick must have a UCS of 3-10.5 MPa and this requirement increases for face bricks (9-12.5 MPa). On the other hand, tiles are classed according to type of tile (extruded or dry pressed) and their water absorption (3% < E < 10%) and thickness (>7.5 mm or <7.5 mm) (Table 2.5). Each of these criteria determines their minimum required strength. Instead of UCS, tiles consider breaking strength (200 N < breaking strength < 800 N) and modulus of rupture (MOR) (8 N/mm^2 < MOR < 18 N/mm^2), also known as flexural strength (ISO, 2018). Breaking strength considers the force required to break the tile down the middle, and modulus of rupture further considers the minimum thickness of the tile. Commercially, the thickness of tiles typically ranges between 6-10 mm. Bio-tiles would be more similar to extruded ceramic tiles than dust-pressed tiles in method of manufacture, so tile thickness is not considered in the standard. The MOR equates to the breaking strength divided by the minimum thickness of the tile along the broken tile edge, with a great MOR meaning a high breaking strength and a thin tile. Therefore, methods of increasing this strength must be considered.

Table 2.5: International Organisation of Standards (ISO) tile classification (ISO, 2018).

Tile type	Water absorption (E; %)	Thickness (mm)	Breaking strength (N)	Modulus of rupture (N/mm^2)
Extruded	6% < E < 10%	N/A	≥ 750	≥ 9
	> 10	N/A	≥ 600	≥ 8
Dry pressed	6% < E < 10%	≥7.5	≥ 800	≥ 18
		< 7.5	≥ 500	≥ 18
	> 10	≥7.5	≥ 600	≥ 15
		< 7.5	≥ 200	≥ 12

BioMASON has commercialised the production of bio-tiles with a thickness of 19 mm and bio-bricks using a patented spraying MICP technique. The process differs from approaches applied in literature but also seems to be limited in achieving high strengths as the tiles meet a modulus of rupture standard

of 3.45 MPa (BioMASON, 2022), while conventional tiles commonly are required to exceed a modulus of rupture of 8.0 MPa (ISO, 2018).

Regardless of the benefits achieved with growing a thinner bio-material, new techniques also need to be implemented that increase the compressive strength of these bio-materials. Properties that are more in line with the conventional construction industry's materials will widen their applicability and their positive impact.

2.5.2 *Conventional tile manufacture*

Tiles are generally produced through two processes: ceramic tile manufacture and handmade cement tile manufacture. Both ceramics and cement sectors are considered energy-intensive industries (EIIs) (European Commission, 2019). Ceramics are inert, inorganic, nonmetal materials made from sintered raw-earth resources (Hamood & Khatib, 2016; Hanagadakar & Kulkarni, 2023). These resources commonly consist of clay, feldspar and quartz sand (Hamood & Khatib, 2016) and are made into powders of different sizes, preparation methods and formulations depending on the purpose and forming operation (Francis, 2016). Ceramics encompass a broad range of products and are generally categorised as either traditional or advanced structural ceramics (Figure 2.4).

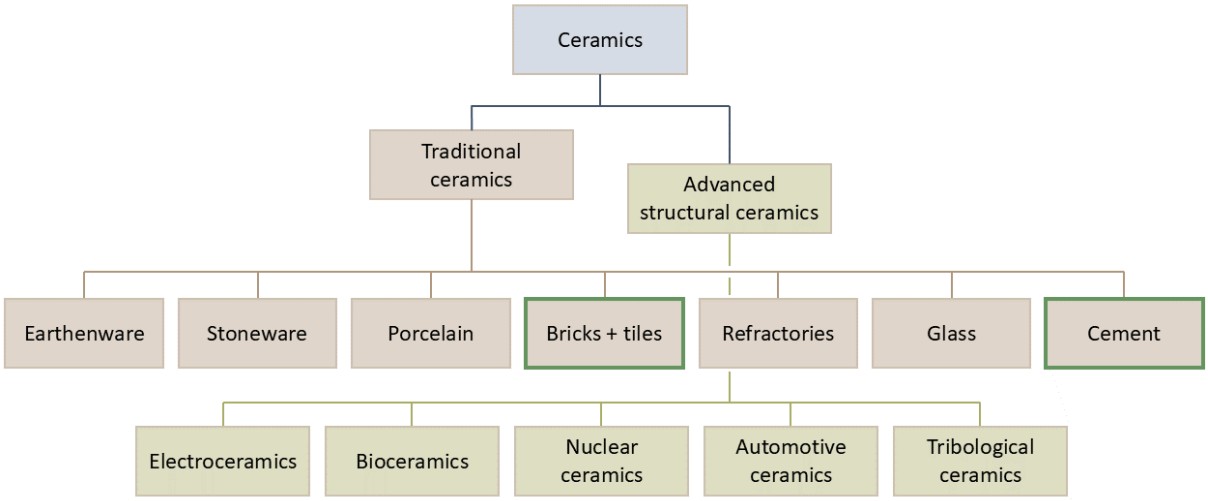

Figure 2.4: Traditional and advanced structural ceramic categories (Melethil & Thomas, 2023).

After the material is formed, it is then usually fired in a kiln at temperatures of up to 1050-1300°C (Melethil & Thomas, 2023). The ceramic tile manufacturing process is energy intensive, with firing and sintering consuming the majority of the energy, at more than 56-60% of the total process energy requirements, atomisation at 30% and drying with 14% (Ciacco *et al.*, 2017). Much of this energy is thermal energy and energy efficiency is considered an issue where about half the energy input to roller kilns is lost to the flue gas and cooling gas stacks of the kilns (Mezquita *et al.*, 2012). Energy costs can constitute up to 30% of total production costs (European Commission, 2019). Globally, much of this energy is sourced from natural gas, although coal is used in South Africa (Ciacco *et al.*, 2017). When coal is the energy source, the flue gas contains substantial amounts of particulate matter, nitrous compounds, oxides and sulphides (Yin & Wang, 2021). The ceramic industry produces more than 1.5 million tons of NO_X, 21.5 million tons of SO_X, and 800,000 tons of dust, heavy metals and other pollutants annually (Yin & Wang, 2021).

Although cement tiles have a global market size about 16 times smaller than ceramic tiles (Data Horizzon Research, 2024; Straits Research, 2023), cement tiles are not insignificant in environmental concern. Cement is an adhesive substance, first developed by the people of Greece as a combination of volcanic ash and lime to bind building blocks (Melethil & Thomas, 2023). Concrete is made by mixing cement with water and an aggregate. The most commonly used cement, Portland cement, was patented in 1824 and in 2016, accounted for more than 98% of concrete usage (Bernal *et al.*, 2016). The primary ingredient in cement is still lime (CaO) or clinker and is produced by calcination of marl or crushed limestone (primarily consisting of $CaCO_3$ and quartz sand) at temperatures of 1400-1450°C using fossil fuels (Melethil & Thomas, 2023; Myhr *et al.*, 2019). The calcination reaction, removing CO_2 from the limestone, usually accounts for over half of the emissions of cement production (Figure 2.5). The low cost, ease of use, flexible properties and general knowledge of this material are the main reasons that there has not been more development of alternative options (Imbabi *et al.*, 2012). The overall process, breakdown of the source of emissions and their possible solutions is shown in Figure 2.5.

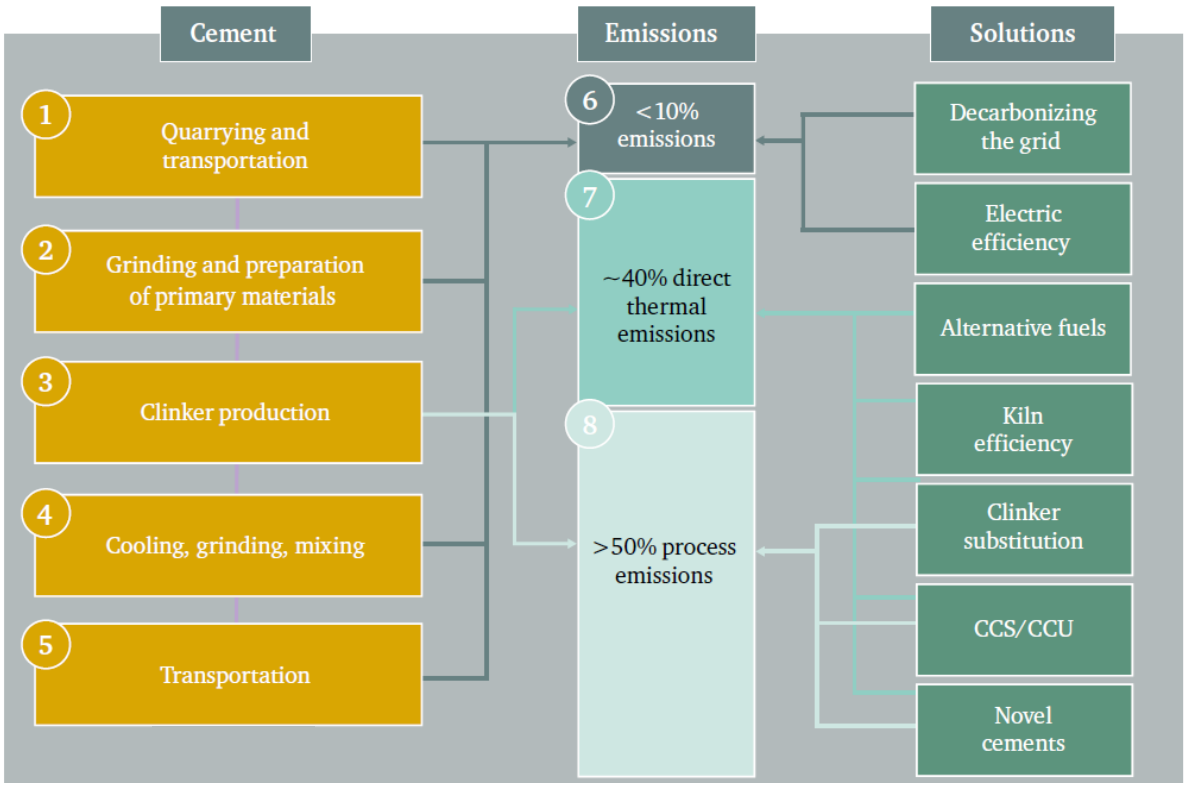

Figure 2.5: An overview of cement production, breakdown of process emissions and possible mitigation interventions (Lehne & Preston, 2018).

Cement tiles are produced using an empirical production process unchanged for over 100 years, involving a hydraulic press and are considered artisanal workmanship (Pires *et al.*, 2022). A cement slab mixture is placed under an iron formwork in two layers. The thicker base layer is a mixture of sand and cement and provides strength. The surface layer is 3-5 mm thick, consists of white cement, fine sand or white marble and pigments, and is responsible for the colour, shine and other resistance properties.

2.6 Enhancing the compressive strength of bio-materials

The primary challenge in the commercialisation of bio-materials produced through MICP is their insufficient strength compared to their conventional counterparts. This is a common occurrence in literature (Bu *et al.*, 2018; Cheng *et al.*, 2020; Lambert & Randall, 2019). Addressing this limitation requires exploring methods to enhance the strength properties of these bio-materials. While increasing the proportion of calcium carbonate ($CaCO_3$) is a known strategy for improving UCS (Al Qabany & Soga, 2013; Choi *et al.*, 2017; van Paassen *et al.*, 2010), this alone is insufficient.

2.6.1 *Selecting for calcium carbonate polymorphs*

The crystals of $CaCO_3$ can take the form of different polymorphs, each with distinct properties. Calcite, the most thermodynamically stable polymorph of $CaCO_3$, is the predominant product in MICP reactions, followed by vaterite and amorphous calcium carbonate (ACC) (Stocks-Fischer *et al.*, 1999; Seifan and Berenjian, 2018). Technically, ACC is not a crystalline structure. There are three non-hydrated crystal polymorphs of $CaCO_3$, namely calcite, vaterite and aragonite (Li *et al.*, 2013). Each polymorph has a different structure, density, hardness and solubility characteristics (Table 2.6). Aragonite, notable for the greatest density (2.95 g/cm^3) and Mohs hardness (3.5-4) of all the polymorphs (Xu *et al.*, 2020), offers superior mechanical properties.

Table 2.6: Properties of the three non-hydrated and two hydrated calcium carbonate crystal polymorphs (Morse & Mackenzie, 1990; Xu et al., 2020).

Mineral	Crystal shape	Density (g/cm^3)	Hardness (Mohs)	Solubility (-log K_{sp})
Calcite	Rhombic	2.71	3	8.48
Vaterite	Hexagonal	2.54	3	7.91
Aragonite	Orthorhombic	2.93	3.5-4	8.34
Monohydrocalcite ($CaCO_3 \cdot H_2O$)	Trigonal	2.43	2-3	7.60
Ikaite ($CaCO_3 \cdot 6H_2O$)	Monoclinic	1.77	3	7.12

The polymorphs that form when $CaCO_3$ crystallises and their sizes have been shown to be influenced by various factors, such as retention time, gentle to vigorous stirring speeds (Sand *et al.*, 2012; Anbu *et al.*, 2016), urea hydrolysis rate and surface area available for crystal growth (Kim *et al.*, 2020; Van Paassen, 2009). The choice of calcium source is also significant: calcium chloride favours the formation of calcite (Chen *et al.*, 2006; Anbu *et al.*, 2016), while calcium lactate and calcium gluconate favour vaterite formation (Anbu *et al.*, 2016), and calcium acetate promotes the formation of aragonite (Chen *et al.*, 2006; Zhang *et al.*, 2015). Additionally, the composition of the growth media or microbial culture may also influence the polymorph present (De Muynck *et al.*, 2008; Anbu *et al.*, 2016).

Finally, magnesium ions enhance the utilisation rate of Ca^{2+} ions to precipitate more $CaCO_3$ between particles and promote aragonite precipitation over calcite (Bischoff, 1968; Xu *et al.*, 2020). As Xu *et al.* (2020) explain, this preference for aragonite over calcite is due to the differences in crystal structure and the size of Mg^{2+} and Ca^{2+} ions. Mg^{2+} cations are smaller than Ca^{2+}, and while it can substitute into the calcite lattice to form magnesium calcite, magnesium calcite has a relatively higher solubility than pure calcite, resulting in a lower driving force for the crystallisation of both overall (Lippmann, 2012). In contrast, aragonite does not accommodate Mg^{2+} due to its denser coordination—Ca^{2+} in aragonite is bonded to nine oxygen atoms, compared to six in calcite. The weaker bonds formed by Mg^{2+} in

aragonite lead to its expulsion, preventing substitution (Lippmann, 2012). As a result, calcite formation is hindered while aragonite formation proceeds, favouring aragonite precipitation.

Zhang *et al.* (2015) and Putra *et al.* (2016) found that the prevalence of aragonite instead of calcite could result in an improvement in the strength properties of bio-materials. Xu *et al.* (2020) reported that Mg^{2+} ions improved the compressive strength of bio-columns by 40%, however, magnesium ions in excess of 0.5 M caused the precipitation of magnesium carbonate, reducing compressive strength (Gawwad *et al.*, 2016). Although $MgCO_3$ has a Mohs hardness of 3.5–4.5, Xu *et al.* (2020) identified that its presence in cemented structures did not yield favourable results, particularly when formed using $MgCl_2$/urea cementation solution. Nonetheless, concentrations of 0.1-0.5 M $MgCl_2$ remain beneficial. Concentrations as high as 0.5 M $MgCl_2$ are still favourable because in the initial stage of MICP, cations like Mg^{2+} and Ca^{2+} will be bonded by water dipoles, and need to dehydrate to bond with CO_3^{2-}. Calcium has a lower hydration enthalpy than magnesium and therefore will more easily attract CO_3^{2-} and favour the precipitation of $CaCO_3$ over $MgCO_3$ (Lippmann, 2012).

2.6.2 *Pore volume saturation with inoculum and cementation solution*

Cheng and Cord-Ruwisch (2012) identified the significance of pore volume saturation in improving the strength of bio-columns. Treating sand columns by injection at low saturation levels (50% pore volume saturation) yielded higher strength compared to treatments at full saturation, despite similar $CaCO_3$ levels. This is due to the distribution of crystals being more restricted to interparticle contact points. Further studies by Cheng *et al.* (2013) confirmed that when the pore volume was 100% saturated by bacterial solution and then by cementation solution treatments, not only did agglomerated crystals precipitate at the interparticle contact points, but also on the whole sand grain surface as well as being suspended in the pore spaces between the grains. Whereas 20% saturation produced a strong coating effect of the grains, likely due to surface tension, allowing the solution to be homogeneously absorbed and access only the full surface of the grains. This phenomenon is conceptualised in Figure 2.6.

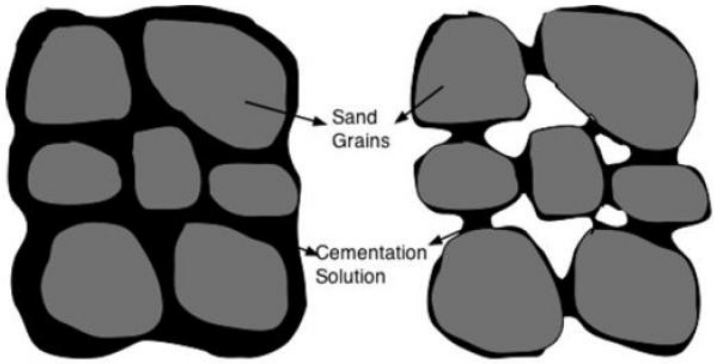

Figure 2.6: Conceptual illustration of the distribution of cementation solution in the sand matrix under different saturation conditions.

In this case, samples treated at 100% and 20% saturation demonstrated similar UCS at 1 and 1.14 MPa, respectively, while the 20% saturation sample had less than half the amount of precipitated $CaCO_3$ crystals. This definitively indicates that the strength of bio-materials is strongly associated with the effectiveness of the formed $CaCO_3$ to hold the grains together, rather than only the mass of $CaCO_3$ in the sample.

This was also illustrated in bio-bricks, where bio-bricks treated at 50% pore volume saturation demonstrated almost twice the strength of those treated at full saturation for the same $CaCO_3$ content (Cheng *et al.*, 2020). The production of bio-bricks has previously been performed under fully saturated conditions by pumping (Lambert & Randall, 2019), surface percolation (Bernardi *et al.*, 2014) and submergence (Bu *et al.*, 2018). Therefore, partial saturation during MICP could enhance the spatial distribution and efficacy of precipitated $CaCO_3$ in each of these techniques, improving the bio-materials' strength and economic viability (Cheng *et al.*, 2020).

2.6.3 *Other potential additives to improve strength properties*

Beyond magnesium (Section 2.6.1), various substances can be added to the cementation solution to enhance bio-material strength. Biopolymers have been investigated for this purpose, including xanthan gum, guar gum, inert polyol-cellulose hydrogels and gelatine (Ahenkorah *et al.*, 2021). These additives increase the cementation solution's viscosity and are thought to concentrate precipitation to the contact points between particles (Hamdan, 2015), similar to the coating effect of partial saturation conditions (Section 2.6.2). Hydrogels can reduce the production of ammonia and CO_2 when using EICP processes, without adverse effects on $CaCO_3$ precipitation (Ahenkorah *et al.*, 2021; Hamdan, 2015).

Biopolymers have shown promising results: xanthan and guar gum additives improved UCS (Dikshit *et al.*, 2021; Hamdan *et al.*, 2016) and formed a thick polymer layer on sand particles that was not easy to remove (Hamdan, 2015). Gelatine, when combined with inoculum and mixed into sand, produced bio-materials with UCS of around 12 MPa and provided self-healing properties (Wang *et al.*, 2022a). Like gelatine, chitosan is also an inexpensive biopolymer and enhances cementation and strength by absorbing Ca^{2+} ions into the hydrogel, accelerating nucleation and forming interparticle bridges, although excessive chitosan could distort crystal shape and lead to agglomerates (Nawarathna *et al.*, 2019).

Other substances like dried non-fat milk have been investigated as a stabiliser in EICP cementation solution (Almajed, 2017; Almajed *et al.*, 2019; Nemati & Voordouw, 2003). Supplementing at 4 g/L improved UCS almost 13-fold to 1.6-1.8 MPa at a very low $CaCO_3$ content (less than 1%), once again through the preferential formation of $CaCO_3$ at the interparticle contact points (Almajed *et al.*, 2019). This improvement is understood to be from the stabilisation of the enzyme and additional nucleation sites for $CaCO_3$ precipitation.

Some researchers have added nutrient broth to the cementation solution to support the metabolism and rapid growth of the bacteria during MICP (Feng *et al.*, 2021; Rittmann *et al.*, 2011; Wen *et al.*, 2020) which can increase urease production (Chuo *et al.*, 2020). Lambert and Randall (2019) found that nutrient broth was the most expensive input when manufacturing bio-bricks, so ideally nutrient broth is not used for every treatment during the MICP process. It has also been found that the addition of nutrient broth can severely affect the compressive strength of bio-materials produced with a submersion technique (De Oliveira *et al.*, 2021).

Furthermore, the inclusion of fibres in particle mixtures has been explored to enhance UCS. Li *et al.* (2020) found that adding 3 wt% of polypropylene or natural coconut fibres improved strength by 50-70%, with synthetic fibres outperforming the coconut fibre. Another study found a four-fold increase in strength with optimal natural sisal fibre ratio and length (Almajed, 2017).

While these additives are effective at improving mechanical properties of bio-materials, they could also offer other benefits for scalability and broader applications. For example, Dikshit *et al.* (2021) found a nearly 6-fold improvement in UCS when using guar gum but when supplementing with chopped glass fibre, a structural reinforcement material, although the strength was lowered slightly, it

made the bio-material more tough. This toughening effect allows the material to withstand greater amounts of strain and be machinable on a conventional lathe, enabling the precise fabrication of free-form shapes, without the need for shape-specific moulds. Therefore, glass fibres make MICP an even more attractive process for producing structures in resource-poor environments, such as extra-terrestrial habitats. In addition, enhancement with additives may lead to reduced bacteria, urea and Ca^{2+} requirements (Ahenkorah *et al.*, 2021). Therefore, the MICP or EICP process has the potential to be more financially viable, more technically feasible and more sustainable when employing additive strategies.

2.7 Problem statement

The exploration of MICP as a method for developing bio-materials presents significant potential for sustainable construction solutions. However, a key challenge of producing bio-materials with MICP is achieving the necessary strength to compete with conventional construction materials. Multiple factors affect MICP, including the urease activity, reagent concentration and resulting ionic strength, choice of $CaCO_3$ polymorph, potential cementation solution supplements and retention time, and offer the potential for varying mechanical properties. Bio-materials produced with MICP often face challenges of pore clogging and fluid penetration that can hinder the uniform distribution of $CaCO_3$. By focusing on the production of a thinner bio-material, bio-tiles, the nutrient transfer limitations and mixing inefficiencies associated with larger bio-materials can be minimised. Achieving bio-tiles with adequate strength properties, particularly in terms of breaking strength and modulus of rupture, is the first step in establishing the proof of concept of the viability of bio-tiles. Therefore, while MICP presents a promising technology for construction materials with a minimised environmental impact, there is a need for targeted research into optimising the factors that influence the strength of bio-materials. Focusing on the production of bio-tiles could offer a sustainable alternative to conventional tiles in the marketplace and pave the way for the broader adoption of MICP in the construction industry, provided the first hurdle of sufficient strength can be crossed.

References

V. Achal & X. Pan. 2014. Influence of calcium sources on microbially Induced calcium carbonate precipitation by *Bacillus* sp. CR2. *Applied biochemistry and biotechnology.* 173(1):307-317. DOI:10.1007/s12010-014-0842-1.

V. Achal, X. Pan & D. Zhang. 2011a. Remediation of copper-contaminated soil by *Kocuria flava* CR1, based on microbially induced calcite precipitation. *Ecological Engineering.* 37(10):1601-1605. DOI:10.1016/j.ecoleng.2011.06.008.

V. Achal, X. Pan & N. Özyurt. 2011b. Improved strength and durability of fly ash-amended concrete by microbial calcite precipitation. *Ecological Engineering.* 37(4):554-559. DOI:10.1016/j.ecoleng.2010.11.009.

V. Achal, A. Mukherjee, P.C. Basu & M.S. Reddy. 2009. Strain improvement of Sporosarcina pasteurii for enhanced urease and calcite production. *Journal of Industrial Microbiology and Biotechnology.* 36(7):981-988. DOI:10.1007/s10295-009-0578-z.

V. Achal, X. Pan, D.-J. Lee, D. Kumari & D. Zhang. 2013. Remediation of Cr(VI) from chromium slag by biocementation. *Chemosphere (Oxford).* 93(7):1352-1358. DOI:10.1016/j.chemosphere.2013.08.008.

I. Ahenkorah, M.M. Rahman, M.R. Karim & S. Beecham. 2021. Enzyme induced calcium carbonate precipitation and its engineering application: A systematic review and meta-analysis. *Construction & Building Materials.* 308:125000. DOI:10.1016/j.conbuildmat.2021.125000.

A. Al Qabany & K. Soga. 2013. Effect of chemical treatment used in MICP on engineering properties of cemented soils. *Geotechnique.* 63(4):331-339. DOI:10.1680/geot.SIP13.P.022.

A. Almajed. 2017. Enzyme induced carbonate precipitation (EICP) for soil improvement Arizona State University.

A. Almajed, H.K. Tirkolaei, E. Kavazanjian & N. Hamdan. 2019. Enzyme induced biocementated sand with high strength at low carbonate content. *Scientific Reports.* 9(1):1135-1135. DOI:10.1038/s41598-018-38361-1.

P. Anbu, C.H. Kang, Y.J. Shin & J.S. So. 2016. Formations of calcium carbonate minerals by bacteria and its multiple applications. *SpringerPlus.* 5:1-26. DOI:10.1186/s40064-016-1869-2.

M.S. Ashraf, M.U. Hassan Shah, A. Bokhari & M. Hasan. 2021. Less is more: Optimising the biocementation of coastal sands by reducing influent urea through response surface method. *Journal of Cleaner Production.* 315:128208. DOI:10.1016/j.jclepro.2021.128208.

M. Bendixen, L.L. Iversen, J. Best, D.M. Franks, C.R. Hackney, E.M. Latrubesse & L.S. Tusting. 2021. Sand, gravel, and UN Sustainable Development Goals: Conflicts, synergies, and pathways forward. *One Earth.* 4(8):1095-1111. DOI:10.1016/j.oneear.2021.07.008.

S.A. Bernal, E.D. Rodríguez, A.P. Kirchheim & J.L. Provis. 2016. Management and valorisation of wastes through use in producing alkali-activated cement materials. *Journal of chemical technology and biotechnology (1986).* 91(9):2365-2388. DOI:10.1002/jctb.4927.

D. Bernardi, J.T. Dejong, B.M. Montoya & B.C. Martinez. 2014. Bio-bricks: Biologically cemented sandstone bricks. *Construction and Building Materials.* 55:462-469. DOI:10.1016/j.conbuildmat.2014.01.019.

BioMASON. 2022. *BioLITH, Material Performance*. Available: https://biomason.com/biolith/ [2022, 11 March].

E. Boquet, A. Boronat & A. Ramos-Cormenzana. 1973. Production of Calcite (Calcium Carbonate) Crystals by Soil Bacteria is a General Phenomenon. *Nature.* 246(5434):527-529. DOI:10.1038/246527a0.

C. Bu, K. Wen, S. Liu, U. Ogbonnaya & L. Li. 2018. Development of bio-cemented constructional materials through microbial induced calcite precipitation. *Materials and Structures/Materiaux et Constructions.* 51(30):1-11. DOI:10.1617/s11527-018-1157-4.

M.J. Castro-Alonso, L.E. Montañez-Hernandez, M.A. Sanchez-Muñoz, M.R. Macias Franco, R. Narayanasamy & N. Balagurusamy. 2019. Microbially induced calcium carbonate crecipitation (MICP) and its potential in bioconcrete: microbiological and molecular concepts. *Frontiers in Materials.* 6. DOI:10.3389/fmats.2019.00126.

N. Chahal, R. Siddique & A. Rajor. 2012. Influence of bacteria on the compressive strength, water absorption and rapid chloride permeability of fly ash concrete. *Construction & building materials.* 28(1):351-356. DOI:10.1016/j.conbuildmat.2011.07.042.

Y. Chen, S. Wang, X. Tong & X. Kang. 2022. Towards the sustainable fine control of microbially induced calcium carbonate precipitation. *Journal of Cleaner Production.* 377:134395. DOI:10.1016/j.jclepro.2022.134395.

L. Cheng & R. Cord-Ruwisch. 2012. In situ soil cementation with ureolytic bacteria by surface percolation. *Ecological Engineering.* 42:64-72. DOI:10.1016/j.ecoleng.2012.01.013.

L. Cheng & R. Cord-Ruwisch. 2014. Upscaling effects of soil improvement by microbially induced calcite precipitation by surface percolation. *Geomicrobiology Journal.* 31(5):396-406. DOI:10.1080/01490451.2013.836579.

L. Cheng, R. Cord-Ruwisch & M.A. Shahin. 2013. Cementation of sand soil by microbially induced calcite precipitation at various degrees of saturation. *Canadian Geotechnical Journal.* 50(1):81-90. DOI:10.1139/cgj-2012-0023.

L. Cheng, M.A. Shahin & D. Mujah. 2017. Influence of key environmental conditions on microbially induced cementation for soil stabilization. *Journal of Geotechnical and Geoenvironmental Engineering.* 143(1). DOI:10.1061/(ASCE)GT.1943-5606.0001586.

L. Cheng, T. Kobayashi & M.A. Shahin. 2020. Microbially induced calcite precipitation for production of “bio-bricks” treated at partial saturation condition. *Construction and Building Materials.* 231(117095):1-9. DOI:10.1016/j.conbuildmat.2019.117095.

S. Choi, K. Wang & J. Chu. 2016. Properties of biocemented, fiber reinforced sand. *Construction & building materials.* 120:623-629. DOI:10.1016/j.conbuildmat.2016.05.124.

S. Choi, J. Chu, R.C. Brown, K. Wang & Z. Wen. 2017. Sustainable biocement production via microbially induced calcium carbonate precipitation: use of limestone and acetic acid derived from pyrolysis of lignocellulosic biomass. *ACS Sustainable Chemistry and Engineering.* 5(6):5183-5190. DOI:10.1021/acssuschemeng.7b00521.

Q. Chunxiang, W. Jianyun, W. Ruixing & C. Liang. 2009. Corrosion protection of cement-based building materials by surface deposition of CaCO3 by *Bacillus pasteurii*. *Materials Science and Engineering: C.* 29(4):1273-1280. DOI:10.1016/j.msec.2008.10.025.

S.C. Chuo, S.F. Mohamed, S.H.M. Setapar, A. Ahmad, M. Jawaid, W.A. Wani, A.A. Yaqoob & M.N.M. Ibrahim. 2020. Insights into the current trends in the utilization of bacteria for microbially induced calcium carbonate precipitation. *Materials.* 13(21):1-28. DOI:10.3390/ma13214993.

E.F.S. Ciacco, J.R. Rocha & A.R. Coutinho. 2017. The energy consumption in the ceramic tile industry in Brazil. *Applied Thermal Engineering.* 113:1283-1289. DOI:10.1016/j.applthermaleng.2016.11.068.

A.B. Cunningham, R. Gerlach, L. Spangler & A.C. Mitchell. 2009. Microbially enhanced geologic containment of sequestered supercritical CO2. *Energy Procedia.* 1(1):3245-3252. DOI:https://doi.org/10.1016/j.egypro.2009.02.109.

A.B. Cunningham, R. Gerlach, L. Spangler, A.C. Mitchell, S. Parks & A. Phillips. 2011. Reducing the risk of well bore leakage of CO2 using engineered biomineralization barriers. *Energy Procedia.* 4:5178-5185. DOI:https://doi.org/10.1016/j.egypro.2011.02.495.

M.O. Cuthbert, M.S. Riley, S. Handley-Sidhu, J.C. Renshaw, D.J. Tobler, V.R. Phoenix & R. Mackay. 2012. Controls on the rate of ureolysis and the morphology of carbonate precipitated by *S. Pasteurii* biofilms and limits due to bacterial encapsulation. *Ecological Engineering.* 41:32-40. DOI:10.1016/j.ecoleng.2012.01.008.

Data Horizzon Research. 2024. *Chemicals and Materials - Cement tiles market research report. Report code: DHR3048*. Fort Collins, United States.

W. De Muynck, N. De Belie & W. Verstraete. 2010. Microbial carbonate precipitation in construction materials: A review. *Ecological Engineering.* 36(2):118-136. DOI:10.1016/j.ecoleng.2009.02.006.

D. De Oliveira, E.J. Horn & D.G. Randall. 2021. Copper mine tailings valorization using microbial induced calcium carbonate precipitation. *Journal of Environmental Management.* 298:113440. DOI:10.1016/j.jenvman.2021.113440.

J.T. DeJong, M.B. Fritzges & K. Nüsslein. 2006. Microbially induced cementation to control sand response to undrained shear. *Journal of Geotechnical and Geoenvironmental Engineering.* 132(11):1381-1392. DOI:10.1061/(ASCE)1090-0241(2006)132:11(1381).

S. Delong & T. Liyan. 2014. *Production method for calcium chloride dihydrate.* China: Ningbo new materials Limited by Share Ltd.

N.K. Dhami, M.S. Reddy & A. Mukherjee. 2012. Improvement in strength properties of ash bricks by bacterial calcite. *Ecological Engineering.* 39:31-35. DOI:10.1016/j.ecoleng.2011.11.011.

N.K. Dhami, M.S. Reddy & A. Mukherjee. 2013. Biomineralization of calcium carbonate polymorphs by the bacterial strains isolated from calcareous sites. *Journal of Microbiology and Biotechnology.* 23(5):707-714.

R. Dikshit, N. Gupta, A. Dey, K. Viswanathan & A. Kumar. 2022. Microbial induced calcite precipitation can consolidate martian and lunar regolith simulants. *PLOS ONE.* 17(4):e0266415-e0266415. DOI:10.1371/journal.pone.0266415.

R. Dikshit, A. Dey, N. Gupta, S.C. Varma, I. Venugopal, K. Viswanathan & A. Kumar. 2021. Space bricks: From LSS to machinable structures via MICP. *Ceramics international.* 47(10):14892-14898. DOI:10.1016/j.ceramint.2020.07.309.

G.K. Dosier. 2016. *Production of masonry with bacteria. Patent number: US9796626B2.* US: BioMason Inc.

N. Erdmann, F. Kästner, K. De Payrebrune & D. Strieth. 2022. *Sporosarcina pasteurii* can be used to print a layer of calcium carbonate. *Engineering in Life Sciences.* 22(12):760-768. DOI:10.1002/elsc.202100074.

Y.C. Ersan, N. Boon & N. De Belie. Eds. 2015. Microbial self-healing concrete: denitrification as an enhanced and environment-friendly apporach. Ghent, 2015. Duke University.

European Commission. 2019. *Making ceramic tile production greener with reused heat*. European Commission, CORDIS. Available: https://cordis.europa.eu/article/id/411496-making-ceramic-tile-production-greener-with-reused-heat [2024, 5 August].

C. Feng, B. Cui, H. Ge, Y. Huang, W. Zhang & J. Zhu. 2021. Reinforcement of recycled aggregate by microbial-induced mineralization and deposition of calcium carbonate—influencing factors, mechanism and effect of reinforcement. *Crystals (Basel).* 11(8):887. DOI:10.3390/cryst11080887.

F.G. Ferris, V. Phoenix, Y. Fujita & R.W. Smith. 2004. Kinetics of calcite precipitation induced by ureolytic bacteria at 10 to 20°C in artificial groundwater. *Geochimica et Cosmochimica Acta.* 68(8):1701-1710. DOI:10.1016/S0016-7037(03)00503-9.

C.P. Flanagan & D.G. Randall. 2018. Development of a novel nutrient recovery urinal for on-site fertilizer production. *Journal of Environmental Chemical Engineering.* 6(5):6344-6350. DOI:10.1016/j.jece.2018.09.060.

L.F. Francis. 2016. Chapter 1 - Introduction to Materials Processing. In *Materials Processing.* L.F. Francis, Ed. Boston: Academic Press. 1-20. DOI:https://doi.org/10.1016/B978-0-12-385132-1.00001-X.

D. Gat, M. Tsesarsky, D. Shamir & Z. Ronen. 2014. Accelerated microbial-induced CaCO3 precipitation in a defined coculture of ureolytic and non-ureolytic bacteria. *Biogeosciences.* 11:2561-2569. DOI:10.5194/bg-11-2561-2014.

H.A. Gawwad, S.A.E.-A. Mohamed & S.A. Mohammed. 2016. Impact of magnesium chloride on the mechanical properties of innovative bio-mortar. *Materials Letters.* 178:39-43. DOI:10.1016/j.matlet.2016.04.190.

T. Ghosh, S. Bhaduri, C. Montemagno & A. Kumar. 2019. *Sporosarcina pasteurii* can form nanoscale calcium carbonate crystals on cell surface. *PLOS ONE.* 14(1):1-15. DOI:10.1371/journal.pone.0210339.

C.M. Gorospe, S.H. Han, S.G. Kim, J.Y. Park, C.H. Kang, J.H. Jeong & J.S. So. 2013. Effects of different calcium salts on calcium carbonate crystal formation by *Sporosarcina pasteurii* KCTC 3558. *Biotechnology and Bioprocess Engineering.* 18(5):903-908. DOI:10.1007/s12257-013-0030-0.

S. Gowthaman, M. Yamamoto, K. Nakashima, V. Ivanov & S. Kawasaki. 2021. Calcium phosphate biocement using bone meal and acid urease: An eco-friendly approach for soil improvement. *Journal of Cleaner Production.* 319:128782. DOI:10.1016/j.jclepro.2021.128782.

M. Grabarek, W. Tabor, P. Krzyżek, A. Grabowiecka, Ł. Berlicki & A. Mucha. 2025. Halogenated N-Benzylbenzisoselenazolones Efficiently Inhibit *Helicobacter pylori* Ureolysis In Vitro. *ACS medicinal chemistry letters.* 16(4):675-680. DOI:10.1021/acsmedchemlett.5c00057.

V. Guichet, S. Almahmoud & H. Jouhara. 2019. Nucleate pool boiling heat transfer in wickless heat pipes (two-phase closed thermosyphons): A critical review of correlations. *Thermal Science and Engineering Progress.* 13:100384. DOI:https://doi.org/10.1016/j.tsep.2019.100384.

C.R. Hackney, G. Vasilopoulos, S. Heng, V. Darbari, S. Walker & D.R. Parsons. 2021. Sand mining far outpaces natural supply in a large alluvial river. *Earth surface dynamics.* 9(5):1323-1334. DOI:10.5194/esurf-9-1323-2021.

N. Hamdan. 2015. Applications of enzyme induced carbonate precipitation (EICP) for soil improvement. Arizona State University.

N. Hamdan & E. Kavazanjian. 2016. Enzyme-induced carbonate mineral precipitation for fugitive dust control. *Geotechnique.* 66(7):546-555. DOI:10.1680/jgeot.15.P.168.

N. Hamdan, E. Kavazanjian, B.E. Rittmann & I. Karatas. 2017. Carbonate mineral precipitation for soil improvement through microbial denitrification. *Geomicrobiology Journal.* 34(2):139-146. DOI:10.1080/01490451.2016.1154117.

N. Hamdan, Z. Zhao, M. Mujica, E. Kavazanjian & X. He. 2016. Hydrogel-assisted enzyme-induced carbonate mineral precipitation. *Journal of Materials in Civil Engineering.* 28(10). DOI:10.1061/(ASCE)MT.1943-5533.0001604.

F. Hammes & W. Verstraete. 2002. Key roles of pH and calcium metabolism in microbial carbonate precipitation. *Reviews in Environmental Science and Biotechnology.* 1(1):3-7. DOI:10.1023/A:1015135629155.

A. Hamood & J.M. Khatib. 2016. 24 - Sustainability of sewage sludge in construction. In *Sustainability of Construction Materials (Second Edition).* J.M. Khatib, Ed.: Woodhead Publishing. 625-641. DOI:https://doi.org/10.1016/B978-0-08-100370-1.00024-X.

M.S. Hanagadakar & R.M. Kulkarni. 2023. 20 - Environmental impacts and benefits of ceramic coatings. In *Advanced Ceramic Coatings.* R.K. Gupta, A. Motallebzadeh, S. Kakooei, T.A. Nguyen and A. Behera, Eds.: Elsevier. 461-487. DOI:https://doi.org/10.1016/B978-0-323-99659-4.00019-X.

J. Henze & D.G. Randall. 2018. Microbial induced calcium carbonate precipitation at elevated pH values (>11) using *Sporosarcina pasteurii*. *Journal of Environmental Chemical Engineering.* 6:5008-5013. DOI:10.1016/j.jece.2018.07.046.

C. Höglund. 2001. *Evaluation of microbial health risks associated with the reuse of source-separated human urine.* Stockholm, Sweden.

X. Huang, J. Zhang & L. Zhang. 2024. Accelerated carbonation of steel slag: A review of methods, mechanisms and influencing factors. *Construction & building materials.* 411:134603. DOI:10.1016/j.conbuildmat.2023.134603.

Y.H. Huang, H.J. Chen, J.P. Maity, C.C. Chen, A.C. Sun & C.Y. Chen. 2020. Efficient option of industrial wastewater resources in cement mortar application with river-sand by microbial induced calcium carbonate precipitation. *Scientific Reports.* 10(1):6742. DOI:10.1038/s41598-020-62666-9.

M.S. Imbabi, C. Carrigan & S. McKenna. 2012. Trends and developments in green cement and concrete technology. *International Journal of Sustainable Built Environment.* 1(2):194-216. DOI:https://doi.org/10.1016/j.ijsbe.2013.05.001.

ISO. 2018. *ISO 13006:2018: Ceramic tiles - definitions, classification, characteristics and marking*. Available: https://www.iso.org/standard/63406.html.

H.M. Jonkers, A. Thijssen, G. Muyzer, O. Copuroglu & E. Schlangen. 2010. Application of bacteria as self-healing agent for the development of sustainable concrete. *Ecological Engineering.* 36(2):230-235. DOI:10.1016/j.ecoleng.2008.12.036.

M. Joseph, L. Boehme, Z. Sierens & L. Vandewalle. 2015. Water absorption variability of recycled concrete aggregates. *Magazine of concrete research.* 67(11):592-597. DOI:10.1680/macr.14.00210.

M. Kahani, F. Kalantary, M.R. Soudi, L. Pakdel & S. Aghaalizadeh. 2020. Optimization of cost effective culture medium for *Sporosarcina pasteurii* as biocementing agent using response surface methodology: Up cycling dairy waste and seawater. *Journal of Cleaner Production.* 253(120022):1-10. DOI:10.1016/j.jclepro.2020.120022.

H.A. Keykha, A. Asadi & M. Zareian. 2017. Environmental factors affecting the compressive strength of microbiologically induced calcite precipitation-treated soil. *Geomicrobiology Journal.* 34(10):889-894. DOI:10.1080/01490451.2017.1291772.

D.M. Kiefer. 2002. Soda Ash, Solvay Style. *Today's Chemist at Work.* 11(2):87–88.

D.H. Kim, N. Mahabadi, J. Jang & L.A.v. Paassen. 2020. Assessing the Kinetics and Pore-Scale Characteristics of Biological Calcium Carbonate Precipitation in Porous Media using a Microfluidic Chip Experiment. *Water Resources Research.* 56(e2019WR02542):1-19. DOI:10.1029/2019WR025420.

S. Kim, Y. Kim, S. Lee & J. Do. 2022. Preliminary Study on Application and Limitation of Microbially Induced Carbonate Precipitation to Improve Unpaved Road in Lateritic Region. *Materials.* 15(7219):1-15. DOI:10.3390/ma15207219.

G.B. Kistiakowsky & W.H.R. Shaw. 1953. Ureolytic activity of urease at pH 8.9. *Journal of the American Chemical Society.* 75(11):2751-2754. DOI:10.1021/ja01107a061.

D. Kumari, X.-Y. Qian, X. Pan, V. Achal, Q. Li & G.M. Gadd. 2016. Microbially-induced carbonate precipitation for immobilization of toxic metals. In *Advances in Applied Microbiology.* Elsevier. 79-108. DOI:10.1016/bs.aambs.2015.12.002.

V. Kyriakou, I. Garagounis, A. Vourros, E. Vasileiou & M. Stoukides. 2020. An electrochemical Haber-Bosch process. *Joule.* 4(1):142-158. DOI:10.1016/j.joule.2019.10.006.

S.E. Lambert & D.G. Randall. 2019. Manufacturing bio-bricks using microbial induced calcium carbonate precipitation and human urine. *Water Research.* 160:158-166. DOI:10.1016/j.watres.2019.05.069.

J. Lehne & F. Preston. 2018. *Making concrete change: Innovation in low-carbon cement and concrete*. (9781784132729). Available: www.chathamhouse.org.

C. Lentner. 1981. *Geigy scientific tables*. Basle, Switzerland. Available: https://trove.nla.gov.au/work/12893997.

W. Li, W.S. Chen, P.P. Zhou, L. Cao & L.J. Yu. 2013a. Influence of initial pH on the precipitation and crystal morphology of calcium carbonate induced by microbial carbonic anhydrase. *Colloids and Surfaces B: Biointerfaces.* 102:281-287. DOI:10.1016/j.colsurfb.2012.08.042.

W. Li, W.S. Chen, P.P. Zhou, S.L. Zhu & L.J. Yu. 2013b. Influence of initial calcium ion concentration on the precipitation and crystal morphology of calcium carbonate induced by bacterial carbonic anhydrase. *Chemical Engineering Journal.* 218:65-72. DOI:10.1016/J.CEJ.2012.12.034.

Y. Li, K. Wen, L. Li, W. Huang, C. Bu & F. Amini. 2020. Experimental investigation on compression resistance of bio-bricks. *Construction and Building Materials.* 265(120751):1-7. DOI:10.1016/j.conbuildmat.2020.120751.

M.G. Lioliou, C.A. Paraskeva, P.G. Koutsoukos & A.C. Payatakes. 2007. Heterogeneous nucleation and growth of calcium carbonate on calcite and quartz. *Journal of colloid and interface science.* 308(2):421-428. DOI:10.1016/j.jcis.2006.12.045.

F. Lippmann. 2012. *Sedimentary carbonate minerals.* Springer Berlin Heidelberg. Available: https://books.google.co.za/books?id=g--PBAAAQBAJ.

L. Ma, A.P. Pang, Y. Luo, X. Lu & F. Lin. 2020. Beneficial factors for biomineralization by ureolytic bacterium *Sporosarcina pasteurii*. *Microbial Cell Factories.* 19(12):1-12. DOI:10.1186/s12934-020-1281-z.

K. Melethil & B. Thomas. 2023. 7 - Photocatalytic applications of ceramics. In *Ceramic Catalysts.* M. Kurian, S. Thankachan and S.S. Nair, Eds.: Elsevier. 169-204. DOI:https://doi.org/10.1016/B978-0-323-85746-8.00003-5.

A. Mezquita, E. Monfort, E. Vaquer, S. Ferrer, M.A. Arnal, J. Toledo & M.A. Cuesta. Eds. 2012. Energy optimisation in ceramic tile manufacture by using thermal oil. Castellón, Spain.

H.L. Mobley & R.P. Hausinger. 1989. Microbial ureases: significance, regulation, and molecular characterization. *Microbiology and Molecular Biology Reviews.* 53(1).

J.W. Morse & F.D. Mackenzie. 1990. *Geochemistry of Sedimentary Carbonate.* Amsterdam: Elsevier.

B.M. Mortensen, M.J. Haber, J.T. DeJong, L.F. Caslake & D.C. Nelson. 2011. Effects of environmental factors on microbial induced calcium carbonate precipitation. *Journal of Applied Microbiology.* 111(2):338-349. DOI:10.1111/J.1365-2672.2011.05065.X.

J.W. Mullin. 2001. Chemical, petrochemical & process. In *Crystallization.* Elsevier Science. Available: https://books.google.no/books?id=Et0EtojQmvsC.

R. Murugan, G.K. Suraishkumar, A. Mukherjee & N.K. Dhami. 2021. Influence of native ureolytic microbial community on biocementation potential of *Sporosarcina pasteurii*. *Scientific Reports.* 11(20856):1-12. DOI:10.1038/s41598-021-00315-5.

A. Myhr, F. Royne, A.S. Brandtsegg, C. Bjerkseter, H. Throne-Holst, A. Borch, A. Wentzel & A. Royne. 2019. Towards a low CO2 emission building material employing bacterial metabolism (2/2): Prospects for global warming potential reduction in the concrete industry. *PLOS ONE.* 14(4):e0208643. DOI:10.1371/journal.pone.0208643.

T.H.K. Nawarathna, K. Nakashima & S. Kawasaki. 2019. Chitosan enhances calcium carbonate precipitation and solidification mediated by bacteria. *International journal of biological macromolecules.* 133:867-874. DOI:10.1016/j.ijbiomac.2019.04.172.

P.G.N. Nayanthara, A.B.N. Dassanayake, K. Nakashima & S. Kawasaki. 2019. Microbial induced carbonate precipitation using a native inland bacterium for beach sand stabilization in nearshore areas. *Applied Sciences.* 9(15):3201. DOI:10.3390/app9153201.

M. Nemati & G. Voordouw. 2003. Modification of porous media permeability, using calcium carbonate produced enzymatically in situ. *Enzyme and microbial technology.* 33(5):635-642. DOI:10.1016/S0141-0229(03)00191-1.

M. Nemati, E.A. Greene & G. Voordouw. 2005. Permeability profile modification using bacterially formed calcium carbonate: comparison with enzymic option. *Process Biochemistry.* 40(2):925-933.

C. Nething, M. Smirnova, J.A.D. Gröning, W. Haase, A. Stolz & W. Sobek. 2020. A method for 3D printing bio-cemented spatial structures using sand and urease active calcium carbonate powder. *Materials & design.* 195:109032. DOI:10.1016/j.matdes.2020.109032.

G.D.O. Okwadha & J. Li. 2010. Optimum conditions for microbial carbonate precipitation. *Chemosphere.* 81(9):1143-1148. DOI:10.1016/j.chemosphere.2010.09.066.

J.V. Parambil & J.Y.Y. Heng. 2017. Seeding in Crystallisation. In *Engineering Crystallography: From Molecule to Crystal to Functional Form.* K.J. Roberts, R. Docherty and R. Tamura, Eds. Dordrecht: Springer Netherlands. 235-245. DOI:10.1007/978-94-024-1117-1_13.

P.H. Pfromm. 2017. Towards sustainable agriculture: Fossil-free ammonia. *Journal of Renewable and Sustainable Energy.* 9(3):034702-034702. DOI:10.1063/1.4985090.

V.P. Pham, A. Nakano, W.R.L. Van Der Star, T.J. Heimovaara & L.A. Van Paassen. 2018. Applying MICP by denitrification in soils: A process analysis. *Environmental geotechnics.* 5(2):79-93. DOI:10.1680/jenge.15.00078.

M. Pires, R. Fidelis, D. Resende & A. Bezerra. 2022. Phosphate rock waste in the production of cement tile. *Results in Engineering.* 16:100701. DOI:10.1016/j.rineng.2022.100701.

S.K. Pradhan, A. Mikola & R. Vahala. 2017. Nitrogen and phosphorus harvesting from human urine using a stripping, absorption, and precipitation process. *Environmental Science & Technology.* 51(9):5165-5171. DOI:10.1021/acs.est.6b05402.

D.F. Putnam. 1971. *Composition and concentrative properties of human urine*. Huntington Beach, CA, United States. Available: https://ntrs.nasa.gov/citations/19710023044.

J. Qiu, D.Q.S. Tng & E.-H. Yang. 2014. Surface treatment of recycled concrete aggregates through microbial carbonate precipitation. *Construction & building materials.* 57:144-150. DOI:10.1016/j.conbuildmat.2014.01.085.

M.M. Rahman & R.N. Hora. Eds. 2017. Unconfined compressive strength of microbial induced calcite precipitation (MICP) treated soils | ISSMGE. Seoul: International Society for Soil Mechanics and Geotechnical Engineering (ISSMGE).

M.M. Rahman, R.N. Hora, I. Ahenkorah, S. Beecham, M.R. Karim & A. Iqbal. 2020. State-of-the-art review of microbial-induced calcite precipitation and its sustainability in engineering applications. *Sustainability.* 12(15):6281-6281. DOI:10.3390/su12156281.

D.G. Randall, M. Krähenbühl, I. Köpping, T.A. Larsen & K.M. Udert. 2016. A novel approach for stabilizing fresh urine by calcium hydroxide addition. *Water Research.* 95:361-369. DOI:10.1016/j.watres.2016.03.007.

S.H. Raut, D.D. Sarode & S.S. Lele. 2014. Biocalcification using *B. pasteurii* for strengthening brick masonry civil engineering structures. *World Journal of Microbiology and Biotechnology.* 30(1):191-200. DOI:10.1007/s11274-013-1439-5.

B.E. Rittmann, B. Mayer, P. Westerhoff & M. Edwards. 2011. Capturing the lost phosphorus. *Chemosphere (Oxford).* 84(6):846-853. DOI:10.1016/j.chemosphere.2011.02.001.

M.A. Rivadeneyra, R. Delgado, A. Del Moral, M.R. Ferrer & A. Ramos-Cormenzana. 1993. Precipitation of calcium carbonate by *Vibrio* spp. from an inland saltern. *FEMS microbiology ecology.* 13(3):197-204. DOI:10.1016/0168-6496(94)90013-2.

K.K. Sahoo, M. Arakha, P. Sarkar, R.D. P & S. Jha. 2016. Enhancement of properties of recycled coarse aggregate concrete using bacteria. *International journal of smart and nano materials.* 7(1):22-38. DOI:10.1080/19475411.2016.1152322.

D. Sarda, H.S. Choonia, D.D. Sarode & S.S. Lele. 2009. Biocalcification by *Bacillus pasteurii* urease: A novel application. *Journal of Industrial Microbiology and Biotechnology.* 36(8):1111-1115. DOI:10.1007/s10295-009-0581-4.

M. Seifan & A. Berenjian. 2018. Application of microbially induced calcium carbonate precipitation in designing bio self-healing concrete. *World Journal of Microbiology and Biotechnology.* 34:168-168. DOI:10.1007/s11274-018-2552-2.

M. Seifan, A.K. Samani & A. Berenjian. 2016. Bioconcrete: next generation of self-healing concrete. *Applied Microbiology and Biotechnology.* 100(6):2591-2602. DOI:10.1007/s00253-016-7316-z.

P. Shao, L. Comolli & R. Bernier-Latmani. 2014. Membrane vesicles as a novel strategy for shedding encrusted cell surfaces. *Minerals (Basel).* 4(1):74-88. DOI:10.3390/min4010074.

A.A. Shubbar, M. Sadique, P. Kot & W. Atherton. 2019. Future of clay-based construction materials – A review. *Construction & building materials.* 210:172-187. DOI:10.1016/j.conbuildmat.2019.03.206.

M. Song, T. Ju, Y. Meng, S. Han, L. Lin & J. Jiang. 2022. A review on the applications of microbially induced calcium carbonate precipitation in solid waste treatment and soil remediation. *Chemosphere (Oxford).* 290:133229-133229. DOI:10.1016/j.chemosphere.2021.133229.

S. Stocks-Fischer, J.K. Galinat & S.S. Bang. 1999. Microbiological precipitation of CaCO3. *Soil Biology and Biochemistry.* 31(11):1563-1571. DOI:10.1016/S0038-0717(99)00082-6.

Straits Research. 2023. *Ceramic tiles market size, growth & analysis by 2031. Report code: SRAM466DR.* Amanora Park Town, India.

W. Stumm & J.J. Morgan. 1981. *Aquatic chemistry.*

T. Tambunan, M.I. Juki & N. Othman. 2019. Mechanical properties of sulphate reduction bacteria on the durability of concrete in chloride condition. *International conference on sustainable civil engineering structures and construction materials (SCESCM 2018).* 258:1024. DOI:10.1051/matecconf/201925801024.

L. Thörneby, K. Persson & G. Trägårdh. 1999. Treatment of liquid effluents from dairy cattle and pigs using reverse osmosis. *Journal of agricultural engineering research.* 73(2):159-170. DOI:10.1006/jaer.1998.0405.

C.E. Turick & C.J. Berry. 2016. Review of concrete biodeterioration in relation to nuclear waste. *Journal of environmental radioactivity.* 151(P1):12-21. DOI:10.1016/j.jenvrad.2015.09.005.

K.M. Udert, T.A. Larsen, M. Biebow & W. Gujer. 2003. Urea hydrolysis and precipitation dynamics in a urine-collecting system. *Water Research.* 37(11):2571-2582. DOI:10.1016/S0043-1354(03)00065-4.

UNEP. 2019. *Sand and Sustainability: Finding new solutions for environmental governance of global sand resources: synthesis for policy-makers*. Geneva, Switzerland.

UNEP. 2022. *Sand and sustainability: 10 strategic recommendations to avert a crisis*. Geneva, Switzerland.

L.A. Van Paassen. 2009. *Biogrout, ground improvement by microbial induced carbonate precipitation.* Delft, The Netherlands.

L.A. van Paassen, R. Ghose, T.J.M.v.d. Linden, W.R.L.v.d. Star & M.C.M. van Loosdrecht. 2010. Quantifying biomediated ground improvement by ureolysis: large-scale biogrout experiment. *Journal*

of Geotechnical and Geoenvironmental Engineering. 136(12):1721-1728. DOI:10.1061/(ASCE)GT.1943-5606.0000382.

J. Wang, B. Vandevyvere, S. Vanhessche, J. Schoon, N. Boon & N. De Belie. 2017. Microbial carbonate precipitation for the improvement of quality of recycled aggregates. *Journal of Cleaner Production.* 156:355-366. DOI:10.1016/J.JCLEPRO.2017.04.051.

S. Wang, S.F. Scarlata & N. Rahbar. 2022a. A self-healing enzymatic construction material. *Matter.* 5(3):957-974. DOI:10.1016/j.matt.2021.12.020.

Y. Wang, K. Soga, J.T. DeJong & A.J. Kabla. 2021. Effects of bacterial density on growth rate and characteristics of microbial-induced CaCO3 precipitates: Particle-scale experimental study. *Journal of Geotechnical and Geoenvironmental Engineering.* 147(6). DOI:10.1061/(ASCE)GT.1943-5606.0002509.

Z. Wang, J. Zhang, M. Li, S. Guo, J. Zhang & G. Zhu. 2022b. Experimental study of microorganism-induced calcium carbonate precipitation to solidify coal gangue as backfill materials: mechanical properties and microstructure. *Environmental Science and Pollution Research.* 29(30):45774-45782. DOI:10.1007/s11356-022-18975-9.

K. Wen, Y. Li, F. Amini & L. Li. 2020. Impact of bacteria and urease concentration on precipitation kinetics and crystal morphology of calcium carbonate. *Acta Geotechnica 2019 15:1.* 15(1):17-27. DOI:10.1007/S11440-019-00899-3.

V.S. Whiffin, L.A. van Paassen & M.P. Harkes. 2007. Microbial carbonate precipitation as a soil improvement technique. *Geomicrobiology Journal.* 24(5):417-423. DOI:10.1080/01490450701436505.

J.Z. Xiao, Y.Q. Wei, H. Cai, Z.W. Wang, T. Yang, Q.H. Wang & S.F. Wu. 2020. Microbial-Induced Carbonate Precipitation for Strengthening Soft Clay. *Advances in materials science and engineering.* 2020:1-11. DOI:10.1155/2020/8140724.

Y. Xiao, X. He, T.M. Evans, A.W. Stuedlein & H. Liu. 2019. Unconfined Compressive and Splitting Tensile Strength of Basalt Fiber–Reinforced Biocemented Sand. *Journal of Geotechnical and Geoenvironmental Engineering.* 145(9). DOI:10.1061/(ASCE)GT.1943-5606.0002108.

X. Xu, H. Guo, X. Cheng & M. Li. 2020. The promotion of magnesium ions on aragonite precipitation in MICP process. *Construction and Building Materials.* 263(120057):1-9. DOI:10.1016/j.conbuildmat.2020.120057.

M. Yang, L. Tan, C. Batchelor-McAuley & R.G. Compton. 2024. The solubility product controls the rate of calcite dissolution in pure water and seawater. *Chemical science (Cambridge).* 15(7):2464-2472. DOI:10.1039/d3sc04063a.

H. Yi, T. Zheng, Z. Jia, T. Su & C. Wang. 2021. Study on the influencing factors and mechanism of calcium carbonate precipitation induced by urease bacteria. *Journal of Crystal Growth.* 564:126113. DOI:10.1016/j.jcrysgro.2021.126113.

W. Yin & K. Wang. 2021. Analysis of energy saving in domestic ceramic industry kilns. *E3S Web of Conferences.* 267:1011. DOI:10.1051/e3sconf/202126701011.

J. Zehner, A. Røyne & P. Sikorski. 2021. Calcite seed-assisted microbial induced carbonate precipitation (MICP). *PLOS ONE.* 16(2):1-15. DOI:10.1371/journal.pone.0240763.

M. Zhan, M. Fu, G. Pan, X. Lu & Y. Wang. 2020. Recycled aggregate mortar enhanced by microbial calcite precipitation. *Magazine of concrete research.* 72(12):622-633. DOI:10.1680/jmacr.18.00417.

Q. Zhao, L. Li, C. Li, H. Zhang & F. Amini. 2014a. A full contact flexible mold for preparing samples based on microbial-induced calcite precipitation technology. *Geotechnical Testing Journal.* 37(5):20130090-20130090. DOI:10.1520/GTJ20130090.

Q. Zhao, L. Li, M. Asce, C. Li, M. Li, F. Amini, F. Asce & H. Zhang. 2014b. Factors affecting improvement of engineering properties of MICP-treated soil catalyzed by bacteria and urease. *Journal of Materials in Civil Engineering.* 26(12):1-10. DOI:10.1061/(ASCE)MT.1943-5533.

H.-M. Zheng, L.-L. Wu, K.-W. Tong, D.-X. Ding, Z.-J. Zhang, Q. Yu & G.-C. He. 2020. Experiment on microbial grouting reinforcement of tailings under the regulation of egg white. *Soils and foundations.* 60(4):962-977. DOI:10.1016/j.sandf.2020.07.004.

T. Zhu & M. Dittrich. 2016. Carbonate precipitation through microbial activities in natural environment, and their potential in biotechnology: a review. *Frontiers in Bioengineering and Biotechnology.* 4:4-4. DOI:10.3389/fbioe.2016.00004.

3 Research outline

This study investigates the biomimetic process of MICP to produce an alternative to conventional ceramic and cement tiles: bio-tiles. Growing bio-tiles utilising the MICP presents numerous potential advantages over conventional tile production. However, current MICP research has yet to explore the specifics of manufacturing tiles. Moreover, the various potential methods for enhancing the strength of bio-materials grown with MICP to ensure their competitiveness with existing commercial products remain largely unexamined.

3.1 Overarching aim

The overarching aim of this study was to manufacture bio-tiles using MICP with three different techniques (submersion, pumping and automated 3D printing) such that they have properties comparable to conventional ceramic tiles.

3.2 Objectives

The primary objectives of this study were to:

1. Investigate the technical feasibility of producing bio-tiles with MICP using a submersion technique while focusing on the effect of particle size distribution (PSD) and other key parameters;
2. Compare the effect of using a different production method, the pumping technique, on the strength properties of the bio-tiles where the benefits of $CaCO_3$ seeding is investigated.
3. Develop and optimise a fully automated process that utilises the advantages and avoids the disadvantages of the first two techniques while optimising for scalability and assessing the effect this production method has on the breaking strength of bio-tiles as well as various process supplements.

3.3 Scope

The scope of this study involved determining the feasibility of producing bio-tiles using MICP. This study only considered the enzymatic urea hydrolysis pathway of MICP by the ureolytic bacteria, *S. pasteurii*. Smaller tiles of 100 x 100 x 10 mm were produced as a proof of concept.

In the development of a feasible process for the manufacturing of bio-tiles, three techniques were investigated: a submersion technique, a pumping technique, and an automated 3D printing technique. This study focused on data collected from these experimental systems using custom designed moulds and machines that were informed by previous research and the materials available. This study does not consider the economic feasibility of the MICP process and the various bio-material production techniques.

4 Materials and methods

This chapter describes the general materials and methods used in this dissertation. The materials and methods relevant to each of the following chapters are discussed within those chapters. Section 4.1 discusses the cultivation and preparation of the microbiological inoculum. Section 4.2 covers the procedures followed for sampling. Section 4.3 outlines the reagents and aggregate used and where they were sourced. Finally, Sections 4.4 and 4.5 detail the analytical techniques utilised and the standards and tests for tiles that were required and followed, respectively.

4.1 Microbiological cultivation and inoculum preparation

The cultivation of ureolytic soil bacteria *S. pasteurii* (ATCC®1859) and inoculation of aggregate with the bacteria was carried out as described by Henze and Randall (2018). In summary, a bacteria colony was cultivated in 10 mL of ammonium-yeast growth medium (ATCC®1376; consisting of: 20 g/L yeast extract, 10 g/L $(NH_4)_2SO_4$ and 0.13 M Tris buffer (pH 9.0 achieved with 32% HCl), autoclaved (Waste and Pipette Sterilization Autoclave E-SA-300VF, Steeledale, South Africa) separately and then aseptically mixed) for 24 hours in a shaking incubator (120 rpm) at 30°C. The 10 mL inoculum was then added to 90 mL of ammonium-yeast medium in a 1 L flask and incubated for a further 16 hours to the late exponential growth phase.

4.1.1 *Analysis of the culture activity for inoculation with standardised activity*

Depending on the quantity of bacteria required for the experiment sets, flasks were combined to obtain 600-1500 mL of bacteria solution and then the ureolytic activity of the batch was determined. When stated, bacteria cell counts of the mixed batch were also performed within 1 hour of the removal from the incubator. Microscope cell counts were used to determine microbial culture density following standard practices with a Helber Bacteria Counting Chamber (Z30000, Hawksley, Sussex, United Kingdom). Each batch of bacteria was analysed for its ureolytic activity by measuring the amount of ammonium ions (NH_4-N) produced in 30 min. Bacteria solution (15 mL) and 1 M urea solution (15 mL) were added aseptically to an autoclaved 250 mL Erlenmeyer flask, sealed with parafilm, and placed on an orbital shaker (262, Scientific, South Africa) at 120 rpm for 30 min. This test and sampling were performed immediately in duplicate and at the end of the 30-minute period.

The batch of bacteria was only used if the ammonium production activity was greater than 2.7 mmol NH_4^+ /L·min. The ureolytic activity was standardised across experimental runs using a dilution method in which the inoculum was diluted or concentrated to achieve the desired activity. When liquid bacteria culture was required, the bacteria cells were harvested by centrifugation (Varispin 12R, Cryste, Bucheon, Korea) at 2570 g for 20 minutes at 5°C. Pending the analysis of the ureolytic activity test, the bacteria pellets were aseptically resuspended in fresh ammonium-yeast growth medium (ATCC®1376) to achieve the desired ureolytic activity and then immediately mixed into the required aggregate to 75% saturation of the pore space (Cheng *et al.*, 2020). The inoculated aggregate was left to colonise and then packed into the bio-tile moulds before starting the experimental run 3-4 hours after inoculation.

4.1.2 *Long term preparations for consistent microbiological cultivation*

ATCC®1376 agar plates were prepared according to the same recipe as the ammonium-yeast growth medium above, but with the addition of 20 g bacteriological agar to the yeast solution. Once aseptically mixed post autoclaving and the bottle was cool enough to hold, the solution was poured into petri

dishes. The agar plates were allowed to solidify overnight and then were stored at 4°C in sealed plastic bags until needed.

Glycerol *S. pasteurii* stock culture was prepared for posterity of the culture. Bacteria culture at the late exponential growth phase was combined aseptically 1:1 with autoclaved 50 vol% glycerol solution in sterile cryogenic vials to a volume of 2 mL (Zhang, 2013). The glycerol stocks were stored at -50°C.

Bacteria was streaked from glycerol stock culture either every 6 months or once 10 plates had been streaked sequentially from the initial stock culture plate, whichever came first. Bacteria cultures were only grown from plates after the 3rd sequential plate was streaked, after 2-3 days of incubation at 30°C.

4.2 Sampling

For the ureolytic activity tests, two 20 µL samples were taken directly from both of the flasks and the pH measured simultaneously from the flasks. Deionised water was added to the sample immediately to a 1 in 100 dilution. When sampling the bio-reactors, the sample contained solid $CaCO_3$ and needed to be filtered before analysis. Bio-reactor samples were extracted and filtered with a 0.22 µm pore size syringe filter (ThermoFisher Scientific, South Africa) into a 2 mL Eppendorf tube and closed immediately. From this, 1 in 100 dilutions were carried out in triplicate. Concentrations were measured immediately, and when needed, a dilute HCl solution (0.1 M) was added to the dilutions to stop the reaction.

4.3 Material inputs

The cementation solution was made up of synthetic urea (≥99.5% purity, Sigma-Aldrich, Darmstadt, Germany) and additional calcium in the form of calcium chloride dihydrate (≥99.1% purity, Kimix, Cape Town, South Africa). When additional nutrients were added to the cementation solution, this was in the form of Nutrient Broth No. 1 (Sigma-Aldrich) at a concentration of 3 g/L. The nutrient broth contained 15 g/L peptone, 3 g/L yeast extract, 6 g/L sodium chloride, 1 g/L D-glucose and was mixed into a small amount of deionised water and autoclaved before use. In experiments that used magnesium chloride, anhydrous $MgCl_2$ (≥98% purity, Sigma-Aldrich) was added to some deionised water before adding it to the cementation solution.

Dune sand sourced from the Cape Flats in Cape Town was used for the bio-tile aggregate as a proof of concept. Greywacke aggregate sourced from Peninsula Quarry (AfriSam), Cape Town, was also used in selected experiments to achieve different PSDs. These aggregates were used as a proxy and any particles with a similar PSD could theoretically be used as an alternative.

4.4 Analytical methods

The concentration of calcium, ammonium, and magnesium ions were measured colorimetrically using a Gallery Discrete Analyser (GDA) (Automated Photometric Analyser: 861, Thermo Fisher Scientific, United States). Each of the ions were calibrated on the GDA weekly. A pH probe (HI1131B, Hanna Instruments, Rhode Island, United States) was used to measure the pH of the solutions. The probe was calibrated using 4 buffers, 4.01, 7.01, 10.01 and 12.592. Hanna pH-buffers were used for all but the highest calibration point, for which a saturated calcium hydroxide solution was used.

X-ray diffraction (XRD) analysis (Bruker D8, Bruker, United States) was used to analyse the crystalline $CaCO_3$ polymorph. The presence of $CaCO_3$ and amorphous $CaCO_3$ was confirmed using a scanning electron microscope (SEM) (MIRA3 RISE, TESCAN, Czech Republic) with the methods described by MyScope (2022) where the samples were adhered to SEM stubs with carbon glue and then coated with carbon in an evaporation coater.

4.5 Standards testing

The International Organisation of Standards (ISO) require tiles to meet a wide array of standards, such as stain, scratch, chemical and UV resistance depending on water absorption, method of manufacture, finish, and intended purpose (ISO, 2018). Of all the required standards to be met for the purposes of this study, breaking strength and modulus of rupture were considered to be key fundamental standards to be cleared and were thus the only ones covered in this feasibility study. These standards and tests differ to that of concrete and bricks, for example, where unconfined compressive strength (UCS) is the specific test used to quantify strength. Therefore, breaking strength and modulus of rupture cannot be directly compared to UCS.

The measurement of breaking strength (S) of each bio-tile was performed according to the ISO 10545-4:2019 standard using a three-point bending device, similar to that in Figure 4.1. Rubber with a thickness (t) coated each of the rods to protect the tile and apply consistent force. The device has unique measurements used to calculate the actual breaking strength from the breaking force (F). Table 4.1 provides the system parameters unique to the testing rig used. The breaking force of each bio-tile was measured using a ProLine Z100 (ZwickRoell 1474, Ulm, Germany).

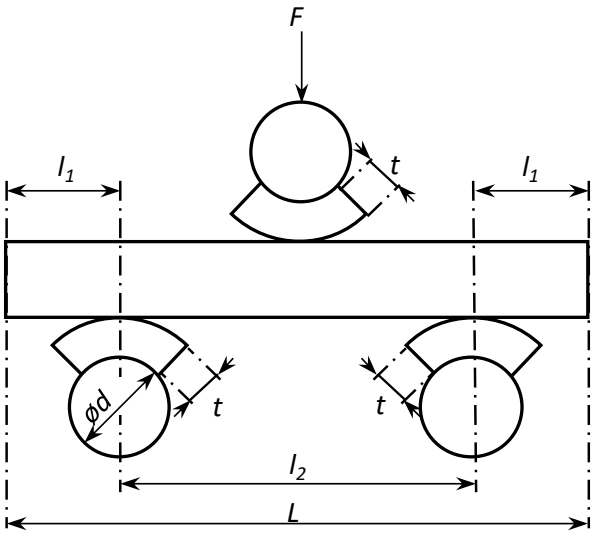

Figure 4.1: Breaking strength testing rig (adapted from ISO (2019)).

Where:

F breaking force (N)
d diameter of rod (mm)
L long side of tile (mm)
l_1 overlap of tile beyond the edge supports (mm)
l_2 span between support rods (mm)
t thickness of rubber (mm)
S breaking strength (N)

Table 4.1: Zwick system parameters.

Parameter	Dimension (mm)
d	12
L	100
l_1	19
l_2	62
t	3

The breaking strength was calculated using these parameters and Equation 7.

$$S = F \times \frac{l_2}{L} \quad (7)$$

Once the bio-tile was broken by the breaking force, the minimum thickness (h_{min}) of the bio-tile along the broken edge could be measured with callipers and the modulus of rupture (σ_r) calculated from Equation 8.

$$\sigma_r = \frac{3 \times S}{2 \times h_{min}^2} \quad (N/mm^2) \quad (8)$$

Bio-tiles were considered to be most similar to extruded ceramic tiles and were compared against these standards (ISO, 2018). The target breaking strength and modulus of rupture were determined by the water absorption of the tiles.

Water absorption is important for tile classification, as it determines the application of the tiles. The analysis of the tiles' water absorption was adapted from the SANS1449 standard (SABS, 2012) where after the tiles were tested for their breaking strength, one of the tile's halves was dried for 12 hours at 105°C and cooled in a desiccator and the dry mass measured. The tile half was then vertically inserted into a water bath at room temperature, so that there was 50 mm of water above and below the tile. The water bath was heated to boiling and held there for 2 hours, then turned off and the tiles left in the water bath to cool to room temperature once more. The tiles were patted dry with paper towel and weighed for their wet mass.

The target breaking strength and modulus of rupture were determined by standards for a set range of water absorption for the bio-tiles (Table 2.5). Therefore, for bio-tiles with a water absorption greater than 10%, the breaking strength to be met or exceeded is 600 N and the modulus of rupture must be a minimum of 8 N/mm^2. For bio-tiles with a water absorption of 6-10%, a minimum of 750 N and 9 N/mm^2, respectively, were required.

References

L. Cheng, T. Kobayashi & M.A. Shahin. 2020. Microbially induced calcite precipitation for production of "bio-bricks" treated at partial saturation condition. *Construction and Building Materials.* 231(117095):1-9. DOI:10.1016/j.conbuildmat.2019.117095.

J. Henze & D.G. Randall. 2018. Microbial induced calcium carbonate precipitation at elevated ph values (>11) using *Sporosarcina pasteurii*. *Journal of Environmental Chemical Engineering.* 6:5008-5013. DOI:10.1016/j.jece.2018.07.046.

ISO. 2018. *ISO 13006:2018: Ceramic tiles - definitions, classification, characteristics and marking*. Available: https://www.iso.org/standard/63406.html.

ISO. 2019. *ISO 10545-4:2019, Ceramic tiles — part 4: Determination of modulus of rupture and breaking strength*. Available: https://www.iso.org/standard/69619.html.

MyScope. 2022. *Scanning electron microscopy | A basic guide to using an SEM*. Microscopy Australia. Available: https://myscope.training/#/SEMlevel_2_11 [2022, 20 August].

SABS. 2012. *South African National standard, ceramic wall and floor tiles*. (978-0-626-25452-0). Pretoria. Available: www.sabs.co.za.

L. Zhang. 2013. Production of bricks from waste materials – a review. *Construction & building materials.* 47:643-655. DOI:10.1016/j.conbuildmat.2013.05.043.

5 Production of bio-tiles using the submersion technique

This chapter reports the findings of the first study on bio-tiles grown with MICP. While investigation into how bio-tiles can be produced using the submersion technique was the primary focus of the study, other fundamental parameters, such as the best-performing ureolytic activity, calcium and urea concentration, and the PSD of the loose particles to be bio-cemented together were also determined. From there, other factors were evaluated to enhance the strength properties of the bio-tiles: the effect of the volume of cementation solution and supplemental magnesium. Specific objectives as well as materials and methodology specific to the submersion technique are outlined and then the findings are discussed.

Chapter 5 is based on the first paper published in relation to this work, *Growing bio-tiles using microbially induced calcium carbonate precipitation*.

5.1 Objectives

The key objectives of this study were to investigate how the following parameters influenced the strength properties of the bio-tiles produced with the submersion technique:

1. Calcium and urea concentration;
2. Particle size distribution (PSD) of aggregate material;
3. Volume of cementation solution; and
4. Magnesium concentration.

Each parameter was assessed subsequently and, in some cases, separately, until the end, where the most effective of each was combined into an 'optimal' experiment.

5.2 Materials and methods

5.2.1 *Bio-tile mould*

A Perspex support enclosure was designed that had a mesh grid for the upper and lower surfaces of the bio-tile, with inside dimensions of 100 x 100 mm (Figure 5.1). Clear acetate and petroleum jelly lined the walls of the mould. The aggregate was compacted into the mould using a flat platform and hammer over a block that filled the bottom mould holes, to prevent bulging.

Geotextile (Sanscape, Cape Town, South Africa) with a density of 40 g/m^2 was used to line the upper and lower mesh surfaces. A number of different geotextiles were tested with the submersion technique. The thicker geotextile (~2 mm) used by Lambert and Randall (2019) in their bio-bricks was initially tried, however the thinner Sanscape geotextile (~0.5 mm) allowed a more solidified and stronger bio-material to form, due to better chemical diffusion.

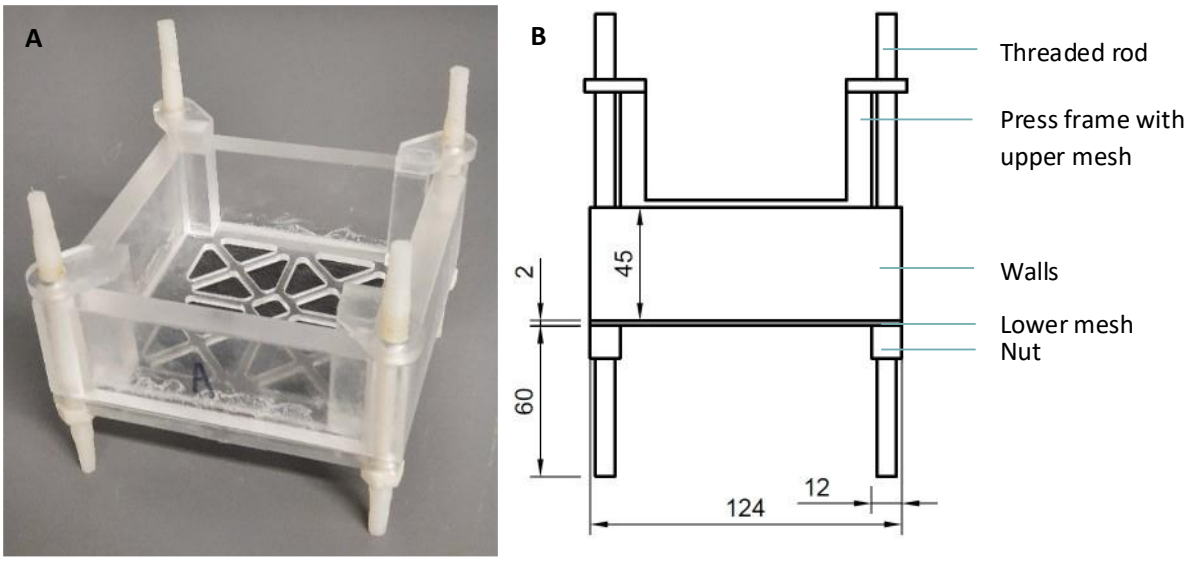

Figure 5.1: Photo (A) and schematic diagram (B) of bio-tile mould where the press frame with upper mesh closes downward with wing nuts to compress a bio-tile of desired height. Dimensions in mm.

5.2.2 *Submersion technique operation*

The submersion technique allows the production of more than one bio-tile at once, where bio-tile moulds were immersed in a stirred batch bio-reactor containing 14 L of cementation solution, unless otherwise specified, of the desired concentration (Cheng *et al.*, 2020). A table of experimental variables tested is given in Table 5.1.

Table 5.1: Experiment condition parameters and ranges.

Experiment	Range	Unit
Ureolytic activity	2.7-7.9	mmol NH_4^+/L·min
Cementation solution concentration	0.1-1.0	M
Particle size distribution (D_{50})	139-978	µm
Cementation solution volume	11.8-18	L
Magnesium concentration	0.1-0.5	M

The inoculated aggregate was compacted into the moulds by first flattening it by hand and then with a plate and hammer. The plate was hit 10 times, with two knocks in the middle and then two in opposite corners and then the final two opposite corners. The aggregate that had squeezed up the walls was flattened down. Each of the four filled bio-tile moulds were secured into each of the quadrants of the bio-reactor over their own dedicated magnetic stirrer at 75% of their maximum speed as shown in Figure 5.2. All reactors were also stirred by a radial flow impeller (WB2000-C, Wiggens, Straubenhardt, Germany) at 250 rpm.

The reaction took place for a period of 7 days at ambient temperature (21-24°C), during which time no further bacteria, nutrients or cementation solution was added to the bio-reactor. The pH and temperature of the reactor were measured simultaneously as samples were extracted.

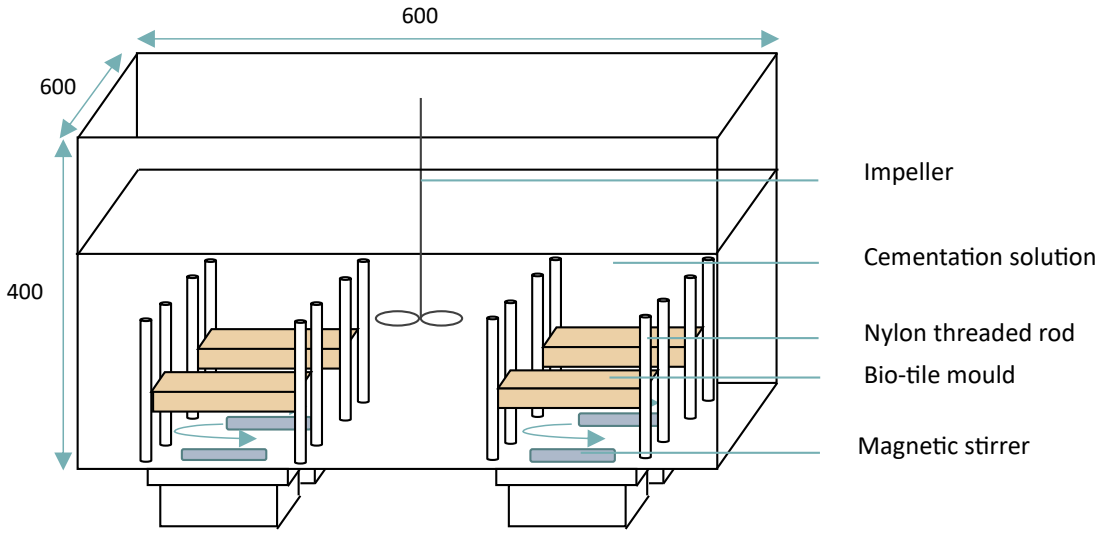

Figure 5.2: Submersion reactor set up with position of the four magnetic stirrers and central impeller.

The bio-tiles were then removed, flushed with tap water and air dried at 30°C for 1 day before performing further tests. During the course of an experiment, at some point during the retention time one of the magnetic stirrer bars may have displaced itself. This resulted in ineffective mixing for part of the experiment, causing inconsistent solidification in that bio-tile and lower strengths. In these situations, the sample size was 3 bio-tiles instead of 4.

5.2.3 *Best-performing cementation solution concentration*

To determine the optimal concentration of cementation solution, equimolar calcium and urea concentrations of 0.1, 0.2, 0.3, 0.4, 0.5, 0.75 and 1.0 M were tested, based on similar concentration ranges from other studies (Al Qabany *et al.*, 2012; Anbu *et al.*, 2016; Lambert & Randall, 2019).

5.2.4 *Best-performing particle size*

Dune sand was used for the bio-tile aggregate as a proof of concept. The Mastersizer (2000, Malvern Panalytical, United Kingdom) with a Hydro2000G dispersion unit was used to analyse the PSD of all aggregates. Unsieved sand with an average particle size of 468.7 µm was used in all experiments. The void ratio and porosity of the sand were calculated to be 0.68 and 40%, respectively, using the density bottle method described by Lambert and Randall (2019). A summary of the PSD findings and the density bottle results are shown in Table A.1 and Table A.2, respectively. To determine the optimal D_{10} of the aggregate, a series of size fractions were selected. Sand was sieved 1:1 with Greywacke aggregate and grains retained between sieves of 75 and 115 µm, 212 and 300 µm, 425 and 600 µm, and 600 and 900 µm were used. These ranges had a D_{50} of 138.5, 330.8, 641.0 and 978.2 µm, respectively. An unsieved 1:1 mixture of sand and Greywacke aggregate sieve was also selected, and divided into two, one with and one without fines smaller than 150 µm removed. These two sand and Greywacke mixtures had a D_{50} of 810 and 825 µm, respectively, and their PSDs are shown in Figure A.2.

5.3 Results and discussion

5.3.1 *Development of design chart*

A novel design chart was developed as a function of breaking strength, modulus of rupture and minimum thickness as a measure of performance of the produced bio-tiles against the required

standards. The water absorption was 9.7-13.7% for all tiles. The design chart in Figure 5.3 was generated for tiles with a water absorption of over 10% which results in the breaking strength target of 600 N and a modulus of rupture of 8 MPa (ISO, 2018). When both conditions are met or exceeded, the tile falls within the green shaded region (Figure 5.3). Tiles within this region meet the most important criteria, proving the feasibility of bio-tiles as a product and that additional studies should be performed on them to ensure they meet other tile standards.

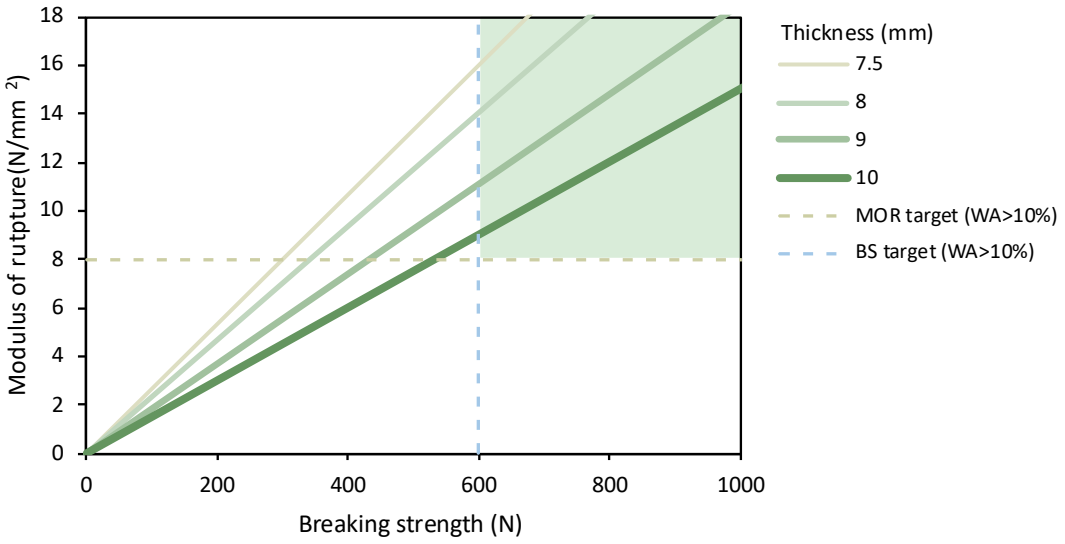

Figure 5.3: Example design chart depicting the relative position of bio-tiles data against the required standards for a water absorption (WA) of greater than 10%. Green lines indicate the minimum thickness in mm of a given tile set. The green shaded area indicates the tiles that meet both the breaking strength (BS) and modulus of rupture (MOR) standards, and the white where one or both are not met.

The diagonal lines on the design chart indicate the minimum thickness of the bio-tile on the broken edge. Each thickness was chosen based on the likely minimum being less than 10 mm. Each diagonal line reflects the relationship of a theoretical breaking strength to the resultant modulus of rupture. Seeing as modulus of rupture is calculated from breaking strength and the square of the minimum thickness along the broken edge, each tile thickness has a corresponding possible set of modulus of ruptures tied to breaking strength. Thicker tiles are apt to be stronger, however, then the modulus of rupture decreases faster. Therefore, the strength benefits of thickness need to be balanced with the required modulus of rupture. The bio-tiles for the specific parameters investigated are discussed in the relevant sections. From Figure 5.3, it is evident that the breaking strength standard is more difficult to reach and therefore, increasing the breaking strength of the bio-tiles was the focus going forward.

5.3.2 *Identifying a suitable ureolytic activity*

The ureolytic activity of the combined inoculum ranged from 5.0-8.0 mmol ammonium produced/L·min. Cell counts indicated similar numbers (3.04-5.52 x 10^9 ± 0.63 cells/mL, N=10) across batches with a Pearson's correlation coefficient of -0.20 to the measured ureolytic activity. This indicated that there was practically no correlation between cell counts and ureolytic activity and that cell counts alone were insufficient in offering a measure of how active the bacteria were, and also posed the problem of inconsistency from test to test. By correlating ureolytic activity with breaking strength and keeping other parameters constant at a retention time of 7 days, it was found that higher activity resulted in lower breaking strength (Figure 5.4). This is contrary to what some researchers have

found where increasing urease activity caused an increase in unconfined compressive strength of bio-columns also grown with the submersion technique (Zhao *et al.*, 2014b). However, methods of measuring and standardising the ureolytic activity were based on the OD_{600} readings (optical density at a wavelength of 600 nm), the measurement of growth phase used by many MICP researchers (Cuzman *et al.*, 2015; Wen *et al.*, 2020; Xu *et al.*, 2020), and the conductivity of the solution which might not always be accurate as non-viable cells can still contribute to the OD_{600} reading.

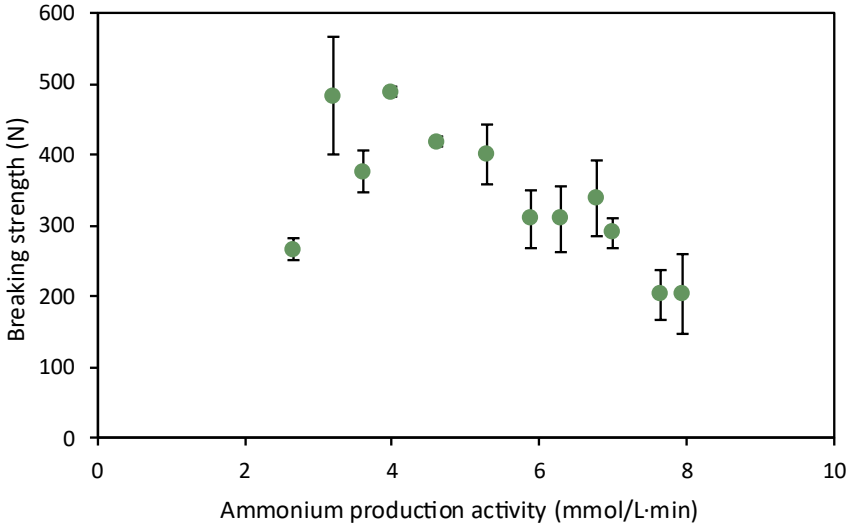

Figure 5.4: The change in breaking strength due to the varying ureolytic activity of the *S. pasteurii* solution. Error bars indicate standard deviation of number of bio-tiles tested, n = 4.

Other researchers (Chunxiang *et al.*, 2009; Wen *et al.*, 2020) have found that bacterial activity has a profound impact on the crystallisation of $CaCO_3$, where higher activity caused a greater secretion of the organic matrix, and a thicker deposit of $CaCO_3$. However, a thicker deposit has also been found to not directly relate to surface permeability resistance, and by extension, the associated strength of the formation (Chunxiang *et al.*, 2009; Kim *et al.*, 2018). This is because the rate of precipitation affects the mineralisation mechanism, where higher initial concentrations of bacteria and urease have a greater rate constant (Wen *et al.*, 2020). A slower reaction rate is favourable as compact and hard $CaCO_3$ forms at very slow rates (Chunxiang *et al.*, 2009). Therefore, the rate of precipitation can be controlled through the ureolytic activity. Mortensen *et al.* (2011) also found that by reducing the precipitation rate a more uniform deposition of $CaCO_3$ is achieved.

Anbu *et al.* (2016) confirmed the findings shown in Figure 5.4, where they observed that the urease activity should not be too high (above 4.0 mmol/L·min) nor too low (under 3.2 mmol/L·min) to achieve improved strength in bio-cemented soil. While an activity of 3.2 mmol NH_4^+/L·min was able to produce bio-tiles almost as strong (483 N) as 4.0 mmol NH_4^+/L·min, an activity of 4.0 mmol/L·min was closer to the activity of the bacteria immediately after they were removed from the incubator and therefore, this activity was selected for all following experiments to reduce the required dilution volumes and potential errors.

5.3.3 *Influence of calcium and urea concentration on breaking strength*

The effect of the cementation solution concentration on the breaking strength of the bio-tiles is shown in Figure 5.5 with the calcium utilisation at the end of the experiment shown in the secondary axis. At

a cementation solution concentration of 0.1 M, the tiles were not solidified and therefore, the breaking strength of the group could not be measured. The equimolar amount of calcium and urea in solution was not enough to form a sufficient amount of $CaCO_3$ to bio-cement the particles together to form a solid.

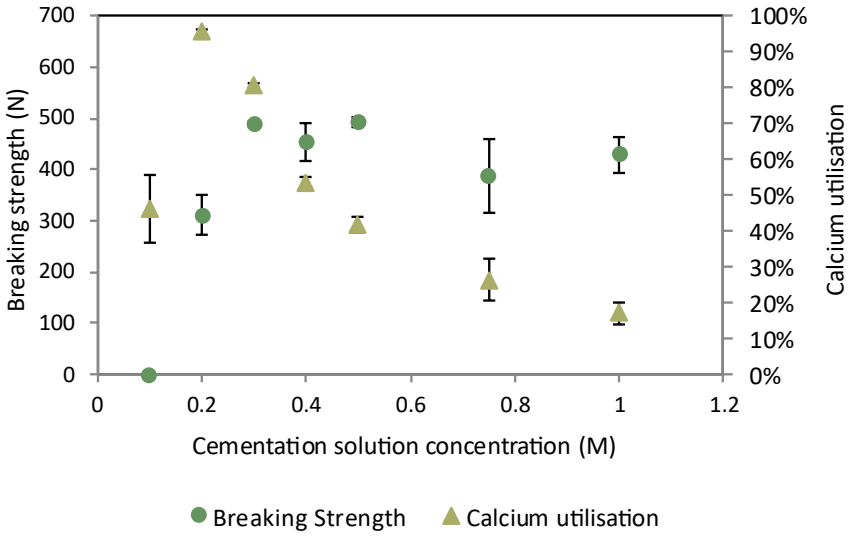

Figure 5.5: The change in breaking strength due to varying the cementation solution concentration and the resulting calcium utilisation at the end of the 7-day retention time. The tiles did not solidify at a concentration of 0.1 M. Error bars represent standard deviation of n = 4 tiles.

Although a concentration of 0.5 M produced a slightly higher breaking strength (491 ± 10 N) than a concentration of 0.3 M (489 ± 6 N), the strength improvement of 0.4% is not worth the additional cost of additional reagents required for higher concentrations, especially when calcium utilisation decreased from 81 to 42%. There is potential for reuse of unspent reagents in the cementation solution for cost recovery. However, build-up of ammonium ions needs to be monitored. This was not pursued for these experiments for consistency. There was a decreasing trend in the utilisation of calcium with increasing cementation solution concentration as the bio-reactor utilised 103 ± 10 g of calcium (excluding 0.1 and 0.2 M bio-reactors) regardless of the cementation solution concentration. At a concentration of 0.2 M, the bio-reactor had utilised 95% of the available calcium (84 g). The calcium utilisation at a cementation solution concentration of 0.1 M was not higher than at 0.2 M and this was likely due to the lower rate of reaction with a lower concentration of calcium driving the process.

The concentration of cementation solution, and in particular calcium, has been shown to affect the strength of bio-materials. Lambert and Randall (2019) suspected that the bacteria are inhibited by a high ionic strength, which was also given as a possible explanation for the reduced precipitation of $CaCO_3$ found by Gorospe *et al.* (2013) as calcium salts add to the electrolytes in the solution. High concentrations of calcium have been reported to have a negative effect on urease activity and as a result, on the precipitation of $CaCO_3$ (Gorospe *et al.*, 2013; Nemati *et al.*, 2005; Rivadeneyra *et al.*, 2000). Zhao *et al.* (2014b) showed increasing strength of the bio-material up to a calcium concentration of 1.5 M, although the majority of the increase occurred between 0.25 M and 0.5 M (a tenfold increase) and the strength only doubled when increasing from 0.5 to 1.5 M. This is similar to the trend shown in Figure 5.5, where low cementation solution concentrations resulted in the poorest breaking strength of the bio-tiles (312 N at 0.2 M). However, in this study, increasing the concentration

above 0.5 M did not have an advantageous impact on the breaking strength of the bio-tiles produced, especially considering the additional input cost required for input chemicals.

Al Qabany *et al.* (2012) found that cementation media with a concentration of 0.25 M could result in a uniform distribution of small crystals of calcite and showed that a concentration of 0.5 M produced larger and more randomly distributed crystals. This is similar to the effect of a lower ureolytic activity allowing the formation of a stronger bonds as the reaction proceeds slower. Therefore, a cementation solution concentration of 0.3 M was used in all following experiments.

5.3.4 *Effect of particle size distribution on breaking strength*

Various particle size groups were categorised (Table A.1) and tested for their effect on the breaking strength of bio-tiles. For each group, the measured porosity and its standard deviation (SD) is also given. The PSD spread of the groups and their resulting breaking strength is given in Figure 5.6. All groups had a particle size uniformity of 0.20-0.27 µm.

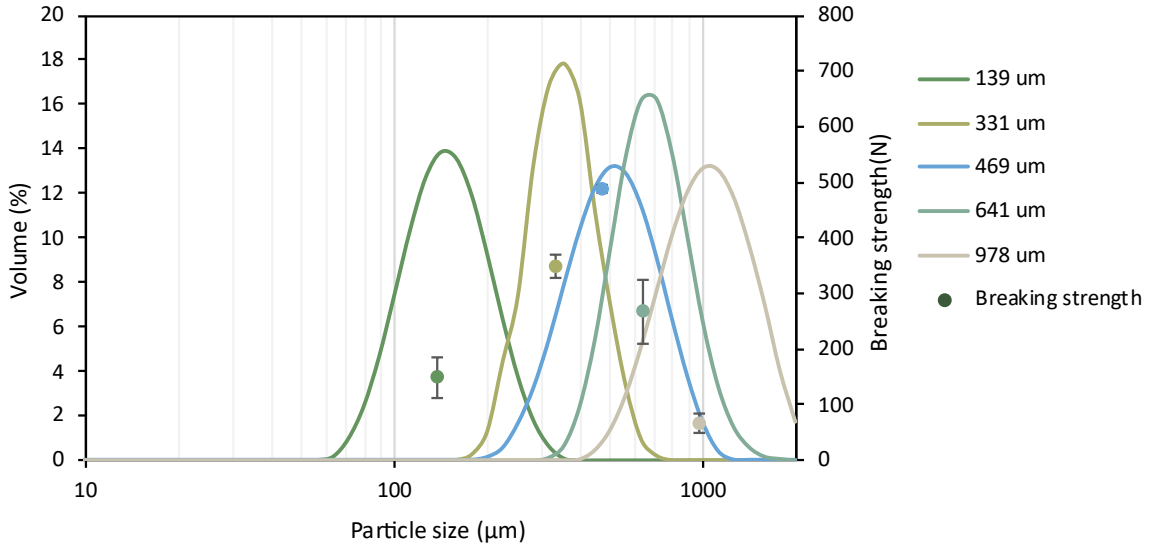

Figure 5.6: Particle size distribution of various aggregate mixtures labelled with their respective D_{50} and the effect on breaking strength. Breaking strength is shown for the respective D_{50}. Error bars represent standard deviation of n = 4 tiles.

The most effective PSD has a D_{50} of 469 µm and results in the highest breaking strength of 489 ± 6 N. This group, the unsieved sand, had a D_{10} of 304 µm, which is almost double the D_{10} recommended by Rahman and Hora (2017). The group has one of the wider PSDs investigated in this study, while containing neither very fine nor very coarse grains, making it a relatively well graded aggregate and confirming previous findings that medium-sized grains facilitate favourable MICP (Mortensen *et al.*, 2011). Rahman *et al.* (2020) reviewed a wide range of literature on MICP and found that UCS displayed high variability due to the variation in soil particle size and shape between studies. Furthermore, they showed that generally larger particle sizes (up to a D_{10} of 650 µm) need a smaller amount of $CaCO_3$ deposited to achieve a greater UCS.

De Oliveira *et al.* (2021) found that when the D_{50} of the aggregate was below 100 µm, even when using inert sand, the bio-column formed a thin bio-cemented crust. However, their results did not indicate the effect of fines in a broad well-graded group. In order to test this, the 1:1 mixture was passed through a 150 µm sieve, and particles remaining on the sieve were used for the experiment. This group

was compared to a 1:1 group that was not passed through the sieve, and therefore, contained fines. The PSD for a 1:1 mixture with less and more fines and the breaking strength of each is given in Figure A.2.

This study shows that the inclusion of too many particles smaller than 400 µm in the aggregate mixture have a negative effect on the breaking strength of bio-tiles (Figure A.2). The breaking strength of the mixture with fines smaller than 150 µm had a breaking strength 4.55 times greater than that of the mixture that contained a greater amount of larger fines (84 N). The "more fines" group also had larger particles, with no particles smaller than 126 µm however, at 224 µm the amount of fines in this group exceeded the amount in the group with less fines. These groups had 10.4% and 8.1% of the mass of particles that were smaller than 400 µm, respectively. When a large amount of fines is included, they reduce the porosity (Table A.1) and therefore, the permeability of the aggregate, causing the reaction to be hindered by poor transport of reagents and oxygen for the aerobic bacteria resulting in poor solidification of the bio-tiles. Additionally, the breaking strength of the bio-tiles using the unsieved sand performed better than using a 1:1 ratio of sand and Greywacke. Lambert and Randall (2019) found that a 1:1 ratio worked well for bio-bricks, but they used a pumping technique to grow the bio-bricks and the thicker form factor of bio-bricks may contribute differently to the interplay of forces under compression for a PSD as wide as the 1:1 mixture and with D_{50} of 810 and 825 µm, respectively. While interlocking of particles in a well-graded aggregate is considered preferable in the construction of bricks, for tiles, the well-graded particle size range needs to be specified to a smaller size. It is possible that thinner bio-tiles require smaller void spaces such that a higher density of $CaCO_3$ can be achieved throughout the volume of aggregate.

5.3.5 *Impact of the volume of cementation solution on breaking strength*

The volume of cementation solution in the bio-reactor was found to influence the breaking strength (Figure 5.7A). While first investigated to improve the overall efficiency of calcium utilisation (81% for 14 L bio-reactor), a greater volume of cementation solution was shown to improve the breaking strength of the bio-tiles, to a point. The utilisation of the mass of calcium is shown in Figure 5.7B.

When using a volume of 15.7 L and a cementation solution concentration of 0.3 M to grow four bio-tiles at the same time, a maximum breaking strength of 546 ± 38 N was recorded. This resulted in a 63% calcium utilisation within the bulk liquid. For a concentration of 0.2 M, the peak breaking strength (407 ± 28 N) occurred at a volume of 17.8 L, resulting in a calcium utilisation of 61%.

We have established that the most favourable equimolar concentration of the cementation solution is 0.3-0.5 M. The amount of $CaCO_3$ precipitated is directly proportional to the calcium concentration present, as the formation of $CaCO_3$ is first order with respect to the calcium concentration (Murugan *et al.*, 2021). However, the bacteria and dynamics of $CaCO_3$ precipitation are also affected by other factors as discussed previously (Rahman *et al.*, 2020).

During the course of the reaction, the calcium concentration decreases while increasing the amount of ammonium ions formed, and hence the ionic strength of the solution. In particular, during the first two days, the calcium concentration of a 14 L reactor decreased from 0.3 to 0.12 M, a 60% decrease. One reason why a larger volume of 0.3 M cementation solution could produce stronger bio-tiles is because when the volume is greater, the total utilisation remains similar, resulting in a smaller total concentration change. Therefore, the instantaneous concentration of calcium will be greater in reactors with a larger volume at each point in time as the reactions progress. The presence of a more

favourable concentration of calcium for a longer period of time positively impacts the reactions and dynamics of $CaCO_3$ precipitation, especially during the particularly active first two to three days, allowing the formation of $CaCO_3$ crystal bindings that are more uniform and compact. This trend continues until the end of the experiment where the reactor with the greater volume contains a greater concentration of calcium. The precipitation of $CaCO_3$ is driven by a higher concentration of calcium throughout the duration of the reaction. However, this is not the full explanation, as there was a maximum in the volume found that resulted in the greatest breaking strength, so an infinitely greater volume is not advantageous. Additionally, it would be expected that a greater volume would result in a greater utilisation of calcium overall due to the higher calcium concentration throughout the reaction period driving the reactions (Rahman & Hora, 2017; Zhao *et al.*, 2014b), yet this was not observed (Figure 5.7B). When comparing Figure 5.7A and Figure 5.7B, it can be seen that a greater mass of calcium utilisation does not correlate with a greater strength within a concentration group, as there is a peak of breaking strength at 76 g and 107 g for 0.2 M and 0.3 M, respectively (Figure A.3) and greater utilisations relate to lower strengths.

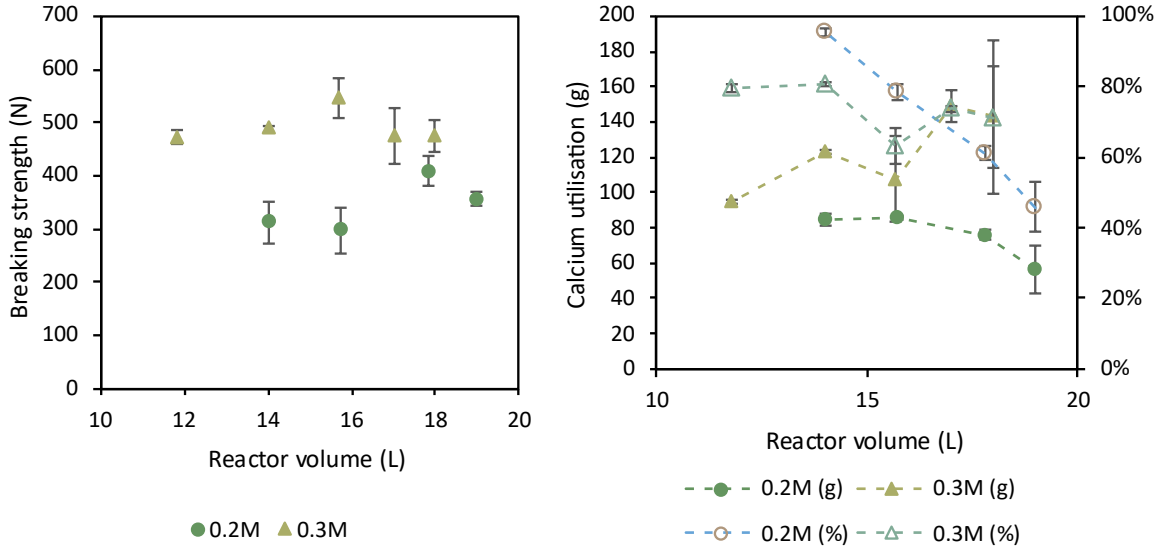

Figure 5.7: The change in breaking strength (A) and calcium utilisation (B) as a result of varying the volume of cementation solution in the bio-reactor. Error bars represent standard deviation of n = 4 tiles.

Unfortunately, a greater volume with an unchanging utilisation in the mass of calcium causes the fraction of calcium utilised to decrease, which results in a reaction with poor usage efficiency and a wastage of reagents. It would be challenging to reuse the cementation solution, as an appropriate amount of additional calcium could be added to the solution once more. However, the progressive build-up of ammonium ions with time would increasingly inhibit the bacteria. It is recommended that ways of recovering the calcium in the solution be investigated in future work.

5.3.6 *Effect of magnesium concentration on parameters*

Anhydrous magnesium chloride was added to the cementation solution to determine its effect on breaking strength. There was a peak breaking strength (620 ± 112 N) at a magnesium concentration of 0.3 M (Figure 5.8), which meets the breaking strength standard of 600 N. This was 21% higher than without magnesium supplementation. However, the error of this data set was very wide (112 N, n =

3). One of the bio-tiles in this group also had a breaking strength of 766 N, 28% above the standard. The effect of magnesium on the breaking strength is significant, and optimisation and reduction of this error should be the focus of future work.

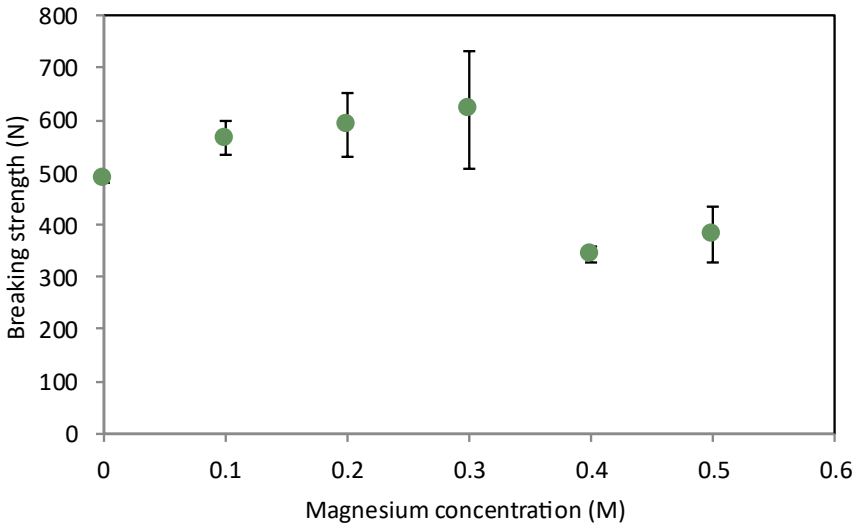

Figure 5.8: The change in breaking strength due to increasing concentrations of magnesium chloride. Error bars represent standard deviation of number of bio-tiles tested, n = 4.

A significant decrease in breaking strength occurs at magnesium concentrations greater than 0.3 M. Xu *et al.* (2020) found that the interaction of magnesium ions in the cementation solution can enhance the physical properties of bio-cemented materials. The authors found that the incorporation of magnesium ions influenced the crystal polymorph, promoting the formation of aragonite while inhibiting calcite growth. The XRD analysis of the optimised bio-tile in the presence of 0.3 M magnesium identified aragonite (73.9 ± 0.4%) in greater proportion than calcite (26.1 ± 0.4%) for the $CaCO_3$ present, while for the experiment with no supplemental magnesium, the proportions of aragonite and calcite were 16.7 ± 0.6% and 83.3 ± 0.4%, respectively. The diffractograms are shown in the Appendix, in Figure A.4 and Figure A.5. Comparison of the SEM images also show a clear shift toward aragonite crystal structures when $CaCO_3$ precipitation occurs in the presence of 0.3 M magnesium (Figure A.6). Aragonite has a Mohs hardness of 3.5-4 while calcite and vaterite are 3 on the Mohs hardness scale (Seifan & Berenjian, 2018), where the Mohs hardness is a measure of the resistance of a smooth surface to scratching or abrasion. In addition to this, aragonite has a higher density (2.95 g/cm^3) than both calcite (2.71 g/cm^3) and vaterite (2.64 g/cm^3) (Xu *et al.*, 2020), allowing the formation of a greater amount of $CaCO_3$ per unit volume and therefore, a stronger bio-material. Putra *et al.* (2016a) used magnesium as an agent that delays the $CaCO_3$ precipitation reaction rate, reducing the size of the precipitated crystals, increasing their density as aragonite forms instead of calcite, thus making the crystals more compact. This aligns with the findings in this research. Xu *et al.* (2020) showed that an additional 0.01 M of magnesium contributed to a 40% higher UCS (Xu *et al.*, 2020). Although these authors identified that UCS doubled further when the magnesium concentration was 0.5 M, findings by Gawwad *et al.* (2016) demonstrate that the UCS of bio-cemented samples decreased with an increase in magnesium ions to 0.5 M due to transformation of the crystal type from $CaCO_3$ to $MgCO_3$, likely due to differences in solubilities of the two compounds. This should be investigated further. Therefore, the formation of $MgCO_3$ over $CaCO_3$ combined with increased ionic

strength inhibiting the bacteria causes high concentrations of magnesium to have adverse effects on the breaking strength of bio-tiles. However, in smaller amounts (0.3 M), the XRD analysis presented no $MgCO_3$ formation and hence, magnesium was beneficial to the strength properties of bio-tiles.

5.3.7 *Calcium carbonate precipitation rate constants for different parameters*

Our results have shown that multiple parameters can affect the breaking strength of bio-tiles Ultimately, it is the rate of $CaCO_3$ precipitation that ultimately affects the breaking strength (Figure 5.9). Each of the parameters had a different effect on the rate constant, however, all parameters followed first order rate kinetics (Equation 9).

$$-r_{precipitation\ of\ CaCO3} = -\frac{dC_{Ca}}{dt} = kC_{Ca} \quad (9)$$

Where $-r_{precipitation\ of\ CaCO3}$ = rate of precipitation reaction [g/L·day]

C_{Ca} = concentration of Ca^{2+} [g/L]

k = rate constant [day^{-1}]

t = time for the reaction to occur [day]

The $CaCO_3$ precipitation rate constant decreased with increasing concentration of cementation solution (Figure A.7 and Table A.3). The Nash-Sutcliffe efficiency (NSE) of the linear relationship in each of these experiments ranged from 0.73 to 0.94, with an average of 0.84. The rate constant did not have a distinct effect on the breaking strength with respect to the cementation solution concentration, except the highest rate constant (0.452 day^{-1}), resulting in the one of the lowest breaking strengths with 0.2 M (312 N). This indicates that a rate constant that is too high has a negative effect on the breaking strength.

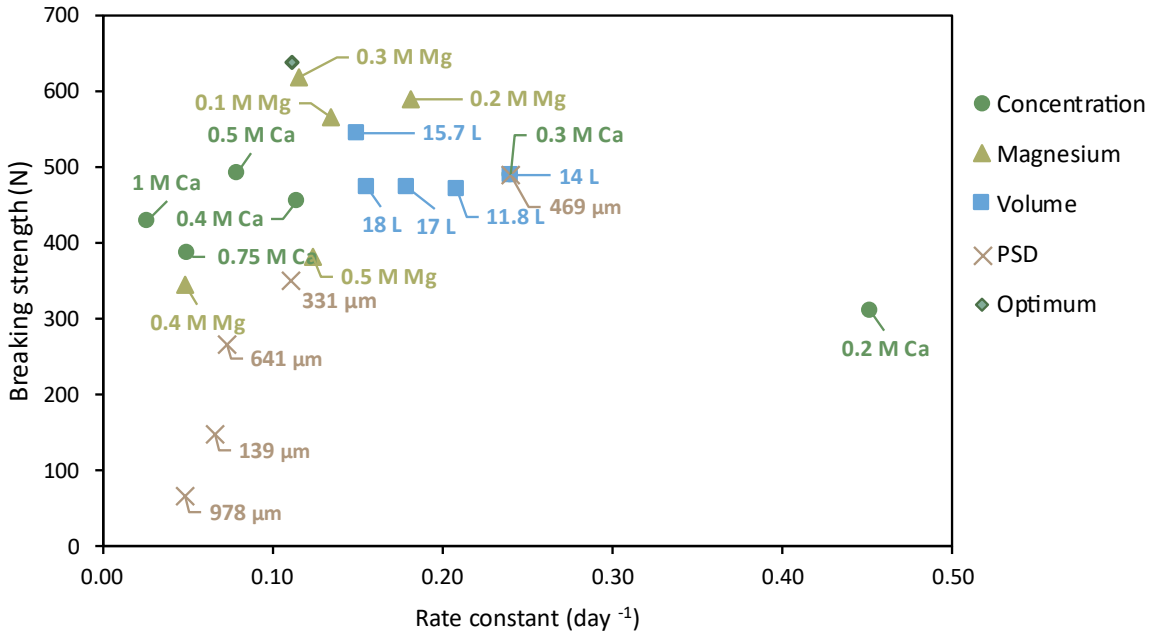

Figure 5.9: Relationship of the $CaCO_3$ precipitation rate constant to the breaking strength of the bio-tiles. 'Optimum' refers to the experiment combining magnesium supplementation (0.3 M) with the best-performing volume of cementation solution identified (15.7 L), other tuned parameters of cementation solution concentration and PSD were already incorporated into both magnesium supplementation and cementation solution volume experiment sets.

The rate constants obtained for different cementation solution volumes (average NSE = 0.89) vary between 0.15-0.24 day^{-1} with little change in breaking strength and the greatest breaking strength (546 N) occurring at the lowest rate constant (0.15 day^{-1}) (Figure 5.9). There is also no consistent trend over changing volume, where 15.7 and 18 L have similar rate constants (0.150 and 0.155 day^{-1}, respectively), but they have almost the greatest difference in breaking strength in the group (546 and 473 N, respectively). Varying the magnesium concentration resulted in $CaCO_3$ precipitation rate constants of 0.05-0.18 day^{-1} with the highest NSE values of 0.95-0.99 amongst all parameters tested (Table A.3). This confirms the findings of Putra *et al.* (2016a) in that magnesium successfully slowed the reaction rate (measured using the evolution of pH as a proxy) and can therefore be used as a delaying agent. The rate constants were higher at lower concentrations of magnesium, peaking at 0.2 M, decreasing sharply and finally increasing slightly at 0.5 M (Figure A.7). The breaking strength followed a similar pattern, but with a peak at 0.3 M magnesium. Generally, these results show that a magnesium concentration above 0.3 M has a negative effect on the breaking strength.

Figure 5.9 illustrates that the rate constant cannot be too high or too low and that there is an ideal range of rate constants that results in the highest breaking strengths. The ideal rate constant should be around 0.11-0.18 day^{-1} to ensure that the breaking strength of the bio-tiles is within the green region of the design chart developed in this study. There are multiple ways of achieving and controlling the rate constant and there are also likely other parameters that affect it that were not investigated in this study. The key parameters affecting the rate constant are concentration of magnesium and volume of cementation solution (Figure 5.9).

The rate constants determined in this study are all lower than those reported in literature, albeit due to different conditions, foremost of which is that values from literature are from flask systems, not the formation of a bio-material. The $CaCO_3$ rate constants identified by Wen *et al.* (2020) are within the same order of magnitude of this study at 0.648-1.152 day^{-1}, while Murugan *et al.* (2021) found rate constants as high as 15.36-18.72 day^{-1}.

5.3.8 *Combining the best performers across all parameters*

This study has shown that each of the parameters investigated can be tuned for the growth of stronger bio-tiles using the submersion technique. Unsieved dune sand was the default aggregate used for all experiments and was found to have the empirically determined best-performing PSD to produce the highest breaking strength of all PSD groups tested (Section 3.4). A ureolytic activity of 4.0 mmol/L·min was used (Section 3.2) for all experiments together with an equimolar cementation solution concentration of calcium and urea of 0.3 M (Section 3.3). Therefore, a final experiment was carried out with all of these parameters in addition to combining the most effective cementation solution volume (15.7 L) with the best magnesium concentration (0.3 M). This resulted in bio-tiles with a breaking strength of 637 ± 60 N. This experiment had a rate constant of 0.112 day^{-1} (Figure 5.9), which is slightly lower than the 0.3 M magnesium experiment (0.116 day^{-1}) and also lower than the 15.7 L experiment (0.150 day^{-1}).

All bio-tiles, excluding the unused PSD experiment groups, had a $CaCO_3$ proportion of 36.7 ± 2.8%. The $CaCO_3$ proportion of the other PSD groups was not measured due to low breaking strengths and low calcium utilisations in the bulk liquid of 31-50%. Bio-tiles grown in the presence of magnesium had a slightly higher proportion of $CaCO_3$ (37.1 ± 2.7%, n = 17) than those with varying volumes (36.5 ± 3.1%, n = 17). The 'optimum' bio-tile had a $CaCO_3$ fraction that was still lower at 35.9 ± 0.5% (n=3). The bio-tiles grown in this study had a water absorption of 11.3 ± 0.5%.

The performance of the four key parameters on the design chart is shown in Figure 5.10 as well as the 'optimum' experiment. This indicates that the novel design chart can be used to aid the optimisation of the bio-tile process for a reference of where the produced bio-tile properties are in relation to the required standards.

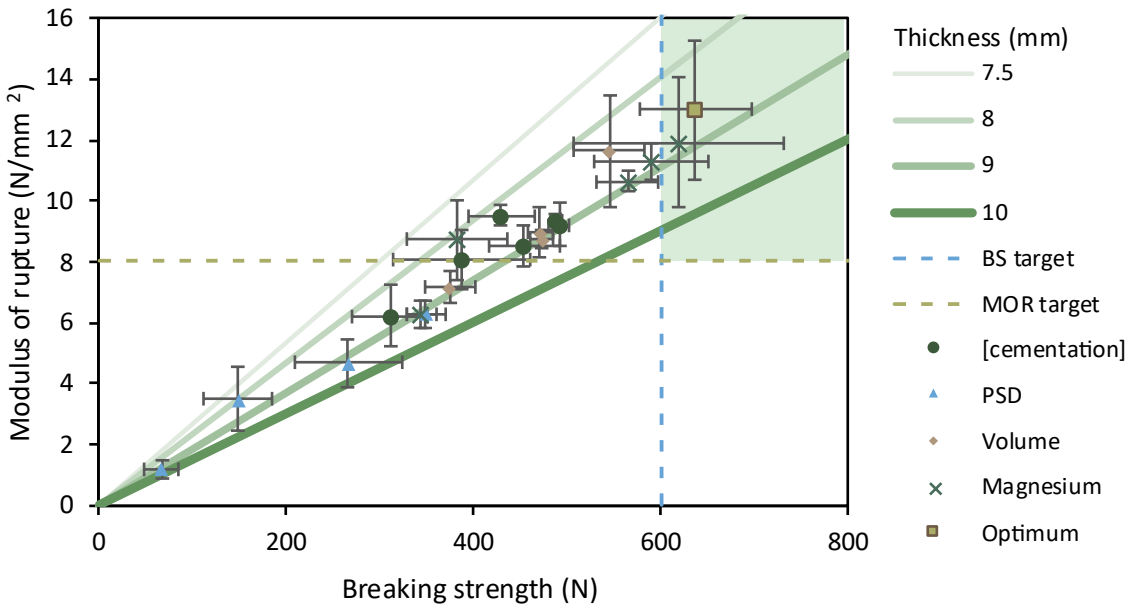

Figure 5.10: Design chart depicting the data for each of the four key parameters tested with diagonal lines showing the minimum thickness (mm) along the broken edge of the bio-tile and the breaking strength (n = 4) and modulus of rupture (MOR) targets to be met. 'Optimum' refers to the experiment combining magnesium supplementation (0.3 M) with the best-performing volume of cementation solution identified (15.7 L), other tuned parameters of cementation solution concentration and PSD were already incorporated into both magnesium supplementation and cementation solution volume experiment sets.

The white region indicates where neither or one of the targets are met and the green region indicates where both the breaking strength and modulus of rupture targets are met.

When the effects of magnesium supplementation are combined with greater volumes of cementation solution, bio-tiles that can consistently meet the modulus of rupture standard are produced. These bio-tiles also meet the breaking strength standard the majority of the time as the error is 60 N while the average is 637 N. Images of the bio-tiles can be seen in Figure A.8. To our knowledge, this is the first time that bio-tiles have been produced using the submergent technique while also investigating holistically the link between key operating parameters and the rate of $CaCO_3$ precipitation.

5.4 Conclusions

This research has shown for the first time that bio-tiles grown using MICP and a submersion technique can achieve a breaking strength and modulus of rupture that meets international standards, provided key conditions are met. A novel design chart was constructed that shows what parameters and operating conditions are important for meeting the standards. It was found that all the bio-tiles produced with a cementation concentration of 0.3 M and dune sand had a water absorption of 11.3 ± 0.5% and a $CaCO_3$ proportion of 36.7 ± 2.8%. An equimolar concentration of calcium and urea of 0.3 M

was found to achieve sufficient breaking strength, as did increased concentrations of cementation solution. However, to reduce input costs, it is recommended that an equimolar concentration of 0.3 M of calcium and urea be used. While a wide PSD with an average size of 469 µm resulted in bio-tiles with the highest breaking strength (489 ± 6 N) and modulus of rupture (9.3 ± 0.3 N), these bio-tiles did not meet the strength standard, however, other PSDs that were larger and smaller on average were at most 71% of this strength. A greater volume of cementation solution that decreases the overall utilisation of calcium in the bulk to around 62% was found to have a positive impact on the breaking strength (546 ± 38 N), even though this resulted in significant loss of reagents. The most beneficial concentration of magnesium was found to be 0.3 M and achieved a breaking strength of 620 ± 112 N, 21% higher than without. This improvement in breaking strength was due to magnesium slowing the reaction and promoting the formation of the aragonite polymorph over calcite. It was also shown that slower $CaCO_3$ precipitation rate constants resulted in stronger bio-tiles than faster rate constants, and the rate constant needs to be within 0.11-0.18 day^{-1} to produce bio-tiles with the highest breaking strengths. Combining the most effective volume (15.7 L) with the best magnesium concentration (0.3 M), bio-tiles with a breaking strength of 637 ± 60 N and a modulus of rupture of 13.0 ± 2.3 N/mm^2 were produced, exceeding conventional tile manufacturing standards.

References

A. Al Qabany, K. Soga & C. Santamarina. 2012. Factors affecting efficiency of microbially induced calcite precipitation. *Journal of Geotechnical and Geoenvironmental Engineering.* 138(8):992-1001. DOI:10.1061/(asce)gt.1943-5606.0000666.

P. Anbu, C.H. Kang, Y.J. Shin & J.S. So. 2016. Formations of calcium carbonate minerals by bacteria and its multiple applications. *SpringerPlus.* 5:1-26. DOI:10.1186/s40064-016-1869-2.

L. Cheng, T. Kobayashi & M.A. Shahin. 2020. Microbially induced calcite precipitation for production of “bio-bricks” treated at partial saturation condition. *Construction and Building Materials.* 231(117095):1-9. DOI:10.1016/j.conbuildmat.2019.117095.

Q. Chunxiang, W. Jianyun, W. Ruixing & C. Liang. 2009. Corrosion protection of cement-based building materials by surface deposition of CaCO3 by Bacillus pasteurii. *Materials Science and Engineering: C.* 29(4):1273-1280. DOI:10.1016/j.msec.2008.10.025.

O.A. Cuzman, K. Richter, L. Wittig & P. Tiano. 2015. Alternative nutrient sources for biotechnological use of *Sporosarcina pasteurii*. *World Journal of Microbiology and Biotechnology.* 31(6):897-906. DOI:10.1007/s11274-015-1844-z.

D. De Oliveira, E.J. Horn & D.G. Randall. 2021. Copper mine tailings valorization using microbial induced calcium carbonate precipitation. *Journal of Environmental Management.* 298:113440. DOI:10.1016/j.jenvman.2021.113440.

H.A. Gawwad, S.A.E.-A. Mohamed & S.A. Mohammed. 2016. Impact of magnesium chloride on the mechanical properties of innovative bio-mortar. *Materials Letters.* 178:39-43. DOI:10.1016/j.matlet.2016.04.190.

C.M. Gorospe, S.H. Han, S.G. Kim, J.Y. Park, C.H. Kang, J.H. Jeong & J.S. So. 2013. Effects of different calcium salts on calcium carbonate crystal formation by *Sporosarcina pasteurii* KCTC 3558. *Biotechnology and Bioprocess Engineering.* 18(5):903-908. DOI:10.1007/s12257-013-0030-0.

ISO. 2018. *ISO 13006:2018: Ceramic tiles - definitions, classification, characteristics and marking*. Available: https://www.iso.org/standard/63406.html.

G. Kim, J. Kim & H. Youn. 2018. Effect of temperature, pH, and reaction duration on microbially induced calcite precipitation. *Applied Sciences.* 8(8):1277. DOI:10.3390/app8081277.

S.E. Lambert & D.G. Randall. 2019. Manufacturing bio-bricks using microbial induced calcium carbonate precipitation and human urine. *Water Research.* 160:158-166. DOI:10.1016/j.watres.2019.05.069.

B.M. Mortensen, M.J. Haber, J.T. DeJong, L.F. Caslake & D.C. Nelson. 2011. Effects of environmental factors on microbial induced calcium carbonate precipitation. *Journal of Applied Microbiology.* 111(2):338-349. DOI:10.1111/J.1365-2672.2011.05065.X.

R. Murugan, G.K. Suraishkumar, A. Mukherjee & N.K. Dhami. 2021. Influence of native ureolytic microbial community on biocementation potential of *Sporosarcina pasteurii*. *Scientific Reports.* 11(20856):1-12. DOI:10.1038/s41598-021-00315-5.

M. Nemati, E.A. Greene & G. Voordouw. 2005. Permeability profile modification using bacterially formed calcium carbonate: comparison with enzymic option. *Process Biochemistry.* 40(2):925-933.

H. Putra, H. Yasuhara, N. Kinoshita, D. Neupane & C.-W. Lu. 2016. Effect of magnesium as substitute material in enzyme-mediated calcite precipitation for soil-improvement technique. *Frontiers in Bioengineering and Biotechnology.* 4:37-37. DOI:10.3389/fbioe.2016.00037.

M.M. Rahman & R.N. Hora. Eds. 2017. Unconfined compressive strength of microbial induced calcite precipitation (MICP) treated soils | ISSMGE. Seoul: International Society for Soil Mechanics and Geotechnical Engineering (ISSMGE).

M.M. Rahman, R.N. Hora, I. Ahenkorah, S. Beecham, M.R. Karim & A. Iqbal. 2020. State-of-the-art review of microbial-induced calcite precipitation and its sustainability in engineering applications. *Sustainability.* 12(15):6281-6281. DOI:10.3390/su12156281.

M.A. Rivadeneyra, G. Delgado, M. Soriano, A. Ramos-Cormenzana & R. Delgado. 2000. Precipitation of carbonates by *Nesterenkonia halobia* in liquid media. *Chemosphere.* 41(4):617-624. DOI:10.1016/S0045-6535(99)00496-8.

M. Seifan & A. Berenjian. 2018. Application of microbially induced calcium carbonate precipitation in designing bio self-healing concrete. *World Journal of Microbiology and Biotechnology.* 34:168-168. DOI:10.1007/s11274-018-2552-2.

K. Wen, Y. Li, F. Amini & L. Li. 2020. Impact of bacteria and urease concentration on precipitation kinetics and crystal morphology of calcium carbonate. *Acta Geotechnica 2019 15:1.* 15(1):17-27. DOI:10.1007/S11440-019-00899-3.

X. Xu, H. Guo, X. Cheng & M. Li. 2020. The promotion of magnesium ions on aragonite precipitation in MICP process. *Construction and Building Materials.* 263(120057):1-9. DOI:10.1016/j.conbuildmat.2020.120057.

Q. Zhao, L. Li, M. Asce, C. Li, M. Li, F. Amini, F. Asce & H. Zhang. 2014. Factors affecting improvement of engineering properties of MICP-treated soil catalyzed by bacteria and urease. *Journal of Materials in Civil Engineering.* 26(12):1-10. DOI:10.1061/(ASCE)MT.1943-5533.

6 Production of bio-tiles using the pumping technique

This chapter describes the findings of the second study on bio-tiles grown with MICP using a pumping technique. The bio-tiles produced with the submersion technique were able to meet international breaking strength standards. However, the results showed minimal operational tolerance, potentially impacting performance for adjustments made at scale. Therefore, a more active flow-through production method, the pumping technique, was tested. During trials, at the end of the reaction, it was observed that the geotextiles were saturated with $CaCO_3$ crystals. Crystallisation theory suggests that seeding the reaction with $CaCO_3$ seeds could aid further $CaCO_3$ precipitation. The key area of investigation of the study was to quantify the effect of $CaCO_3$ seed loading on the strength of bio-tiles, as well as bacteria activity and the retention time of each treatment cycle. Specific objectives as well as materials and methodology specific to the pumping technique are outlined and the results discussed.

Chapter 6 is derived on the second paper published in connection to this work, *Seeding improves the strength of bio-tiles grown with microbially induced calcium carbonate precipitation*.

6.1 Objectives

The key objective of this study was to assess the effect seeding with $CaCO_3$ crystals has on the strength properties of bio-tiles produced with a pumping technique. Additional objectives were to investigate how the breaking strength of bio-tiles produced with the pumping technique is affected by:

1. The bacteria activity; and
2. The treatment cycle duration.

6.2 Materials and methods

6.2.1 *Bio-tile pumping technique set up and procedure*

Moulds were designed in which the bio-tile (100 x 100 x 10 mm) was situated horizontally, and the solution was pumped in from beneath the flat (100 x 100 mm) surface of the tile. The moulds had one inlet and one outlet, offset from each other in opposite corners (Figure 6.1). Before each experiment, the moulds and pipes were cleaned with 0.1 M HCl solution. The walls of the moulds were coated with petroleum jelly and lined with clear acetate for easy removal of the bio-tile from the chamber.

The concentrated suspension of *S. pasteurii* was mixed into an appropriate amount of unsieved dune sand (Cape Flats, Cape Town) with the best-performing particle size distribution (PSD) previously identified by Horn *et al.* (2023) to achieve a 75% saturation of the pore space. The colonised sand was packed into the moulds and compacted between non-woven needle-punched geotextile (the same geotextile as that used by Lambert and Randall (2019) for their pumping system) and 15 mm thick foam, ensuring the bacteria had 3-4 hours of colonisation time before the first feeding. The thicker geotextile compared to that used in the submersion technique experiments allowed better retention of the colonised sand inside the mould during pumping and for a wide range of $CaCO_3$ seed loadings to be possible.

A 4-head Jebao 3.4 Wi-Fi dosing pump (Jebao, Zhongshan City, China) was programmed and used for the pumping requirements. Each pump was calibrated to administer a dosage of 110 ± 3 mL of cementation solution. This volume was calculated from the pore space of the aggregate (0.27) (Table A.1) and foam (0.75) (Lambert & Randall, 2019). The cementation solution consisted of 0.3 M calcium chloride dihydrate and 0.3 M urea. This cementation solution was retained in the mould for a stipulated time (retention time) and then fresh cementation was pumped in again, displacing the spent solution. These treatments are repeated for the duration of the experiment, usually 4 days.

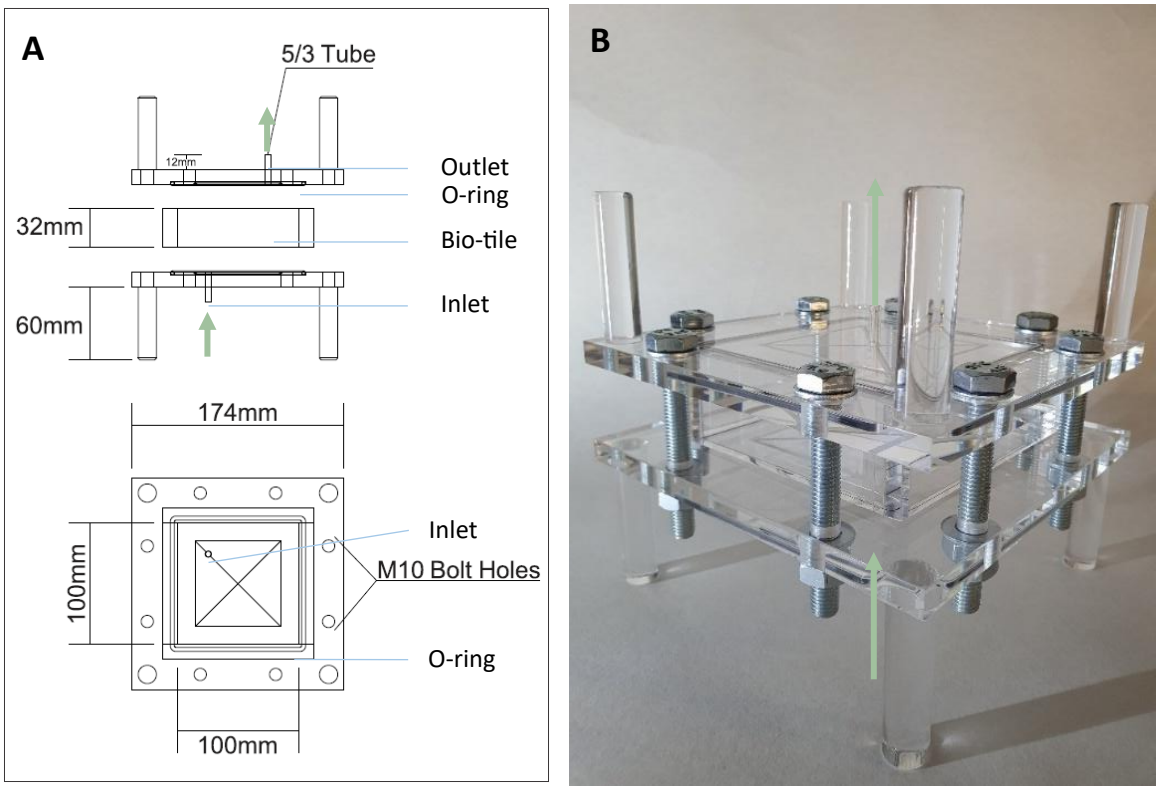

Figure 6.1: A) Schematic and B) photograph of pumping moulds used for bio-tiles (100 x 100 mm). Inlet and outlet directions shown with arrows.

When performed, sampling was carried out one, two or three minutes before the next feed for reactors A, B and C, respectively. A Y-splitter with an attached syringe was used to sample the reactor contents at the inlet feed port. The feed pipe was kinked to prevent fresh feed being pulled into the sample. After discarding the first approximate 2 mL of sample considered to be fresh feed from between the syringe and mould inlet, accounting for the dead volume of the tube, 10-16 mL of sample was extracted and diluted in for concentration analysis.

Daily inversion of the bio-tile mould and swapping of the inlet and outlet ports was part of the standard method based on the study by Lambert and Randall (2019). Unless otherwise stated, each experiment was carried out for four days.

To measure the effect bacteria concentration and activity have on breaking strength, three different concentrations were assessed: 8, 16 and 40 mmol NH_4-N/L·min. These experiments were run for two days in triplicate with one inversion of the bio-tile mould occurring at 24 h. The effect of treatment cycle duration on breaking strength was measured through testing 1, 2 and 4 h retention times. These experiments were run for four days and inverted daily.

6.2.2 *Bio-tiles grown with different materials seeded with calcium carbonate and the effect of mould inverting*

In previous experiments, inversion of the bio-tile mould, where inlet and outlet ports were switched and the mould turned upside-down, was usually carried out daily. Instead, the effect of a single inversion that was performed after the first treatment was measured through the monitoring of calcium utilisation over four days. Following this, the influence of pre-seeding with $CaCO_3$ on the utilisation of calcium was quantified. Dry foam and geotextile recovered from previous bio-tile pumping experiments containing $CaCO_3$ seeds were compared to each other. The mould was inverted

after three treatments and calcium utilisation monitored for a further three treatments. Next, seeded geotextiles were used with unseeded foam and the mould was inverted after a single treatment and the effect on calcium utilisation and breaking strength was measured. Examples of seeded foam and geotextile used in seeding experiments are shown in Figure A.1.

6.2.3 *Bio-tiles grown with geotextiles containing different masses of calcium carbonate seeds*

The influence of the mass of $CaCO_3$ seeds on breaking strength was also evaluated. The loading of the bio-tiles with seeds was carried out through the utilisation of geotextiles impregnated with seeds in place of the fresh geotextiles which lined both flat edges of the bio-tile. Therefore, the seeding took place at the 100 x 100 mm surfaces of the bio-tiles. Geotextiles with different masses of $CaCO_3$ seeds were obtained through multiple MICP treatments of separate geotextiles. The geotextiles were soaked in bacteria solution concentrated to 40 mmol NH_4-N/L·min for three hours using 5 mL bacteria per geotextile. The inoculated geotextiles were then immersed in cementation solution for two hours and drained. To obtain different masses of seeds, sets of geotextiles were subjected to increased numbers of immersion treatments. Four different seed masses were investigated. For example, four treatments with 0.6 M cementation solution were performed to achieve 7.24 g seeds per geotextile or 0.072 g seeds per cm^2 geotextile. The pre-seeded geotextiles were then dried at 30°C until a stable weight was achieved and the mass of seeds compared to initial seed-free masses. The dried pre-seeded geotextiles were used in combination with unseeded foam to grow bio-tiles and the effect of seed mass on breaking strength was quantified.

To meet the objectives of the study, the parameters shown Table 6.1 in were investigated.

Table 6.1: Parameters investigated for improving calcium utilisation and breaking strength.

Parameter	Range or item	Unit
Bacteria activity	8, 16, 40	mmol NH_4-N/L·min
Retention time between treatments	1, 2, 4	h
Timing of mould inversion	1, 24	h
Materials seeded with $CaCO_3$ in previous bio-tile experiments	Geotextile, foam	-
Mass of $CaCO_3$ seeds in geotextiles	2.1, 6.9, 7.8, 14.5	g

6.2.4 *Alternative bio-tile aesthetic*

A shiny bio-tile surface was investigated with a vertical mould (Figure 6.2) with the 100 x 100 mm surfaces being flat and lined with petroleum jelly and transparent acetate. Seeded geotextile was used and inversion was performed after the first treatment only. The experiment was run for 4 days.

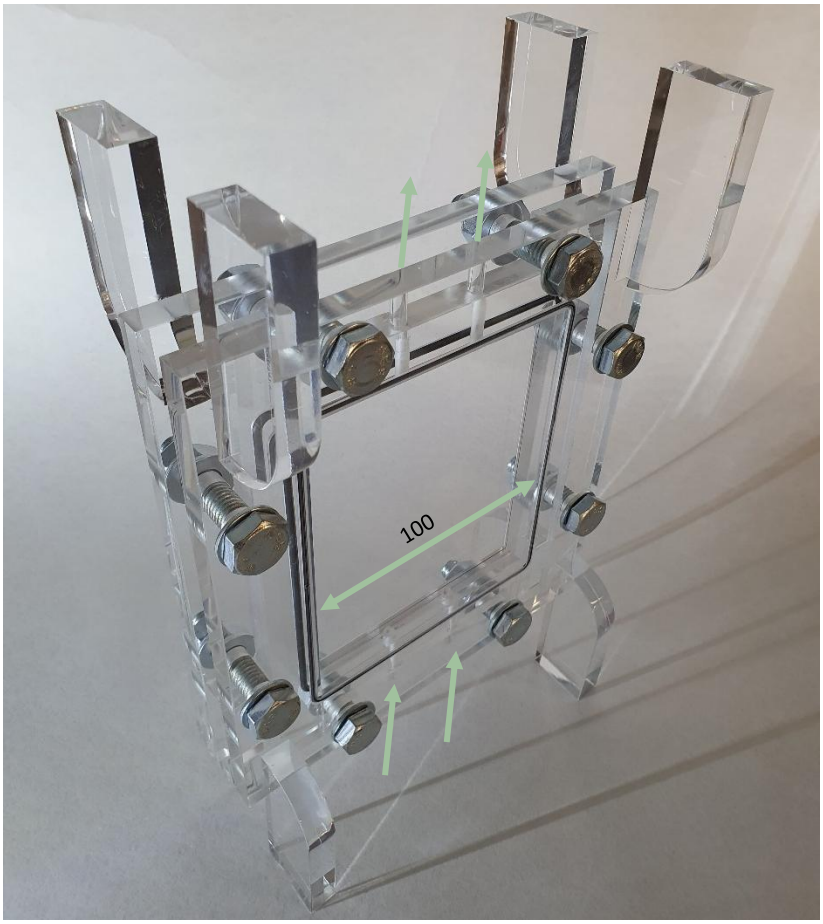

Figure 6.2: Pumping technique mould for bio-tile (100 x 100 mm) in a vertical position. The flat surfaces allow for the $CaCO_3$ precipitate to form smooth and reflective. Feed inlet was from below.

6.3 Results and discussion

6.3.1 *Influence of bacteria activity on bio-tile properties*

Bacteria activity has been found to significantly affect the strength of bio-tiles produced with the submersion technique (Figure 5.4) and therefore, bacteria activity was investigated with the pumping technique. In this reactor system, cementation solution was pumped through a mould periodically and consequently, had different fluid dynamics to a well-mixed batch reactor. The purpose of this initial experiment was not to necessarily achieve a breaking strength that meets the standards, but to determine the influence of bacteria activity on breaking strength. Therefore, to reduce the duration of the experiment, these bio-tiles were run for two days.

As in previous work (Horn *et al.*, 2023), to achieve a desired bacteria activity, the bacteria pellet from the centrifuge was diluted to a volume dependent on the measured ureolytic activity. This allowed the bacterial suspension to be many times more concentrated than when initially removed from the incubator, if desired. Seeing as ureolytic activity is directly proportional to bacteria concentration, ureolytic activity was taken as a proxy for bacteria concentration. Before centrifugation, the ureolytic activity was found to be 5.0-9.0 mmol NH_4-N/L·min and was then centrifuged and rehydrated with fresh media. It was found that the more concentrated the bacterial suspension was, the higher the breaking strength (Figure 6.3). This is contrary to previous findings (Figure 5.4), where an effective bacteria activity of 3.2-4.0 mmol/L·min was identified, and higher activities resulted in poorer breaking strengths. Higher urease activity is correlated to faster $CaCO_3$ precipitation rates (Wen *et al.*, 2020).

The precipitation rate is also a factor that controls the type of polymorph produced (Mitchell & Ferris, 2006), with small, less compact crystals forming at faster rates (Chunxiang *et al.*, 2009; Zehner *et al.*, 2021). Studies (Xiao *et al.*, 2020; Zheng *et al.*, 2020) have found that the resultant crystal size is dependent on the aggregate particle size, however, seeing as the same dune sand was used in previous submersion experiments (Horn *et al.*, 2023) as this study, there was another factor influencing the preferred bacteria activity. Regardless of the polymorph formed and the crystal size, there was a discrepancy in the bacteria activity which produced the strongest bio-tiles with the pumping technique (Figure 6.3) and submersion reactors (Figure 5.4). This indicates that bacteria activity is a key parameter that needs to be optimised for the specific reactor system being used.

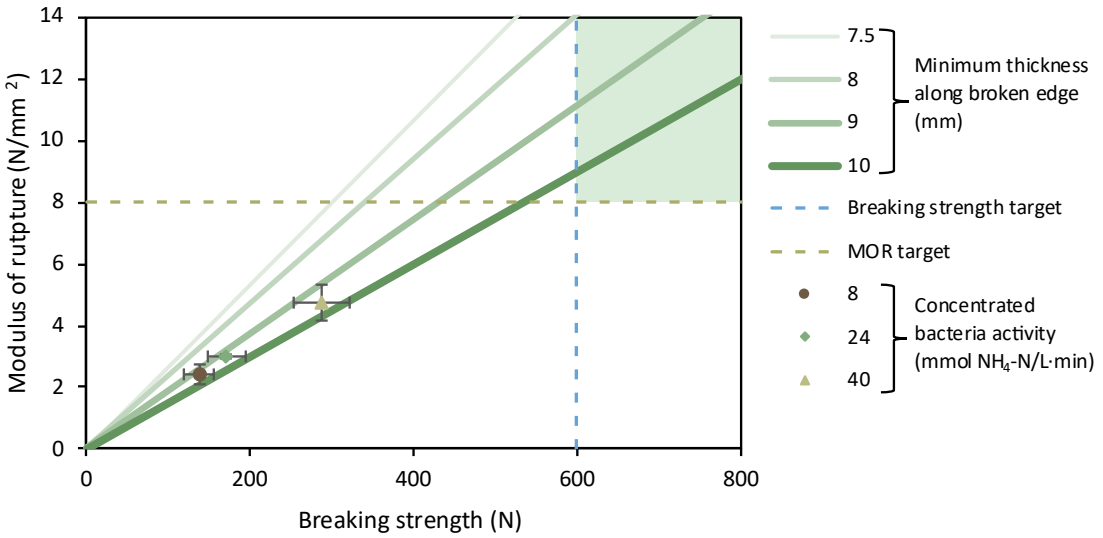

Figure 6.3: Bio-tile design chart showing the effect bacteria activity has on the breaking strength and modulus of rupture of bio-tiles after two days of reaction. Error bars represent the standard deviation of n = 3 bio-tiles. MOR = modulus of rupture.

Concentrated bacteria activities higher than 40 mmol NH_4-N/L·min were not feasible due to the volumes of bacteria solution required. Therefore, a concentrated bacteria activity of 40 mmol NH_4-N/L·min was used in the subsequent experiments.

The design chart (Figure 6.3), shows that when the breaking strength meets the standard for tiles with minimum thicknesses of 9-10 mm, the modulus of rupture will exceed the required standard. Modulus of rupture has a squared inverse dependence on the minimum thickness, with variations exhibiting a degree of randomness due to the influence of factors such as mould packing and surface imperfections. On the other hand, breaking strength shows a responsive increase or decrease to a given parameter. Breaking strength is a key parameter and was therefore used for determining the technical feasibility of the bio-tiles produced.

6.3.2 *Retention time that produces bio-tiles with the highest breaking strength*

The effect of retention time on breaking strength was investigated. Three different treatment cycles were programmed into the pump which in effect changed the retention time between treatments. Experiments were run in triplicate for four days, resulting in 96, 48 and 24 treatments for retention times of 1, 2 and 4 h. Therefore, lower cumulative amounts of cementation solution were delivered to reactors with longer retention times. While the retention time of four hours resulted in higher utilisations of calcium (72-88%) than the two hour (15-77%) and one hour retention times (6-47%) (Figure A.9), the effect of longer retention times on breaking strength was detrimental (Figure 6.4).

Lambert and Randall (2019) found that retention time generally had a small effect on the calcium utilisation, with the utilisation increasing from 86.0% for a retention time of one hour to 97.3% or greater for longer retention times.

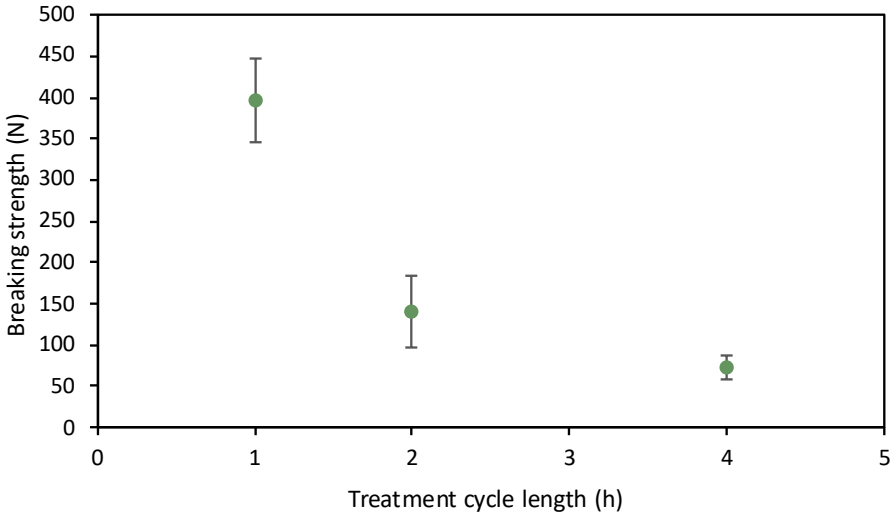

Figure 6.4: The effect of treatment cycle duration on the breaking strength of bio-tiles. Error bars indicate number of bio-tiles, $n_{1h} = 3$, $n_{2h} = 6$, $n_{4h} = 6$.

Shortening the retention time from four hours to one hour caused the breaking strength of the bio-tiles to increase 5.4 times, and from two hours to one hour resulted in a 2.8 times improvement in the breaking strength (Figure 6.4). Therefore, a treatment cycle duration of one hour was chosen and proceeded with for the following experiments.

6.3.3 *Effects of mould inversion and resultant seeding on breaking strength and calcium utilisation*

During the retention time experiments, it was observed that the standard method of inverting the mould and swapping inlet and outlet ports every 24 hours resulted in an improvement in calcium utilisation after the first inversion (Figure 6.5). Notably, inverting the mould again following the first inversion did not result in an improvement in calcium utilisation once more. It was hypothesised that inverting had a positive effect on the calcium utilisation due to seeding. Therefore, instead of waiting 24 hours to invert the mould, inversion was done as soon as possible, after one hour, and not again. When the inversion was performed at one hour, the reactors were able to reach calcium utilisations of 77.4%, compared to 47.0% when inverting at 24 hours (Figure 6.5). The improved utilisation with earlier inversion translated to an increase in breaking strength from 395 ± 51 N to 517 ± 43 N, indicating improvement in solidification and MICP efficiency of 31%, with respect to breaking strength. Therefore, inverting as soon as possible (after one hour) was integrated into the methodology going forward.

The clogging of pore volumes at the inlet site because of not changing the site of injection was a concern for Cheng and Cord-Ruwisch (2014) and Wang *et al.* (2022b), however, for bio-tiles grown with a pumping technique, any pore clogging or $CaCO_3$ depositions that occurred due to not inverting repeatedly were more beneficial than disadvantageous.

The $CaCO_3$ seeds deposited in the geotextile were most beneficial when the mould was inverted as early as possible, allowing calcium utilisation and $CaCO_3$ precipitation to be maximised in the following treatments. This is possibly due to the initial $CaCO_3$ crystals that form when the cementation solution

of the first treatment comes into contact with the inoculum that saturates the aggregate pore space. These early crystals encase the live bacteria which produce urease. Hence, urease active $CaCO_3$ crystals are formed (Cheng & Shahin, 2016). The desirable seeding effects likely occurred because urease active seeds not caught in the pore space of the aggregate were filtered through and caught in the geotextile and foam before being pumped out. In particular, when the bio-tile was inverted and these urease active seeds were at the inlet, underneath the bio-tile, the fresh cementation solution passed by them into the bio-tile and triggered additional $CaCO_3$ precipitation. This explanation is consistent with seed crystallisation in MICP (Zehner *et al.*, 2021).

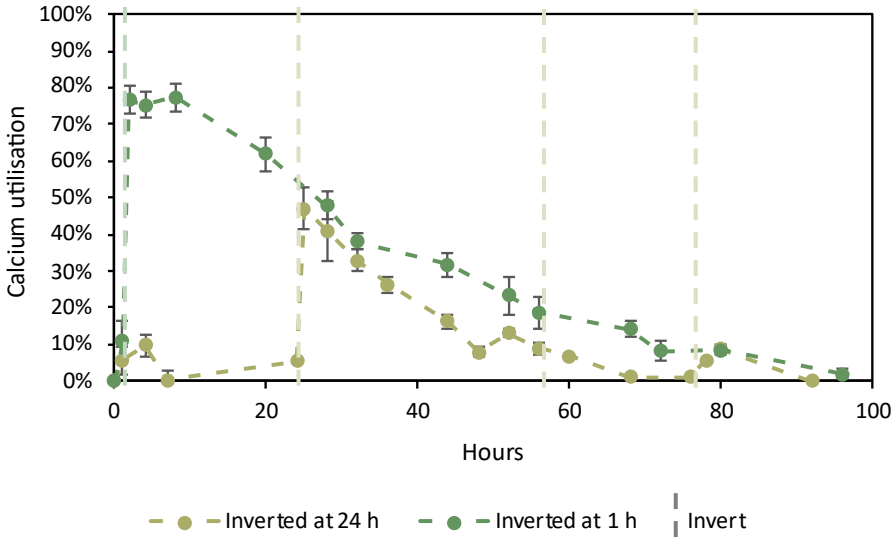

Figure 6.5: The effect mould inversion has on calcium utilisation over the course of the experiment. Error bars represent the standard deviation of number of bio-tiles tested, n = 3.

Furthermore, regardless of inversion after 24 hours or one hour, there was a decrease in calcium utilisation over time (Figure 6.5). Most literature covering MICP on the topic of kinetics shows ureolytic activity decreasing with time in a batch reactor system (Ferris *et al.*, 2004; Horn *et al.*, 2023; Murugan *et al.*, 2021). In pumping experiments by Lambert and Randall (2019), almost 100% efficiency was achieved throughout the two to four day experiment duration, however the authors generally used a four hour retention time and lower calcium concentrations of <0.13 M. Bacteria activity loss was more gradual for two and four hour than one hour retention times in the current study (Figure A.9) even though longer retention times unfortunately resulted in significantly decreased strength (Figure 6.4). Lambert and Randall (2019) found that higher calcium concentrations resulted in lower efficiencies because of increased ionic strength of the solution. When the calcium concentration was maintained at 0.13 M, there was a gradual decrease in calcium utilisation from 99% to 85%. This confirms that higher concentrations result in decreasing performance with time for the pumping technique, even for longer retention times. Considering the concentrations of calcium used in this study were 0.3 M, it follows that the loss in performance with time would have been more pronounced.

Meanwhile, inverting the mould earlier likely allowed the MICP reaction to better utilise the peak bacteria activity at the start of the experiment and thereby, increased calcium utilisations were obtained and resulted in improved strengths. Therefore, considering the benefits gained from using shorter retention times (Figure 6.4) and a higher concentration of 0.3 M (Figure 5.5) , further methods of improving the calcium utilisation needed to be explored to achieve a breaking strength higher than 600 N.

6.3.4 *Impact of pre-seeded materials on breaking strength*

The beneficial seeding effect induced through mould inversion was investigated further to see whether having external seeds present at the onset could further improve the MICP efficiency. The utilisation of foam seeded with $CaCO_3$ from a previous bio-tile experiment resulted in a reduced calcium utilisation efficiency (Figure A.10). However, the utilisation of geotextiles that had been seeded in a previous experiment resulted in an improvement in calcium utilisation before inverting (36-54% compared to 11%, Figure A.10), unlike when seeded foam was used (0% utilisation). Following inverting, seeded and unseeded geotextiles performed with similar utilisations, albeit about 10% greater for seeded geotextiles at some points (Figure A.10). It is likely that the pre-seeded geotextile in contact with the inoculated sand allowed some of the newly formed $CaCO_3$ to be washed into the pore space of the sand during feeding and this helped lower the activation energy of nucleation. However, the exact mechanism could not be determined with this set up and an additional study would be required to better understand this.

When inverting at one hour was combined with geotextile seeding, the breaking strength improved to over the required ISO standard of 600 N to 894 ± 32 N, from 517 ± 43 N for the bio-tiles grown with unseeded geotextile (Figure 6.6). This was an improvement of 73%. This confirmed that not only was pre-seeding of the geotextile crucial for improving the strength of bio-tiles, but the seeds added through inverting were still beneficial to the process.

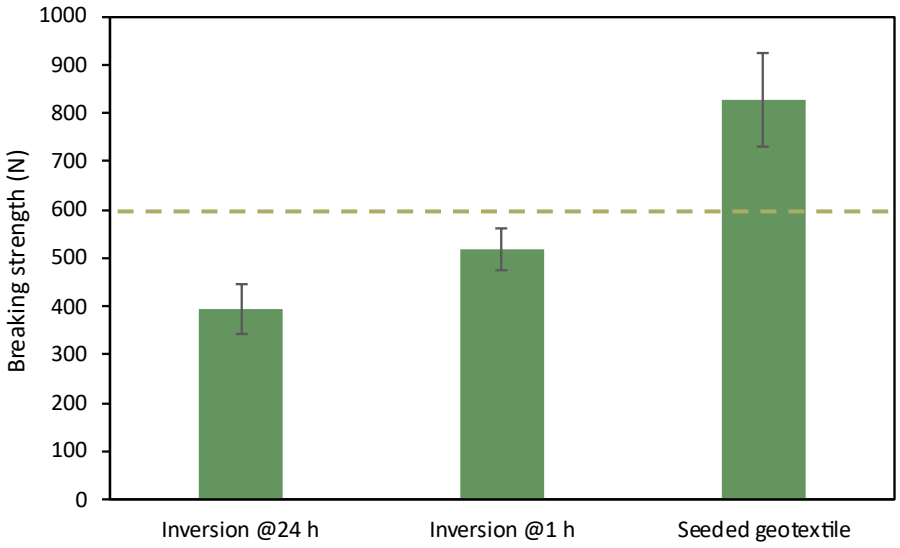

Figure 6.6: Bio-tile breaking strength when inverting the mould at 24 hours and one hour and when using seeded geotextile and inverting at one hour. Horizontal dashed line indicates the ISO minimum breaking strength target of 600 N. Error bars represent the standard deviation of n = 3 bio-tiles.

6.3.5 *The effect that mass of calcium carbonate seeds has on breaking strength*

The experiment utilising seeded geotextiles (Figure 6.6) resulted in a high breaking strength and modulus of rupture. Preliminary results focused on measuring the effect of seeding and therefore, the mass of seeds contained in the geotextiles was not measured in these experiments. From the higher mass of seeds in the top material and greater density in the geotextile compared to the foam (Figure A.11), in subsequent investigations, the effect that the mass of seeds had on breaking strength was quantified.

Using consecutive cementation solution treatments of inoculated geotextiles to achieve various seed loadings, it was found that increasing masses of $CaCO_3$ seeds had a direct effect on breaking strength

(Figure 6.7). Whether through lower supersaturation requirements, higher nucleation rates or bypassing nucleation completely (Kim *et al.*, 2020), increasing the mass of $CaCO_3$ seeds in the geotextile materialised in the bio-tiles having higher breaking strengths. Generally, increasing seed load results in faster utilisation of reagents and the size distribution of the crystal products follows that of the seeds more closely and becomes more uniform as nucleation is increasingly avoided (Loï Mi Lung-Somarriba *et al.*, 2004; Parambil & Heng, 2017). It has also been identified that crystal growth rate is greatly dependent on crystal size, where a 0.4 mm crystal can grow three times faster than a 1 mm crystal (Loï Mi Lung-Somarriba *et al.*, 2004). Smaller mean crystal sizes cause the formation of more crystals that are also smaller, while larger seed crystals tend to grow larger crystals, but slowly (Zubaidah Adnan & Asma Fazli Abdul Samad, 2023).

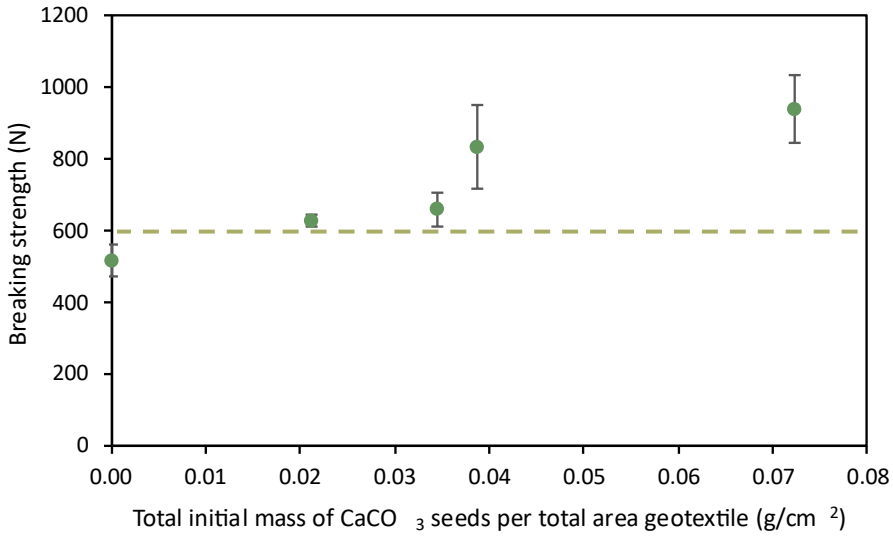

Figure 6.7: The effect that initial mass of $CaCO_3$ seeds contained in the geotextiles has on breaking strength of bio-tiles, normalised for the total area of geotextile per tile. Error bars represent the standard deviation of n = 3 bio-tiles.

The use of geotextiles with the lowest mass of seeds of 0.021 g seeds per cm^2 of geotextile resulted in a breaking strength of 628 ± 18 N. A breaking strength of 940 ± 92 N was achieved with the maximum seed loading tested in this study (0.072 g seeds per cm^2 geotextile). Given that the ISO standard requires the breaking strength to be a minimum of 600 N, it was not necessary to test greater masses of seeds, however, further studies could investigate the influence even greater masses of seeds would have on the process.

6.3.6 *Bio-tiles produced with a vertically-oriented mould*

Bio-tiles produced from a pumping technique using a mould in which they could be positioned vertically, with the two 100 x 100 mm sides flat against the Perspex achieved only breaking strengths of 326 ± 58 N, for inversion once after 1 hour and daily (results not shown). Only when additional bacteria was injected through the feed port at around 48 hours, did the strength increase to 483 ± 41 N. The seeding of geotextiles was less effective for this mould as the geotextiles were only an area of approximately 100 x 10 each, and this, combined with the channelling flow patterns of the feed likely caused the reduced breaking strength of the vertical mould bio-tiles. While breaking strengths were inadequate, the reflective surface aesthetic was a success (Figure 6.8) and could pose an opportunity for further research.

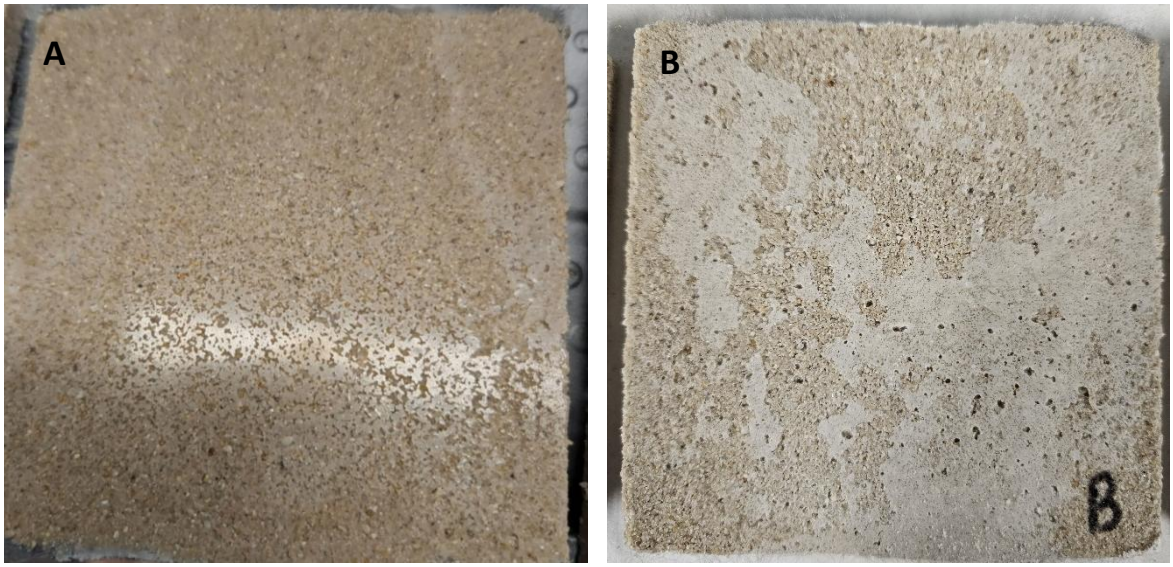

Figure 6.8: Examples of bio-tiles (100 x 100 mm) produced with a vertically-oriented pumping mould to achieve flat and reflective bio-tile surfaces as an alternative aesthetic.

6.3.7 *Summary of bio-tiles produced and adherence to standards*

The design chart in Figure 6.9 shows that the bio-tiles grown with a geotextile seed loading of 0.021 g/cm^2 meet the breaking strength and modulus of rupture targets for extruded tiles with a water absorption of greater than 10% at 628 ± 18 N and 10.5 ± 1.1 N/mm^2 (water absorption = 11.5%). It is also noted that two bio-tiles have a water absorption lower than 10% and therefore fall into the next water absorption category (6-10%) which has a breaking strength requirement of 750 N with a modulus of rupture of at least 9 N/mm^2. Bio-tiles with a seed loading of 0.072 g/cm^2 geotextile meet the targets and have a water absorption of 8.7%. Hence, it is advised that bio-tiles with a seed loading of approximately 0.02 g/cm^2 of geotextile are recommended going forward for bio-tiles with a water absorption of >10%. However, if tiles with a water absorption of 6-10% are desired, bio-tiles that have a seed loading of approximately 0.07 g/cm^2 geotextile are recommended. Seeing as the associated breaking strength and water absorption far exceed the requirements, it is possible that a lower seed loading will still produce bio-tiles that meet the requirements for tiles with a water absorption of 6-10%.

Therefore, bio-tiles produced with MICP and a pumping technique can be categorised into two classes of water absorption and have more broad applicability than tiles produced in previous work with a submersion technique (Horn *et al.*, 2023) where only the water absorption class of >10% was obtained. This means that the bio-tiles produced with a pumping technique and seeding can be utilised in interior and exterior environments with low humidity or that will not go below freezing. Places such as bathrooms should be avoided because of high humidity. Furthermore, the potential strength of both classes can be much higher depending on the seed loading and allows for performance trade-offs associated with scale up and optimisation. Potential optimisations include shortening the time required to produce a bio-tile as well as incorporation of waste materials such as fly ash, crushed reclaimed tiles or unrecyclable glass and reagents derived from waste streams like urine (Lambert & Randall, 2019) or dairy waste (Kahani *et al.*, 2020).

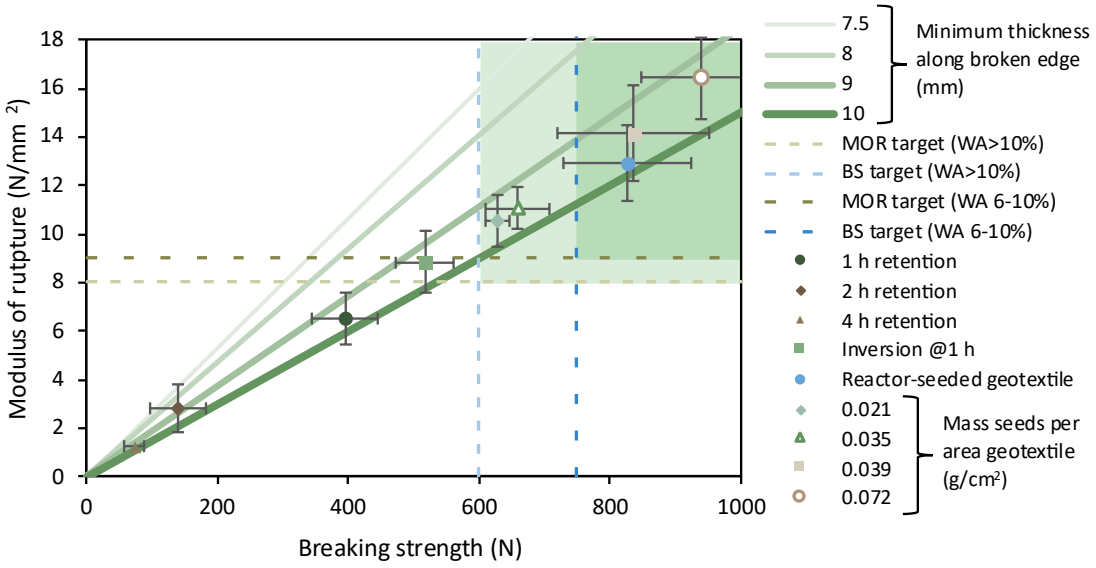

Figure 6.9: Bio-tile design chart comparing effect of treatment cycle duration, inverting at one hour and two kinds of seeded geotextiles. Light green region indicates that breaking strength and modulus of rupture are satisfactory for bio-tiles with a water absorption of greater than 10%. Darker green region indicates the target region for bio-tiles with water absorption of 6-10%. Open data points indicate tiles with 6-10% water absorption, all other tiles have a water absorption >10%. Error bars represent the standard deviation of number of tiles tested, n = 3, except for two and four hour retention time experiments where n = 6. BS = breaking strength; MOR = modulus of rupture; WA = water absorption.

Many of the data points have an error that was relatively large (e.g. ± 98 N for the "seeded geotextile" experiment, i.e. 12% of the group average of 862 N). Other MICP researchers have also illustrated approximate strength standard deviations that equated to errors ranging from 2-27% (Li *et al.*, 2020) and 2-25% (Zhao *et al.*, 2014b), for example. Based on this, we chose an error of up to 15% to be acceptable. This equates to a smaller range for smaller strengths and a standard deviation of almost 100 N for the strongest tiles. While a smaller error limit would be preferred, it was recognised that this variation was representative of the nature of MICP reactions and of the many steps that go into producing bio-materials that each have their own error. Additionally, bio-materials formed through MICP processes are prone to inhomogeneous cementation (Bu *et al.*, 2018; Kim *et al.*, 2022) and areas with less $CaCO_3$ deposits become fracture points, increasing strength variation. A summary of the breaking strength error across all bio-tile experiments is given in Table A.4. The errors of the two- and four-hour retention time experiments exceeded 15%, even when repeated (n = 6 bio-tiles) and the outliers were statistically removed. While not ideal, this was deemed acceptable as these retention times were not pursued because the breaking strengths achieved were far lower (140 N and 73 N, respectively) than the one-hour retention time experiment (395 N). Additionally, the high standard deviation of these two experiments was taken as representative of the dynamics within the bio-tile due to there being fewer treatments. As a result of less cementation solution passing through the system, there was less solidification overall, and the $CaCO_3$ likely occupied the pore space unevenly due to minor channels in the packed particles solidifying first from preferential flows delivering more fresh reagents. With more treatments, the pore space is occupied more evenly as the solution is forced through the particles and channels are increasingly filled with $CaCO_3$.

6.4 Conclusions

Bio-tiles that meet two international breaking strength and modulus of rupture standards were grown with MICP and $CaCO_3$ seeding for the first time. It was identified that the highest ureolytic activity tested (40 mmol NH_4-N/L·min) resulted in bio-tiles with the greatest breaking strengths when utilising a pumping technique. Shorter treatment cycles resulted in higher bio-tile breaking strengths, with the shortest retention time of one hour between cementation solution treatments being most effective. Seeding significantly improved the resulting bio-tile breaking strength by 21-82%, depending on the seed loading. Bio-tiles with a breaking strength of 940 ± 92 N and a modulus of rupture of 16.4 ± 1.7 N/mm^2 (water absorption of 8.7%) were produced with a seed loading of 0.072 g/cm^2, meeting international targets for extruded tiles that have a water absorption of 6-10%. When a seed loading of 0.021 g/cm^2 was used instead, bio-tiles meeting targets for tiles with a water absorption of >10% were produced at 628 ± 18 N and 10.5 ± 1.1 N/mm^2 with 11.5% water absorption.

References

C. Bu, K. Wen, S. Liu, U. Ogbonnaya & L. Li. 2018. Development of bio-cemented constructional materials through microbial induced calcite precipitation. *Materials and Structures/Materiaux et Constructions.* 51(30):1-11. DOI:10.1617/s11527-018-1157-4.

L. Cheng & R. Cord-Ruwisch. 2014. Upscaling effects of soil improvement by microbially induced calcite precipitation by surface percolation. *Geomicrobiology Journal.* 31(5):396-406. DOI:10.1080/01490451.2013.836579.

L. Cheng & M.A. Shahin. 2016. Urease active bioslurry: a novel soil improvement approach based on microbially induced carbonate precipitation. *Canadian Geotechnical Journal.* 53(9):1376-1385. DOI:10.1139/cgj-2015-0635.

Q. Chunxiang, W. Jianyun, W. Ruixing & C. Liang. 2009. Corrosion protection of cement-based building materials by surface deposition of CaCO3 by Bacillus pasteurii. *Materials Science and Engineering: C.* 29(4):1273-1280. DOI:10.1016/j.msec.2008.10.025.

F.G. Ferris, V. Phoenix, Y. Fujita & R.W. Smith. 2004. Kinetics of calcite precipitation induced by ureolytic bacteria at 10 to 20°C in artificial groundwater. *Geochimica et Cosmochimica Acta.* 68(8):1701-1710. DOI:10.1016/S0016-7037(03)00503-9.

E.J. Horn, R. Huddy & D.G. Randall. 2023. Growing bio-tiles using microbially induced calcium carbonate precipitation. *Science of The Total Environment.* 895(165050):1-11. DOI:https://doi.org/10.1016/j.scitotenv.2023.165050.

M. Kahani, F. Kalantary, M.R. Soudi, L. Pakdel & S. Aghaalizadeh. 2020. Optimization of cost effective culture medium for *Sporosarcina pasteurii* as biocementing agent using response surface methodology: Up cycling dairy waste and seawater. *Journal of Cleaner Production.* 253(120022):1-10. DOI:10.1016/j.jclepro.2020.120022.

D.H. Kim, N. Mahabadi, J. Jang & L.A.v. Paassen. 2020. Assessing the Kinetics and Pore-Scale Characteristics of Biological Calcium Carbonate Precipitation in Porous Media using a Microfluidic Chip Experiment. *Water Resources Research.* 56(e2019WR02542):1-19. DOI:10.1029/2019WR025420.

S. Kim, Y. Kim, S. Lee & J. Do. 2022. Preliminary Study on Application and Limitation of Microbially Induced Carbonate Precipitation to Improve Unpaved Road in Lateritic Region. *Materials.* 15(7219):1-15. DOI:10.3390/ma15207219.

S.E. Lambert & D.G. Randall. 2019. Manufacturing bio-bricks using microbial induced calcium carbonate precipitation and human urine. *Water Research.* 160:158-166. DOI:10.1016/j.watres.2019.05.069.

Y. Li, K. Wen, L. Li, W. Huang, C. Bu & F. Amini. 2020. Experimental investigation on compression resistance of bio-bricks. *Construction and Building Materials.* 265(120751):1-7. DOI:10.1016/j.conbuildmat.2020.120751.

B. Loï Mi Lung-Somarriba, M. Moscosa-Santillan, C. Porte & A. Delacroix. 2004. Effect of seeded surface area on crystal size distribution in glycine batch cooling crystallization: a seeding methodology. *Journal of Crystal Growth.* 270(3-4):624-632. DOI:10.1016/j.jcrysgro.2004.07.015.

A.C. Mitchell & F.G. Ferris. 2006. The influence of *Bacillus pasteurii* on the nucleation and growth of calcium carbonate. *Geomicrobiology Journal.* 23(3-4):213-226. DOI:10.1080/01490450600724233.

R. Murugan, G.K. Suraishkumar, A. Mukherjee & N.K. Dhami. 2021. Influence of native ureolytic microbial community on biocementation potential of *Sporosarcina pasteurii*. *Scientific Reports.* 11(20856):1-12. DOI:10.1038/s41598-021-00315-5.

J.V. Parambil & J.Y.Y. Heng. 2017. Seeding in Crystallisation. In *Engineering Crystallography: From Molecule to Crystal to Functional Form.* K.J. Roberts, R. Docherty and R. Tamura, Eds. Dordrecht: Springer Netherlands. 235-245. DOI:10.1007/978-94-024-1117-1_13.

Z. Wang, J. Zhang, M. Li, S. Guo, J. Zhang & G. Zhu. 2022. Experimental study of microorganism-induced calcium carbonate precipitation to solidify coal gangue as backfill materials: mechanical properties and microstructure. *Environmental Science and Pollution Research.* 29(30):45774-45782. DOI:10.1007/s11356-022-18975-9.

K. Wen, Y. Li, F. Amini & L. Li. 2020. Impact of bacteria and urease concentration on precipitation kinetics and crystal morphology of calcium carbonate. *Acta Geotechnica 2019 15:1.* 15(1):17-27. DOI:10.1007/S11440-019-00899-3.

J.Z. Xiao, Y.Q. Wei, H. Cai, Z.W. Wang, T. Yang, Q.H. Wang & S.F. Wu. 2020. Microbial-Induced Carbonate Precipitation for Strengthening Soft Clay. *Advances in materials science and engineering.* 2020:1-11. DOI:10.1155/2020/8140724.

J. Zehner, A. Røyne & P. Sikorski. 2021. Calcite seed-assisted microbial induced carbonate precipitation (MICP). *PLOS ONE.* 16(2):1-15. DOI:10.1371/journal.pone.0240763.

Q. Zhao, L. Li, M. Asce, C. Li, M. Li, F. Amini, F. Asce & H. Zhang. 2014. Factors affecting improvement of engineering properties of MICP-treated soil catalyzed by bacteria and urease. *Journal of Materials in Civil Engineering.* 26(12):1-10. DOI:10.1061/(ASCE)MT.1943-5533.

H.-M. Zheng, L.-L. Wu, K.-W. Tong, D.-X. Ding, Z.-J. Zhang, Q. Yu & G.-C. He. 2020. Experiment on microbial grouting reinforcement of tailings under the regulation of egg white. *Soils and foundations.* 60(4):962-977. DOI:10.1016/j.sandf.2020.07.004.

S. Zubaidah Adnan & N. Asma Fazli Abdul Samad. 2023. Effects of different seed forms on crystal size distribution for seeded batch crystallization process. *Materials today: proceedings.* Article in Press:1-6. DOI:10.1016/j.matpr.2023.06.110.

7 Production of bio-tiles using an automated binder jet 3D printing technique

This chapter details the final study on bio-tiles grown with MICP using an automated binder jet 3D printing prototype. The prototype was designed to combine the beneficial attributes of both the submersion and pumping techniques. The system continued the progression towards the more active flow-through process of the pumping technique. The key driver behind the prototype was to have greater potential for scalability through a lower human intervention requirement as in the submersion technique and enhanced modularity where many bio-tiles could be produced at once. On principle, this system could be adapted to produce different bio-materials through incorporating different chambers and operations. The focus of the study was to quantify the effect of various additives on the strength properties of the bio-tiles produced with the automated technique and freeze-dried bio-slurry. In particular, additional nutrients, $CaCO_3$ seeds and supplemental magnesium were investigated.

Chapter 7 is based on the third paper submitted as part of this research, *Supplementation of bio-tile production with magnesium, calcium carbonate seeds and nutrient broth for an automated, modular microbially induced calcium carbonate precipitation process*.

7.1 Objectives

The key objectives of this study were to develop and optimise an automated technique for growing bio-tiles and evaluate its impact on breaking strength of bio-tiles with:

1. And without $CaCO_3$ seeds;
2. Additional nutrients in the form of a daily nutrient broth-enriched treatment; and
3. Supplemental magnesium.

7.2 Materials and methods

7.2.1 *Preparation of the urease active bio-slurry powder*

A batch of 12-15 flasks of bacteria solution was cultivated according to the usual method. Following ureolytic activity tests, the remaining bacteria solution (1.17-1.47 L) was used to make bio-slurry. The urease-active bio-slurry powder was formed from freeze-drying the conventional bacteria solution after mixing in calcium and urea to form protective $CaCO_3$ capsules around the bacteria. Once powderised, the bio-slurry essentially delivers the bacteria as well as $CaCO_3$ seeds.

To make the bio-slurry, the pH of the bacteria culture was corrected to 7.9 with 85% H_3PO_4 (Nething *et al.*, 2020). The solution was added to an autoclaved 5 L Schott bottle to allow a headroom with sufficient oxygen for the aerobic bacteria. Masses of synthetic urea and calcium chloride dihydrate ($CaCl_2{\cdot}2H_2O$; ≥99.1% purity, Kimix, Cape Town, South Africa) resulting in 0.4 M concentrations (Cheng *et al.*, 2020; Nething *et al.*, 2020) were added to the bacteria in portions while mixing. The lid of the bottle was lightly screwed on. The solution was stirred at 60% speed for 6 hours on a magnetic stirrer (Labcon M5250, Laboratory Equipment, Chamdor, South Africa). The precipitated material was then allowed to settle for 14 hours (Nething *et al.*, 2020). At this point, as much of the supernatant as possible was extracted by syringe and the remainder drained using a Buchner funnel. The bio-slurry was then freeze dried (Varian 801, Vacuum Technologies, Cape Town, South Africa) for 72 hours at 450 mTorr and -33℃. The lyophilised bio-slurry was gently powderised in a mortar and pestle, and then vacuum sealed and stored at -20℃ (Nething *et al.*, 2020). About 46 g of bio-slurry was made from 1 L of bacteria solution.

For quantifying the ureolytic activity of the freeze-dried bio-slurry, a similar procedure as for liquid bacteria was followed where 1 g of bio-slurry powder was resuspended in 15 mL of deionised water in an autoclaved flask and mixed with 15 mL of 1 M urea solution, the flask was sealed and shaken at 120 rpm for 30 minutes. The change in ammonium ion concentration was once again compared.

To assess ways of improving bio-slurry performance, the bacteria was prepared with growth medium consisting of a double and triple concentration of yeast extract and ammonium sulphate (Nething *et al.*, 2020) and the ureolytic activity was compared to bacteria grown with single concentrated medium. Bio-slurry was produced from each bacteria solution, lyophilised and ureolytic activity compared as previously stated.

7.2.2 *Design of the 3D printer*

The 3D printer prototype was designed with the principle of a binder jet 3D printer. Sand that was inoculated with bioslurry (the activator) was used as the solid base. Cementation solution was deposited on the sand in automated sequential treatments, causing a reaction to occur that resulted in the production of bio-cement (the binder).

The prototype was designed by Amnova Tech, Johannesburg, South Africa. The crucial parts of the prototype for understanding its operation are given in Figure 7.1. Detailed drawings are available in the Appendices in Figure A.12 to Figure A.15. In the material selection process for the prototype, as far as possible, metal parts that can rust were avoided and instead, acrylic, silicone, stainless steel and aluminium were used. The 3D printed parts used in the prototype were primarily made from PLA filament, as well as PET-G and ABS.

The reaction chamber consisted of a square platform (100 x 100 mm) with drainage holes and a silicone edge, such that the platform could raise and lower vertically within an acrylic chute. The silicone edging allowed a seal to be maintained around the sides where it meets the chute, keeping sand and solution from escaping at the edges.

When the platform was in a raised position, the holes within the platform allowed spent solution to drain through the bio-tile and the platform. In the lowered position, the platform rested against a registering silicone seal, blocking the holes and preventing solution from draining. The acrylic chute was secured to the main assembly frame through a custom 3D printed part. The main silicone seal was secured in place by the same 3D printed part.

The linear actuator (200 mm stroke, Robotzone, Suzhou, Taiwan) that powers the vertical movement of the platform was paired with a second matching linear actuator that powers a second platform that compacted the bio-tile from above as desired. These linear actuators could each apply 80 kg of force.

The cementation solution deposition was carried out using a diaphragm pump (600-800 L/h, AHEADPUMP AW500S, Qingdao Ahead Electric Co., Shandong, China), and a custom 3D printed showerhead (with a dosing area of 90 x 90 mm), and airlocks were maintained at the feed container and at the outlet. A pair of solenoids (0.02-0.8 MPa, Meishuo, Yueqing City, China) in series at the showerhead, were used to ensure accurate dosing of cementation solution and no leaks. The solution was showered over the bio-tile using a 3D printed shower head. Stepper motors (NEMA17) were used to roll the showerhead into place over the tile for each deposition and rolled out of the way following the deposition.

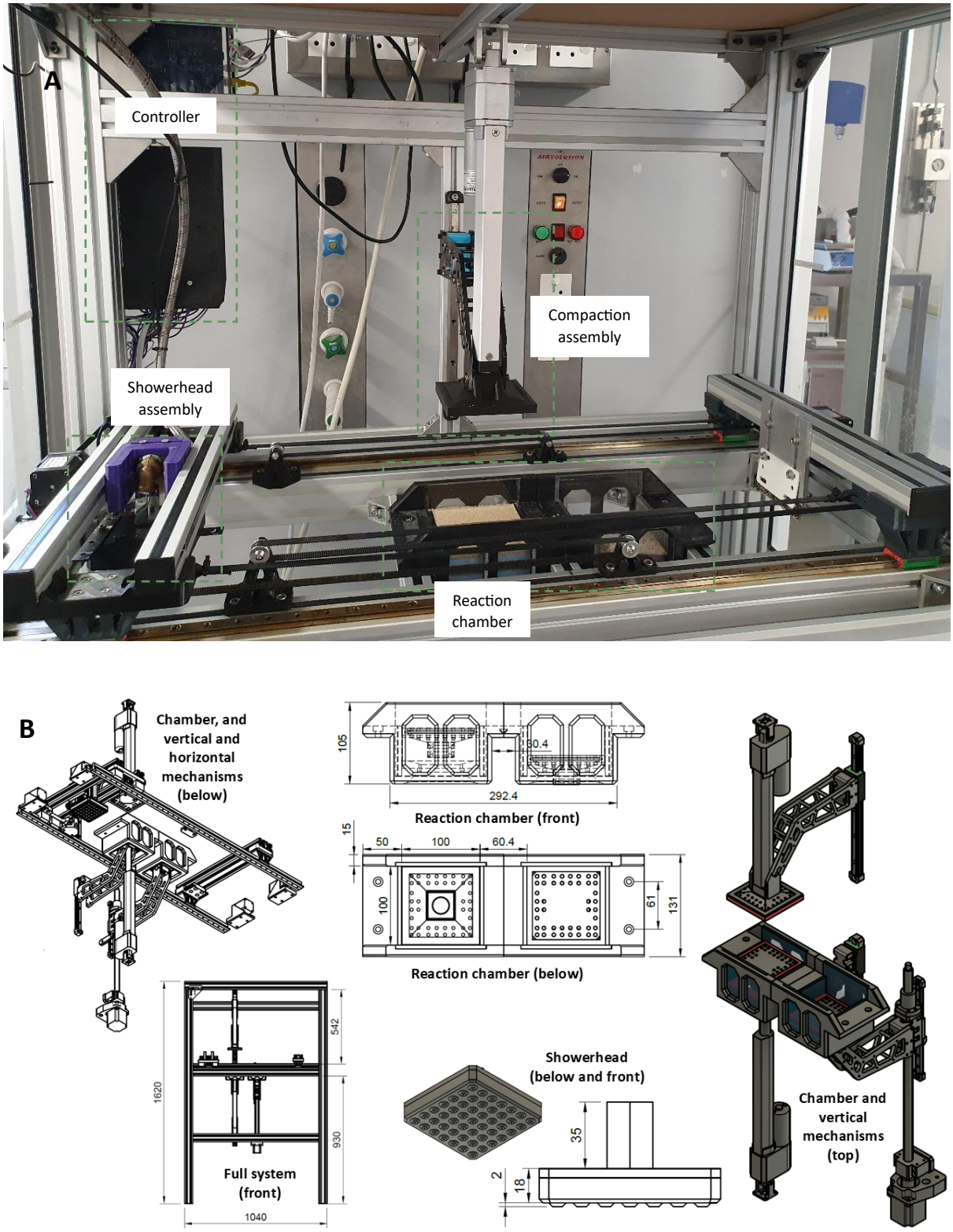

Figure 7.1: Photo (A) and diagrams (B) of the prototype automated MICP system.

7.2.3 *Additive manufacturing process*

For each bio-tile of 100 x 100 x 10 mm, freeze-dried bio-slurry (3 wt%, 3.28 g) was carefully mixed into the required amount of sand for at least 5 minutes (Nething *et al.*, 2020), resulting in a visually even distribution of the white bioslurry throughout the dry sand mixture. The walls of the chute were coated with petroleum jelly and lined with clear acetate for structural support of the bio-tile edges and its

easy removal from the chute. A non-woven needle-punched polypropylene geotextile lined the interface between the platform and the inoculated sand, preventing sand from passing through the platform holes. The inoculated sand was carefully packed on to the platform, flattened and compressed into the chute. A geotextile was also placed on top of the inoculated sand, this was critical in preventing the cementation solution depositions from disturbing the cementation of the surface of the bio-tile.

The working instructions for the automated system were written in a G-code file, which was processed by a 3D printing motion software (Duet Web Control, United Kingdom), sent to the microprocessor (Duet 3 Main Board 6XD, Duet3D, Peterborough, United Kingdom). The microprocessor then sent control commands to the various system outputs including microcontrollers (Arduino Mega and Uno, Arduino, Ivrea, Italy) that control the actuators. Each deposition of cementation solution was run for 3.5 s which equated to 84 ± 2.5 mL, such that there was about 15 mm of pooling above the surface of the bio-tile. Over a run-time of 8 days, each treatment cycle was held for a retention time of one hour and 45 minutes, followed with 15 minutes for draining of the spent solution. The bio-tile was compacted after every second treatment for the first two days of treatment cycles.

Initially, the bio-slurry-sand mixture was completely dry and therefore, a double deposition was carried out at the start of the program. However, when the process was supplemented with additional nutrients, the bio-tile was first treated manually with a single deposition (84 mL) of nutrient-enriched cementation solution, and then a single deposition of regular cementation solution to start. Thereafter, manual nutrient-enriched treatments were carried out daily in place of the corresponding treatment of the regular cementation solution.

7.3 Results and discussion

This prototype represents one perspective on how the various beneficial attributes of both the submersion and pumping techniques could be combined. The following outlines how the chosen set up was engineered and parameters controlled to achieve bio-tiles that meet the breaking strength and modulus of rupture targets.

7.3.1 *Comparison of the urease-active bio-slurry powder to conventional liquid bacteria solution*

The use of freeze-dried bio-slurry allows production from anywhere, increasing accessibility to the technology. The bio-slurry allowed for the bacteria to be mixed into the sand beforehand, resulting in even distribution of the bacteria-$CaCO_3$-seeds throughout the sand and a dry mixture. For the ureolytic activity tests, the final concentration of bio-slurry solids was 33.3 mg/mL, which was similar to the concentration used in the activity tests ran by Cheng and Shahin (2016) who mixed 5 g bio-slurry (about 15% solid content) with 15 mL 3 M urea solution and 10 mL deionised water, to give a final concentration of 25.6 mg bio-slurry solids/mL. When Nething *et al.* (2020) adapted the method, 540 µL resuspended freeze-dried bio-slurry was added to 60 µL 0.1 M urea solution, to give a final bio-slurry solids concentration of 1.17 mg/mL. The ureolytic activity of regular bacteria solution was compared to freeze-dried bio-slurry made from the same batch (Figure 7.2). Bio-slurry was found to have almost double the ammonium production of regular liquid bacteria solution.

Nething *et al.* (2020) utilised ammonium-yeast growth medium constituted from double the concentration of yeast extract and ammonium sulphate for growing the bacteria solution used in the bio-slurry. When compared to original growth medium, the ammonium produced was similar for the bacteria solution prepared with double and triple concentrated growth medium, however, the bio-slurry activity decreased by 29% and halved, respectively (Figure 7.2). This suggests that bio-slurry activity does not benefit from double or triple concentration of growth medium but rather reduces

with increasing concentration of medium. Hence, the original growth medium recipe was followed for bio-slurry preparation.

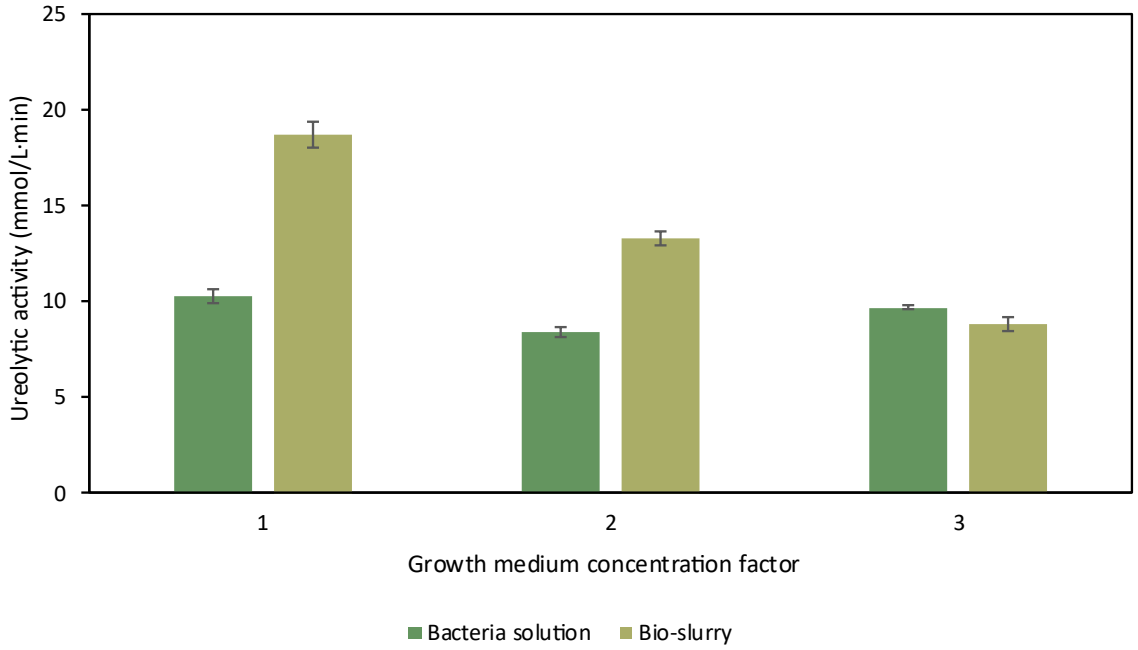

Figure 7.2: Comparison of ureolytic activity from bacteria solution and bio-slurry, and each made from double and triple concentrated ammonium-yeast nutrient medium.

7.3.2 *Supplementation with calcium carbonate seeds, magnesium and nutrient broth*

The bio-tiles produced with the automated technique were relatively poor in breaking strength and needed additives for the corners to be intact and to form more solidly, such that breaking strength tests could be conducted. Even with some additives, solidification was so poor in some cases that a minimum thickness could not be measured, and the modulus of rupture was incalculable. The water absorption of bio-tiles supplemented with magnesium was 10.3 ± 0.9% (n = 5, Figure A.16), and therefore, the breaking strength and modulus of rupture targets were 600 N and 8 N/mm^2, respectively. The effect of additional $CaCO_3$ seed loading (over and above that provided by the bio-slurry), a daily nutrient broth-enriched treatment and cementation solution supplemented with magnesium are shown in Figure 7.3. Most of the bio-tile breaking strengths were widely dispersed over the seed loadings tested, with few exceptions. This was likely influenced by uneven seeding of the geotextiles, the fluid dynamics of the process and reliability concerns of the software, although there was a clear enhancement of breaking strength when supplementing with magnesium. Previous studies (Horn *et al.*, 2024; Li *et al.*, 2020) have also reported variability in the strength of MICP-produced bio-materials ranging 2-27%, especially those with low strengths.

The breaking strength is mostly independent of additional seed loading (Figure 7.3). In bio-tiles supplemented with nutrient broth, the breaking strength was 188 ± 60 N for all tiles (n = 8), across the various seed loadings. This standard deviation is 32% of the average breaking strength, which shows the inhomogeneity of the bio-cementation that occurred, albeit across the seed loadings. In contrast, when no additional seeds where added, the bio-tile has a breaking strength of 198 N. While this is a singular result, it is likely that the bio-cementation was limited and so variable that seeds had little effect on the low breaking strength of bio-tiles supplemented with nutrient broth. When no additional seeds were used in the presence of 0.3 M magnesium, a bio-tile with the lowest and highest strength

of all magnesium-supplemented bio-tiles occurred (498 and 715 N), indicating that additional seeds had little effect on the strength of bio-tiles produced with this technique.

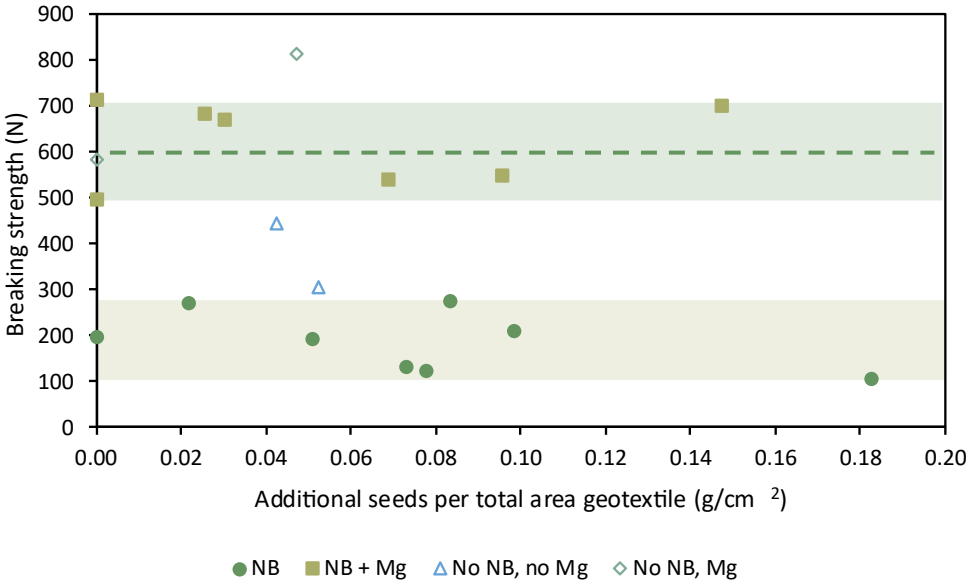

Figure 7.3: Influence of supplementary nutrient broth, $CaCO_3$ seeds and magnesium on bio-tile strength properties produced using an automated technique. Each data point represents a single bio-tile due to the 3D printer prototype having one reaction chamber. The top darker green shaded band shows the range of breaking strengths that bio-tiles treated with both daily nutrient broth treatments and magnesium-supplemented cementation solution spanned. The lower lighter green shaded band indicates the range for bio-tiles treated with only daily nutrient broth treatments.

There was already 3.28 g of bio-slurry (~3 wt% of bio-tile), or urease active $CaCO_3$ seeds, added to each bio-tile. It follows that the additional seed loading of geotextiles would have had less of an effect on the strength of bio-tiles because there is a threshold beyond which nucleation can be bypassed entirely (Kim *et al.*, 2020; Lioliou *et al.*, 2007) and crystals grow bigger instead. At this point, the advantage of seeding to increase the rate of nucleation no longer applies. However, previously (Figure 6.7) bio-tiles were seeded with up to a total of 14.5 g of additional seeds (0.07 g/cm^2 geotextile) and consistently saw increasing breaking strength, with no threshold reached. In this study, a maximum of 36.5 g of additional seeds (0.18 g/cm^2) was supplemented to the bio-tile on the geotextiles, with seed loading having little effect on breaking strength. It is possible that the threshold for the effect seeding has on breaking strength was lower when seeds are added directly to the bio-material. This was because the seeds were mixed amongst the bio-tile particles, in comparison to applied on the surface of the bio-tiles in both geotextiles, as in the pumping technique (Figure A.1). Additionally, the urease active nature of bio-slurry seeds, preserved at -20°C until use, could be compounding the seeding benefit.

It was hypothesised that the nutrient broth would improve the bacterial metabolism and enhance the breaking strength of the bio-tiles. While some authors found that supplementing all cementation solution with nutrient broth was deleterious to the compressive strength measured (De Oliveira *et al.*, 2021), others also noted nutrient broth would be one of the highest contributors to overall cost of production should the process commercialise (Lambert & Randall, 2019). Consequently, a daily treatment using 3 g/L nutrient broth-enriched cementation solution was utilised in this study to lower costs and still offer a boost to bacterial metabolism. Preliminary tests showed that the breaking strength of bio-tiles benefit from the addition of daily nutrients (Figure A.17). When the final tests were run after the bulk of the seed loading experiments, nutrient broth was found not to improve

breaking strength. Instead, bio-tiles without daily nutrient broth treatments and without magnesium supplementation (n = 2) had breaking strengths that were 100% greater than those with only nutrient broth supplementation (n = 8) and for bio-tiles supplemented with magnesium (n = 2), an improvement of 12% was found (Figure 7.3). However, there was still a large difference (139 and 231 N, respectively) in breaking strengths for these bio-tiles without additional nutrients that was not correlated with seed loading.

The effect of supplementing the cementation solution with 0.3 M magnesium ions was the most remarkable of the three supplements. On average, supplementary magnesium and daily nutrient broth treatments resulted in breaking strengths of 622 ± 84 N across seed loadings (n = 7). This standard deviation is 13% of the average breaking strength for magnesium-supplemented bio-tiles, supporting that bio-tiles with higher strengths have less strength variability. The presence of magnesium improved the breaking strength of nutrient broth-enriched bio-tiles 3.3 times. This increase was greater than the previous bio-tile study using the submersion technique (13%, Figure 5.8) as well as the two-fold increase in compressive strength of bio-columns produced with an injection technique (Xu *et al.*, 2020). Magnesium favourably interacts with the precipitation of $CaCO_3$, such as reducing the crystal size (Putra *et al.*, 2016b) and increasing the selection of the aragonite polymorph over others (Nayanthara *et al.*, 2019; Xu *et al.*, 2020). Prevalence of aragonite increases the density of the precipitated $CaCO_3$ and the Moh's hardness from 3 or less to 3.5 (Seifan & Berenjian, 2018). The $CaCO_3$ content of bio-tiles supplemented with both magnesium and nutrient broth (Figure A.16) was marginally higher (39.7±1.8%) than those supplemented with nutrient broth alone (35.7±1.3%). Both are within the range of $CaCO_3$ contents of bio-tiles grown with the pumping technique (36.7 ± 2.8%). Supplementing with magnesium alone could be a more cost-effective strategy than adding nutrient broth.

7.3.3 *Performance of the prototype automated system*

The automated system which was designed and tested was one way of combining the beneficial aspects of the submersion and pumping techniques. However, the pumping technique has one important aspect which was not incorporated into the design: that of forcing solution through the pore space during pumping. This action of solution being driven through interparticle channels allows them to be more thoroughly filled by precipitate than by gravity alone, as is the case with the automated technique. Due to this gravity-driven mechanism of the automated technique, supplemental magnesium was required to produce bio-tiles with a breaking strength higher than the standard. In comparison, the bio-tiles produced by the pumping technique met the standard with just 4.2 g (0.021 g/cm^2 geotextile) of additional $CaCO_3$ seeds and no supplementary magnesium (Figure 6.9). Therefore, the amount of inputs for the automated system was greater than for the pumping system.

The design chart in Figure 7.4 shows that multiple bio-tiles that were supplemented with nutrient broth, additional $CaCO_3$ seeds as well as magnesium, meet the breaking strength and modulus of rupture targets for extruded tiles with a water absorption of greater than 10%. Water absorption of tiles is classified into tiles exceeding a water absorption of 10%, those between 6-10%, between 3-6% and those with a water absorption of less than 3%. Each class has use in different applications. For example, bathrooms require tiles with almost no water absorption, such as vitrified tiles. All but one of the bio-tiles were produced with a water absorption exceeding 9.6%, as with bio-tiles produced with the submersion technique (9.7-13-7%), and do not have as broad applicability as bio-tiles produced with the pumping technique (Figure 6.9). These bio-tiles could be used for wall and floor tiles in more general areas of buildings, especially where bespoke products with interesting aesthetics would be appreciated.

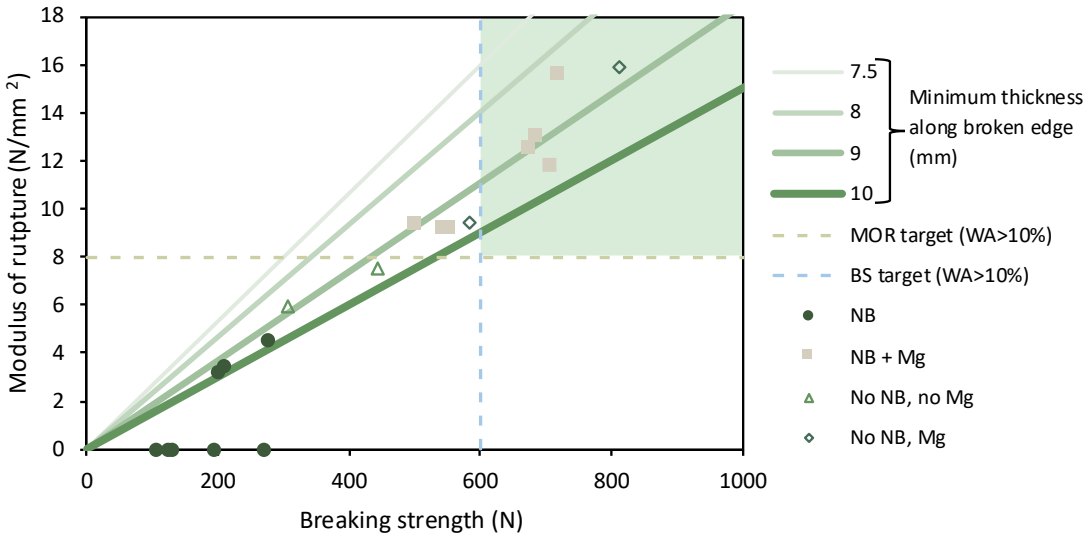

Figure 7.4: Design chart depicting the influence of additional $CaCO_3$ seeds, daily nutrient broth treatments and cementation solution supplemented with 0.3 M magnesium. MOR = modulus of rupture; WA = water absorption; BS = breaking strength. Some bio-tiles were not fully solidified (such as those grown with liquid bacteria and without magnesium) and the minimum thickness along the broken edge could not be accurately measured, and therefore these data points have a zero for modulus of rupture.

Bio-slurry was found to be beneficial to the formation of bio-tiles and improved solidification, when liquid bacteria solution was used instead, bio-tiles were not fully formed and had two distinct layers that were not bio-cemented together (Figure 7.5A). While additional seeds had minimal effect on the breaking strength of bio-tiles produced with the prototype, aesthetically, they did aid in overall solidification of bio-tile and formation of $CaCO_3$ at the corners and edges. Figure 7.5B, C and D were all grown with geotextiles without seeds. However, even the strongest bio-tiles produced with magnesium require improvement to dimensional and surface quality (Figure 7.5E), compared to those produced with the pumping technique. Therefore, the addition of extra seeds is still recommended for bio-tiles produced with this automated technique. It is speculated that the additional seeds at the edges and corners allowed precipitation to form there better than without through improved support of the edges with the seeded geotextile being more structurally supportive with the $CaCO_3$ deposits.

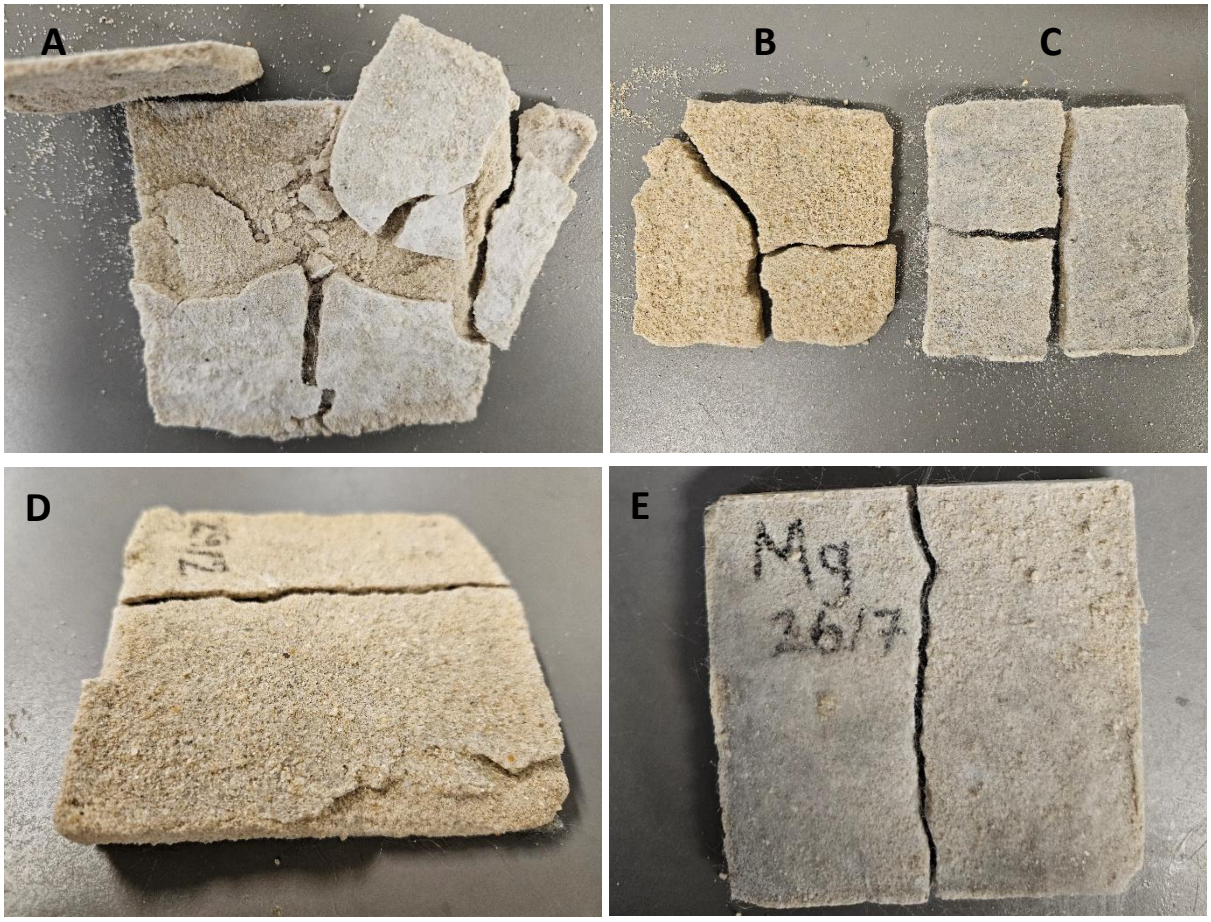

Figure 7.5: Bio-tiles (roughly 100 x 100 mm) grown with liquid bacteria solution (A) instead of bio-slurry, a daily nutrient broth-enriched treatment and no additional $CaCO_3$ seeds (B and C) compared to a bio-tile grown with nutrient broth and additional seeds (D), and a bio-tile grown with nutrient broth and additional seeds and magnesium (E). All bio-tiles are cracked because the picture was taken after determining the breaking strength.

7.3.4 *Conceptualising scalability*

The prototype was designed to be automated and modular. While this prototype had a single reaction chamber, it was postulated that it could be configured to have an array of reaction chambers along the rails that are serviced by a row of showerheads corresponding to the number of reaction chambers in a row (Figure 7.6). The showerheads would deposit row by row and return 'home'. At the specified timing, the platforms would be raised for draining, and so on. This would allow scalability and time efficiency. This system has only been tested for thin materials, such as tiles, however, there is potential for larger bio-materials to be grown. Future research should investigate ways of layering such that larger bio-materials can be bio-cemented.

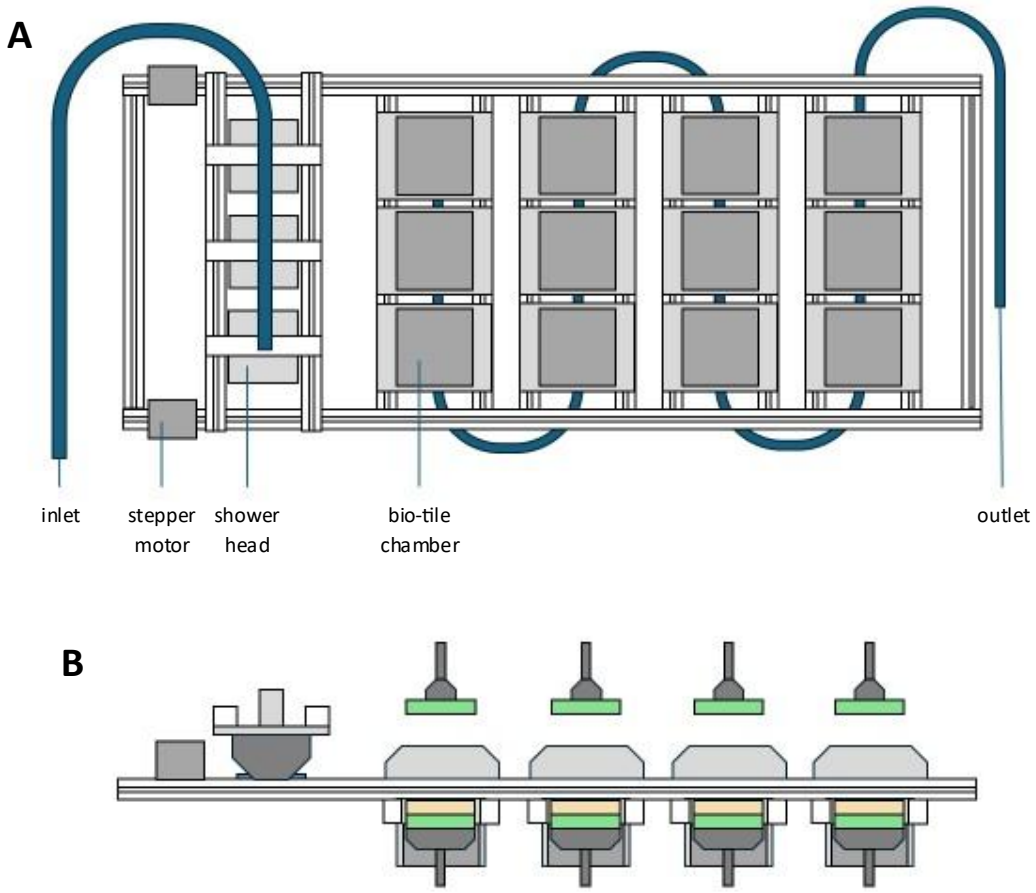

Figure 7.6: Conceptualised configuration of multiple bio-tiles growing at once, top view (A) and side view (B). The blue shows the axis that moves horizontally and the green those that move vertically.

7.4 Conclusions

An automated 3D printing prototype was developed and its design and operations iterated such that bio-tiles that meet international breaking strength and modulus of rupture standards were produced using freeze-dried urease active bio-slurry for the first time. The effect of three additives was quantified and 0.3 M magnesium was found to have the greatest impact on the breaking strength of bio-tiles produced with an automated 3D printing technique. Magnesium supplementation increased the breaking strengths of bio-tiles 3.3 times to 622 ± 84 N. Seeding with additional $CaCO_3$ crystals was found to have little effect on breaking strength, however, was important for improving the solidification on the bio-tiles at the corners and edges. Bio-tiles grown without daily nutrient broth-enriched cementation solution treatments were 12-100% stronger. Multiple bio-tiles that were produced through an automated process supplemented with all three additives had breaking strengths that exceeded the ISO standard, for example, 681, 671 and 702 N and modulus of ruptures of 13.1, 12.6 and 11.9 N/mm^2 for and water absorptions of greater than 10%.

References

L. Cheng & M.A. Shahin. 2016. Urease active bioslurry: a novel soil improvement approach based on microbially induced carbonate precipitation. *Canadian Geotechnical Journal.* 53(9):1376-1385. DOI:10.1139/cgj-2015-0635.

L. Cheng, T. Kobayashi & M.A. Shahin. 2020. Microbially induced calcite precipitation for production of “bio-bricks” treated at partial saturation condition. *Construction and Building Materials.* 231(117095):1-9. DOI:10.1016/j.conbuildmat.2019.117095.

D. De Oliveira, E.J. Horn & D.G. Randall. 2021. Copper mine tailings valorization using microbial induced calcium carbonate precipitation. *Journal of Environmental Management.* 298:113440. DOI:10.1016/j.jenvman.2021.113440.

E.J. Horn, R. Huddy & D.G. Randall. 2023. Growing bio-tiles using microbially induced calcium carbonate precipitation. *Science of The Total Environment.* 895(165050):1-11. DOI:https://doi.org/10.1016/j.scitotenv.2023.165050.

E.J. Horn, R. Huddy & D.G. Randall. 2024. Seeding improves the strength of bio-tiles grown with microbially induced calcium carbonate precipitation. *Science of The Total Environment.* 951(175652):1-9. DOI:https://doi.org/10.1016/j.scitotenv.2024.175652.

D.H. Kim, N. Mahabadi, J. Jang & L.A.v. Paassen. 2020. Assessing the Kinetics and Pore-Scale Characteristics of Biological Calcium Carbonate Precipitation in Porous Media using a Microfluidic Chip Experiment. *Water Resources Research.* 56(e2019WR02542):1-19. DOI:10.1029/2019WR025420.

S.E. Lambert & D.G. Randall. 2019. Manufacturing bio-bricks using microbial induced calcium carbonate precipitation and human urine. *Water Research.* 160:158-166. DOI:10.1016/j.watres.2019.05.069.

Y. Li, K. Wen, L. Li, W. Huang, C. Bu & F. Amini. 2020. Experimental investigation on compression resistance of bio-bricks. *Construction and Building Materials.* 265(120751):1-7. DOI:10.1016/j.conbuildmat.2020.120751.

M.G. Lioliou, C.A. Paraskeva, P.G. Koutsoukos & A.C. Payatakes. 2007. Heterogeneous nucleation and growth of calcium carbonate on calcite and quartz. *Journal of colloid and interface science.* 308(2):421-428. DOI:10.1016/j.jcis.2006.12.045.

P.G.N. Nayanthara, A.B.N. Dassanayake, K. Nakashima & S. Kawasaki. 2019. Microbial induced carbonate precipitation using a native inland bacterium for beach sand stabilization in nearshore areas. *Applied Sciences.* 9(15):3201. DOI:10.3390/app9153201.

C. Nething, M. Smirnova, J.A.D. Gröning, W. Haase, A. Stolz & W. Sobek. 2020. A method for 3D printing bio-cemented spatial structures using sand and urease active calcium carbonate powder. *Materials & design.* 195:109032. DOI:10.1016/j.matdes.2020.109032.

H. Putra, H. Yasuhara, N. Kinoshita, D. Neupane & C.W. Lu. 2016. Effect of magnesium as substitute material in enzyme-mediated calcite precipitation for soil-improvement technique. *Frontiers in Bioengineering and Biotechnology.* 4(MAY). DOI:10.3389/fbioe.2016.00037.

M. Seifan & A. Berenjian. 2018. Application of microbially induced calcium carbonate precipitation in designing bio self-healing concrete. *World Journal of Microbiology and Biotechnology.* 34:168-168. DOI:10.1007/s11274-018-2552-2.

X. Xu, H. Guo, X. Cheng & M. Li. 2020. The promotion of magnesium ions on aragonite precipitation in MICP process. *Construction and Building Materials.* 263(120057):1-9. DOI:10.1016/j.conbuildmat.2020.120057.

8 Concluding remarks

8.1 Key findings

This study highlights the critical role of calcium carbonate precipitation rates, $CaCO_3$ seeding, and magnesium supplementation in enhancing the mechanical properties of bio-tiles produced using MICP. The first bio-tiles production technique explored was the submersion technique. Under tuned conditions, these bio-tiles met international standards for breaking strength and modulus of rupture with a water absorption of greater than 10%. An equimolar concentration of calcium and urea (0.3 M) was found to balance strength and reagent-efficiency over the 7-day retention time. A wide PSD with an average size of 469 µm yielded bio-tiles with the highest breaking strength (489 ± 6 N) and modulus of rupture (9.3 ± 0.3 N/mm²), although this did not meet all strength standards. A design chart was developed as a tool to assess the effect of critical parameters of breaking strength and modulus of rupture. Improvements in both were observed (breaking strength of 546 ± 38 N, modulus of rupture of 11.6 ± 1.8 N/mm²) with a greater volume of cementation solution (15.7 L instead of 14 L), albeit with reduced calcium utilisation efficiency. Magnesium supplementation (0.3 M) enhanced breaking strength to 620 ± 112 N by promoting the formation of the aragonite polymorph of calcium carbonate. An additional key finding was that lower $CaCO_3$ precipitation rates (0.11–0.18 day^{-1}) resulted in stronger bio-tiles, and when all best-performing parameters were combined, a breaking strength of 637 ± 60 N and a modulus of rupture of 13.0 ± 2.3 N/mm² we achieved, surpassing conventional tile standards.

When the pumping technique was adapted to the production of bio-tiles, for the first time, bio-tiles meeting two international standards for breaking strength and modulus of rupture were produced using MICP. First, it was found that the highest ureolytic activity tested (40 mmol NH_4-N/L·min) generated the strongest bio-tiles (288 ± 35 N) when using a pumping technique for two days, contrary to the lower zone identified for the submersion technique. Shorter treatment cycles (one-hour retention times over the full 4-day duration) maximised breaking strength (395 ± 51 N), while pre-seeding the utilised geotextiles improved breaking strength by 21–82%, depending on seed loading. Bio-tiles with seed loading of 0.072 g/cm² achieved breaking strength of 940 ± 92 N and modulus of rupture of 16.4 ± 1.7 N/mm², meeting standards for extruded tiles with 6–10% water absorption. A seed loading of 0.021 g/cm² produced bio-tiles with breaking strength of 628 ± 18 N and modulus of rupture of 10.5 ± 1.1 N/mm², aligning with standards for tiles with water absorption of greater than 10%.

A novel prototype was developed to automate bio-tile production, achieving international standards for breaking strength and modulus of rupture for tiles with a water absorption of greater than 10%. While seeding with additional $CaCO_3$ crystals minimally affected breaking strength, it improved solidification at corners and edges. The breaking strength showed fluctuation with changing seed loading, however, this change was without a clear trend, however, the bio-tiles were more likely to maintain their form for breaking strength and minimum thickness measuring when supplemented with $CaCO_3$ seeds. Magnesium supplementation (0.3 M) significantly improved breaking strength (622 ± 84 N), increasing it 3.3 times compared to bio-tiles without supplementary magnesium. Daily nutrient broth-enriched cementation treatments were found to reduce strength by 12–100%. Bio-tiles produced with magnesium supplementation and other optimised additives achieved breaking strengths of 681, 671, and 702 N and modulus of rupture values of 13.1, 12.6, and 11.9 N/mm², meeting standards for tiles with water absorption of greater than 10%.

Collectively, these findings demonstrate that slower calcium carbonate precipitation rates, controlled magnesium supplementation, and strategic seeding significantly enhance the mechanical properties

of bio-tiles. These factors can be tailored to optimise bio-tile production for varying performance requirements, establishing a strong foundation for the development of sustainable, high-performance building materials. These findings underscore the feasibility of MICP-based bio-tiles as sustainable alternatives to conventional materials, with opportunities for further optimisation and industry adoption.

8.2 Implications of this work

While sand and Greywacke was used in this study as a proof of concept, any aggregate of an adequate PSD could be used. For example, Song *et al.* (2022) reported several authors using calcium-rich solid waste such as fly ash, chrome slag and recycled aggregate mixed with various ratios of cement in MICP studies. Wang *et al.* (2022b) successfully used coal gangue of particle size 0.18-0.5 mm in an MICP process. Reusing and recycling waste aggregate material would create a more circular tile manufacturing process, ultimately benefiting the environment since the waste would no longer be disposed of. While unrecyclable plastic is an aggregate option, attention must be paid to the end-of-life ramifications of tiles impregnated with plastic that could break down and further add to microplastics pollution of the environment. For this reason, waste plastic aggregate material is not recommended. The only restriction is that the aggregate material should be the correct PSD and should not harm the bacteria used in the MICP process. Different waste aggregate material for producing bio-tiles using MICP should be investigated further though.

The most significant environmental and sustainability contribution is the reduced energy requirements for making tiles using MICP compared to conventional kiln-fired tiles. A full techno-economic analysis is recommended to ascertain the potential impact improvements. A direct energy comparison cannot be made at this stage because of differences in size of equipment (lab-scale) and bio-tiles (100 x 100 mm). However, the only power required for the bio-tiles produced with the submersion technique is for mixing (20.9 W) compared to approximately 4497 W typically required for powering a ceramic kiln with natural gas (Ferrer *et al.*, 2019). Additionally, the MICP process would indirectly sequester CO_2 while conventional tile manufacturing contributes up to 16.42 kg of CO_2 per m^2 of tiles (Peng *et al.*, 2012) as well as SO_x, NO_x and CO, depending on the fuel source. Beyond this, the highest potential greenhouse gas reductions (70-83%) will be from achieving faster hardening and efficiency that translates to stronger products, as well as maximising public acceptance which will increase willingness to pay for the bio-materials (Myhr *et al.*, 2019).

The cost efficiency of bio-materials made with MICP is starting to be addressed. It is estimated that materials constitute about a quarter of the cost of bio-brick production and this material price alone is about 10% higher than for conventional concrete bricks (Myhr *et al.*, 2019). This is comparable to what a bio-tile production process would entail. Therefore, the development of more efficient production methods, in particular, reducing the number of treatments required, is essential for bio-materials to compete with traditional products at their current scales (Myhr *et al.*, 2019). This is especially so in the face of the production speed being considerably longer (days) than for conventional fired building materials (hours), which constitute most of the market.

The MICP process produces an ammonium rich by-product solution which can be detrimental to the environment (De Muynck *et al.*, 2010), but researchers have shown that a similar rich nitrogen solution could be used to manufacture ammonium sulphate (Pradhan *et al.*, 2017), a type of fertiliser. This could make the bio-tile manufacturing process more circular and provide an additional source of income through the sale of the fertiliser (Lambert & Randall, 2019).

In this study, we used synthetic urea as a source of urea for the MICP process, but human urine could also be used, either as stabilised urine (Lambert & Randall, 2019) or as a concentrate (Courtney & Randall, 2022). This would result in the recycling of another 'waste' stream, but at an additional cost. It is therefore suggested that future work look at a detailed economic and life cycle assessment of the proposed process for a range of products (bricks, pavers, roof tiles, etc.) and different operational conditions.

While bio-materials have considerable potential, they face hurdles that must be addressed to achieve widespread use. Bio-tiles could serve as a springboard for exploration of other bio-cemented construction materials, with efforts focused on optimising production processes, enhancing strength and efficiency, and reducing production times to establish a viable alternative to traditional construction materials.

References

C. Courtney & D.G. Randall. 2022. Concentrating stabilized urine with reverse osmosis: How does stabilization method and pre-treatment affect nutrient recovery, flux, and scaling? *Water Research.* 209:117970. DOI:https://doi.org/10.1016/j.watres.2021.117970.

W. De Muynck, N. De Belie & W. Verstraete. 2010. Microbial carbonate precipitation in construction materials: A review. *Ecological Engineering.* 36(2):118-136. DOI:10.1016/j.ecoleng.2009.02.006.

S. Ferrer, A. Mezquita, V.M. Aguilella & E. Monfort. 2019. Beyond the energy balance: Exergy analysis of an industrial roller kiln firing porcelain tiles. *Applied Thermal Engineering.* 150:1002-1015. DOI:10.1016/j.applthermaleng.2019.01.052.

S.E. Lambert & D.G. Randall. 2019. Manufacturing bio-bricks using microbial induced calcium carbonate precipitation and human urine. *Water Research.* 160:158-166. DOI:10.1016/j.watres.2019.05.069.

A. Myhr, F. Royne, A.S. Brandtsegg, C. Bjerkseter, H. Throne-Holst, A. Borch, A. Wentzel & A. Royne. 2019. Towards a low CO2 emission building material employing bacterial metabolism (2/2): Prospects for global warming potential reduction in the concrete industry. *PLOS ONE.* 14(4):e0208643. DOI:10.1371/journal.pone.0208643.

J. Peng, Y. Zhao, L. Jiao, W. Zheng & L. Zeng. 2012. CO2 emission calculation and reduction options in ceramic tile manufacture - The Foshan case. *Energy Procedia.* 16:467-476. DOI:10.1016/j.egypro.2012.01.076.

S.K. Pradhan, A. Mikola & R. Vahala. 2017. Nitrogen and phosphorus harvesting from human urine using a stripping, absorption, and precipitation process. *Environmental Science & Technology.* 51(9):5165-5171. DOI:10.1021/acs.est.6b05402.

M. Song, T. Ju, Y. Meng, S. Han, L. Lin & J. Jiang. 2022. A review on the applications of microbially induced calcium carbonate precipitation in solid waste treatment and soil remediation. *Chemosphere (Oxford).* 290:133229-133229. DOI:10.1016/j.chemosphere.2021.133229.

Z. Wang, J. Zhang, M. Li, S. Guo, J. Zhang & G. Zhu. 2022. Experimental study of microorganism-induced calcium carbonate precipitation to solidify coal gangue as backfill materials: mechanical properties and microstructure. *Environmental Science and Pollution Research.* 29(30):45774-45782. DOI:10.1007/s11356-022-18975-9.

“The more our world functions like the natural world, the more likely we are to endure on this home that is ours, but not ours alone.”

— Janine M. Benyus

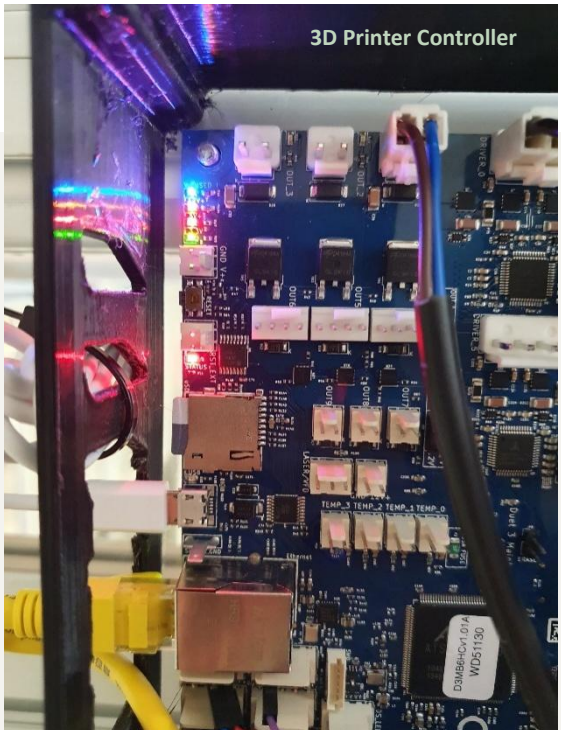
3D Printer Controller


Edge of Strongest Bio-tile

9 Appendices

The following are supplemental information, tables and figures that enhance the body of the thesis.

9.1 Materials and methods

9.1.1 *Submersion technique experimental set up*

The inoculated aggregate was compacted into the moulds by first flattening it by hand and then with a plate and hammer. The plate was hit 10 times, with two knocks in the middle and then two in opposite corners and the final two corners. The aggregate that had squeezed up the walls was flattened down. Each of the four bio-tile moulds were secured into each of the quadrants of the bio-reactor over a magnetic stirrer.

9.1.2 *Appearance of seeded geotextile and foam*

Examples of seeded foam and geotextiles seeded manually as well as in previous bio-tile reactors are show in Figure A.1.

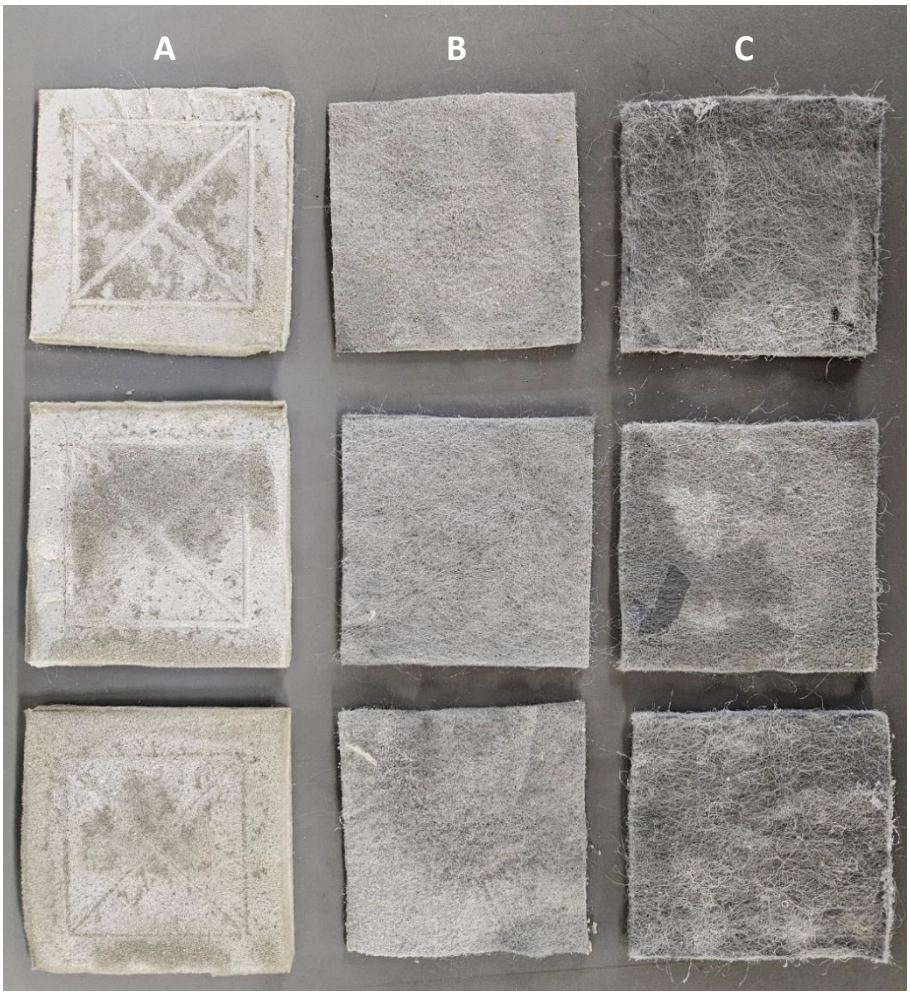

Figure A.1: Seeded materials used in seeding experiments. A) foam and B) geotextile recovered from previous bio-tile experiments. C) Geotextile seeded manually, externally from bio-tile reactors.

9.2 Submersion technique

9.2.1 *Effect of particle size on bio-tile properties*

Various particle size groups were assessed for their effect on the breaking strength of bio-tiles. The particle size distribution (PSD) of each group was measured using a Mastersizer which provided the results shown in Table A.1 for the D_{10}, D_{50} and D_{90} of each group, and its porosity and the standard deviation (SD) thereof.

Table A.1: Key particle size categories (µm) and associated porosity fraction of each particle size distribution (PSD) group. Standard deviation (SD) was calculated from n = 3.

Sieve size	D_{10}	D_{50}	D_{90}	Porosity	SD
75-150	92	139	209	0.50	0.020
212-300	241	331	457	0.45	0.007
Unsieved sand	304	469	707	0.40	0.036
425-600	456	641	919	0.43	0.007
600-900	633	978	1474	0.42	0.008
1:1* less fines	423	810	1428	0.28	0.002
1:1* more fines	393	825	1465	0.32	0.017

*sand:Greywacke aggregate

The density bottle method was carried out according to British Standard (BS1377, 1990), as described by Lambert and Randall (2019) for each PSD group. Briefly, 10 mL of tapped-down sample was placed into a density bottle after weighing (M_1) and weighed with the sample (M_2). Enough de-aired deionised water was added to cover the sample and then placed in a desiccator until all air was removed (at least an hour). Air-free water at 25°C was then added to the rim, the stopper was inserted and then the bottle placed in a 25°C water bath until constant temperature was reached. The bottle was dried, the stopper capillary filled if need be and bottle and contents weighed (M_3). The bottle was cleaned thoroughly, filled with deionised water of 25°C, the stopper inserted and weighed (M_4). From these measurements, the specific gravity, void ratio and porosity of each particle size group was determined (Table A.2).

Table A.2: Selected input, measured and calculated values from the density bottle method.

		Parameter value					Standard deviation				
D50	**µm**	**139**	**331**	**469**	**641**	**825**	**139**	**331**	**469**	**641**	**825**
G_1		1	1	1	1	1	0	0	0	0	0
Vt	mL	10	10	10	10	10	0	0	0	0	0
M_1	g	36.7	34.5	34.5	34.4	35.8	0.28	0.29	0.21	0.48	1.13
M_2	g	50.0	49.0	50.4	49.8	54.2	0.42	0.39	0.31	0.48	0.84
M_3	g	96.6	93.6	94.3	93.8	98.4	0.35	0.25	0.35	0.63	1.60
M_4	g	88.3	84.6	84.2	84.1	86.8	0.26	0.20	0.59	0.63	1.66
M	g	13.3	14.5	15.8	15.4	18.4	0.16	0.11	0.12	0.040	0.44
Gs	g/mL	2.65	2.65	2.78	2.68	2.72	0.081	0.018	0.16	0.002	0.007
Vs	mL	5.02	5.47	5.72	5.73	6.77	0.20	0.066	0.36	0.017	0.17
e		0.99	0.83	0.76	0.75	0.48	0.079	0.022	0.11	0.005	0.038
n		0.50	0.45	0.43	0.43	0.32	0.020	0.007	0.036	0.002	0.017

The effect of fines on the strength of bio-tiles was measured between two different groups, one with a small fraction of fines below 110 µm and another with a larger amount of fines under 400 µm but

not smaller than 103 µm. The PSD curves for these two groups are given in Figure A.2 with the breaking strength of each of the groups.

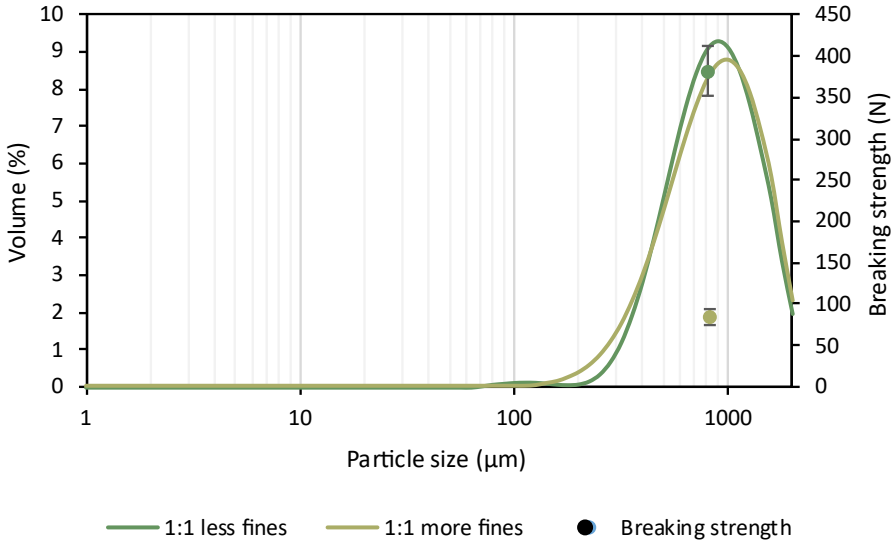

Figure A.2: Particle size distribution comparing 1:1 sand to Greywacke with and without fines and the corresponding breaking strength. Error bars represent standard deviation, n = 4. Fines were considered the particles that are smaller than 400 µm.

It must be noted that for this PSD analysis, particles over the size of 2000 µm had to be sieved out as the Mastersizer only measures up to 2000 µm and therefore, the graph is cut off there. For the 1:1 group with less and more fines, the fraction greater than 2000 µm removed accounted for 24.9% and 18.4% of the total mass, respectively.

9.2.2 *Impact of cementation solution volume on breaking strength*

Cementation solution volume was decreased to improve the utilisation efficiency of calcium within the bio-reactor, however this had the effect of lowering the breaking strength of the bio-tiles. When greater volumes were tested, the utilisation efficiency decreased. Generally, a greater volume resulted in a greater mass of calcium utilised, likely due to precipitation in the bulk. However, it was found that the breaking strength was not directly proportional to the mass of calcium utilised. Separating the two cementation solution concentration datasets of 0.2 and 0.3M, both had a negative correlation (-0.48 and -0.38, respectively) due to the greatest breaking strength for each being achieved for the second lowest calcium utilisation (Figure A.3).

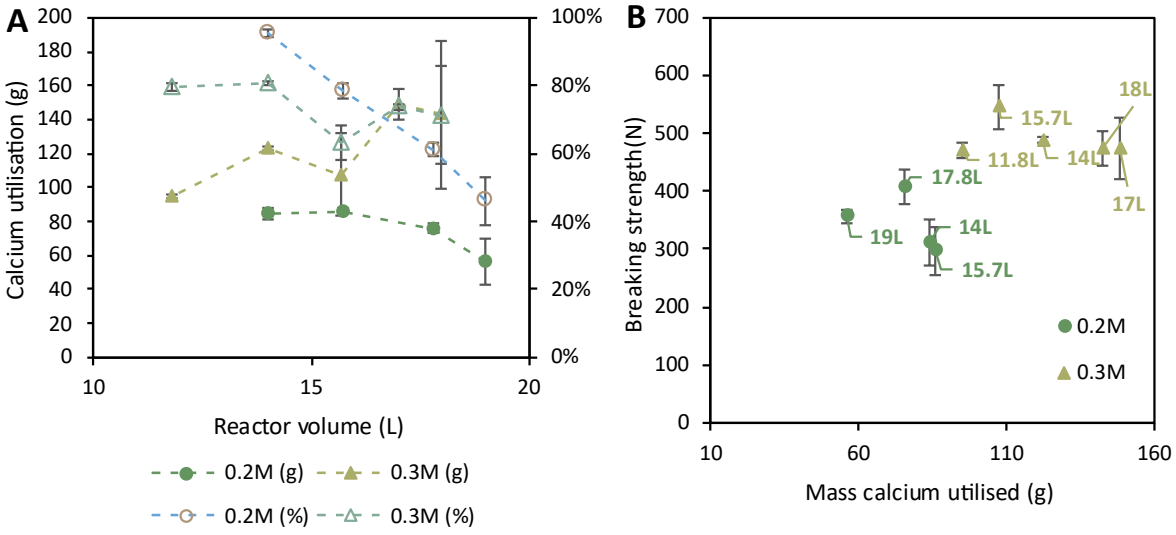

Figure A.3: Relationship between breaking strength (error bars are standard deviation, n = 3 or 4) and mass of calcium utilised for different cementation solution volumes and concentrations of 0.2 M and 0.3 M. The volumes are given in L as text on the graph for each data point.

9.2.3 *Water absorption of the bio-tiles produced with the submersion technique*

The bio-tiles grown had a water absorption of 9.7-13-7%. All but one group of bio-tile experiments (15.7 L) had a water absorption of greater than 10%, confirming the breaking strength and modulus of rupture standard of 600 N and 8 N/mm^2. Bio-tiles grown in the presence of magnesium had a greater water absorption (12.3 ± 1.1%, n = 17) than bio-tiles grown in varying volumes of cementation solution in the absence of magnesium (10.5 ± 0.7%, n = 17).

9.2.4 *Comparison of bio-tiles with and without magnesium*

Calcite crystals are generally rhombohedral in shape, vaterite, hexagonal and aragonite has orthorhombic and needle-like structures (Seifan & Berenjian, 2018). The XRD analysis showed the presence of both calcite and aragonite in bio-tiles with and without magnesium (Figure A.4). The raw XRD diffractograms are shown in Figure A.5.

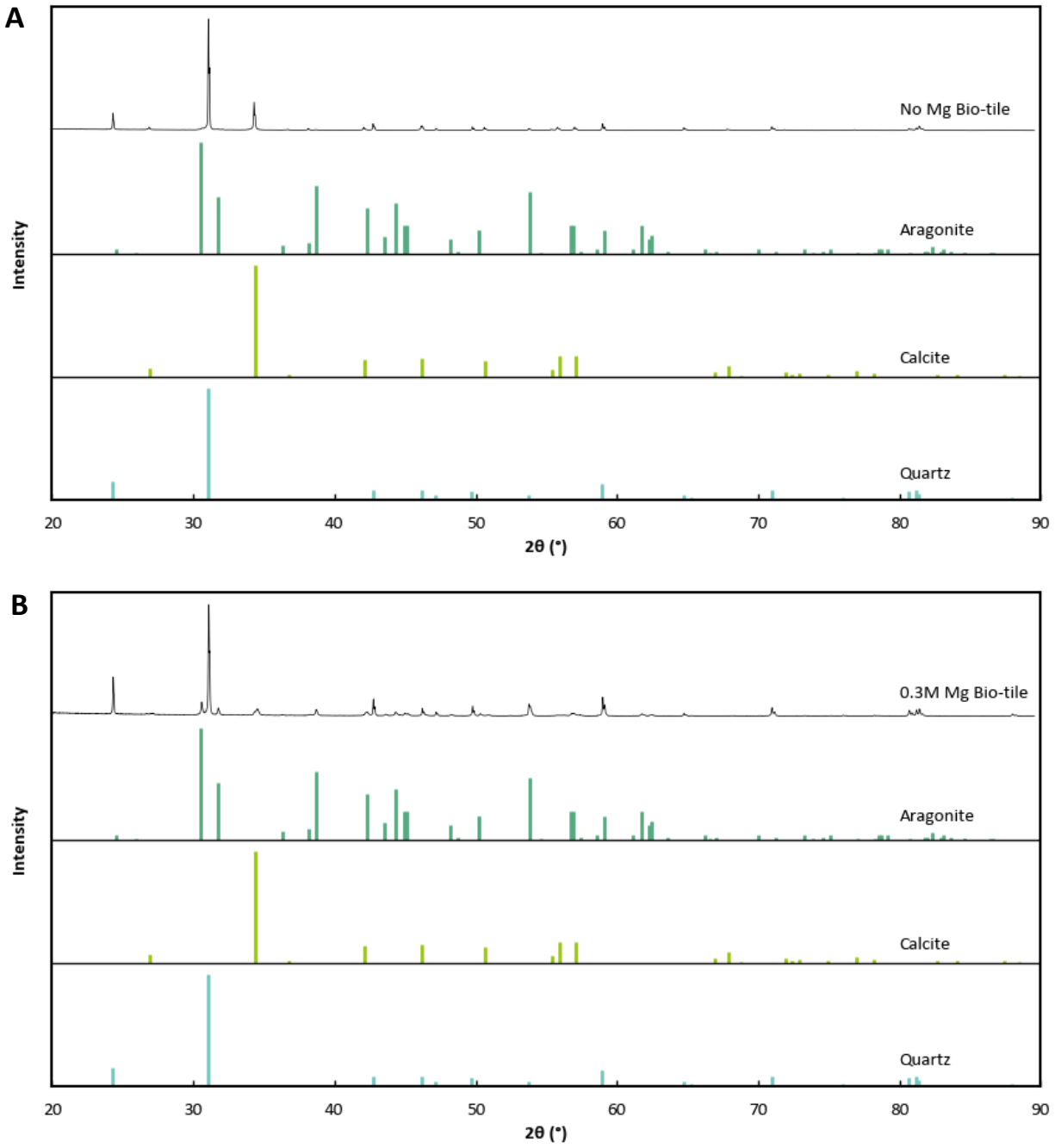

Figure A.4: XRD analysis of bio-tiles grown with a cementation volume of 15.7 L without magnesium (A) and with the presence of 0.3 M magnesium (B), compared to references of aragonite, calcite and quartz.

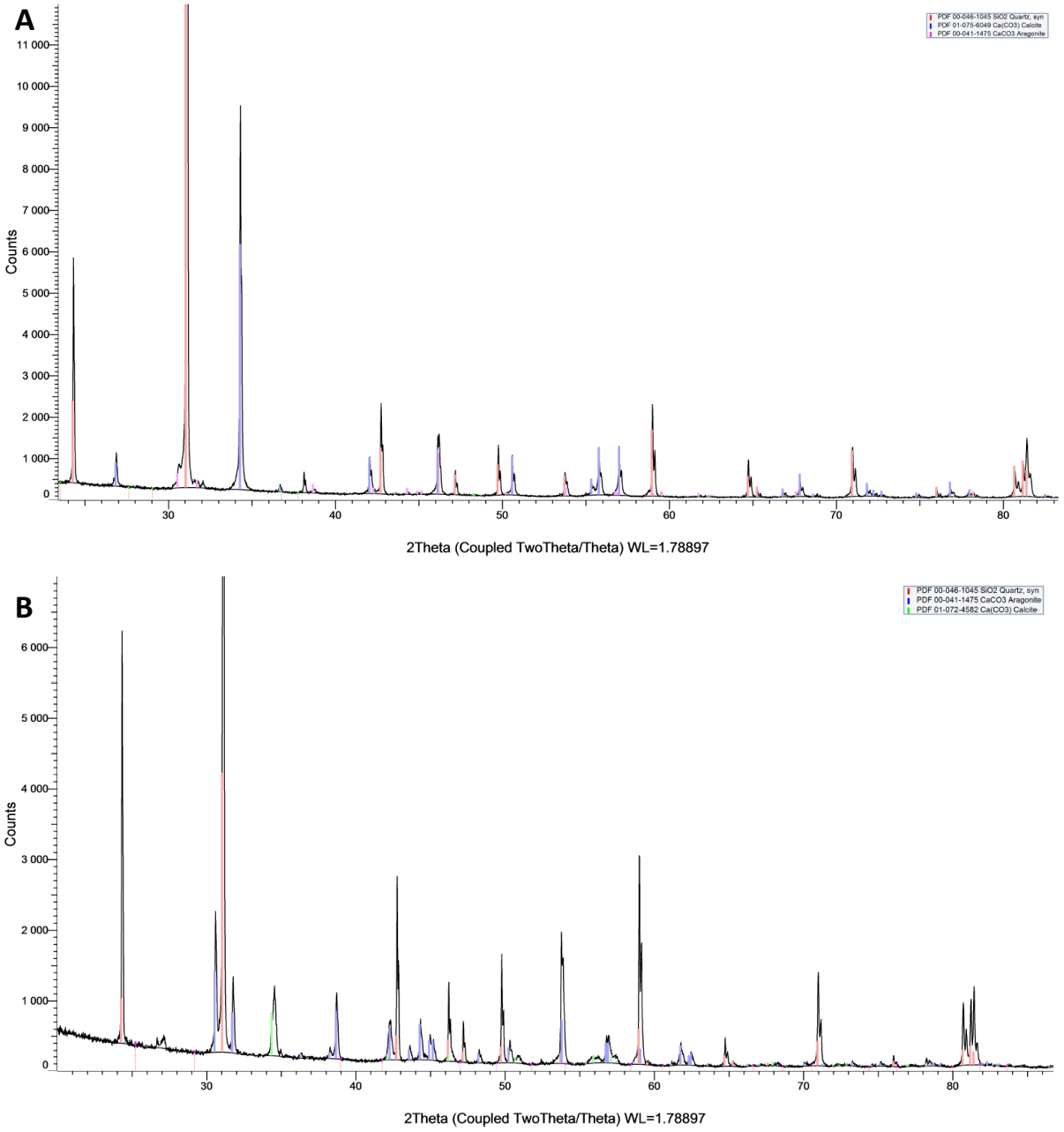

Figure A.5: Raw XRD diffractograms of bio-tiles grown with a cementation volume of 15.7 L without magnesium (A) and with the presence of 0.3 M magnesium (B).

In Figure A.6, the SEM images show the difference in the dominant crystal structures between the two types of bio-tiles. Figure A.6A and B both show the dominance of rhombohedral shapes while Figure A.6C and D have many needle-like structures. This confirms that the presence of magnesium causes the $CaCO_3$ to shift more towards aragonite over calcite.

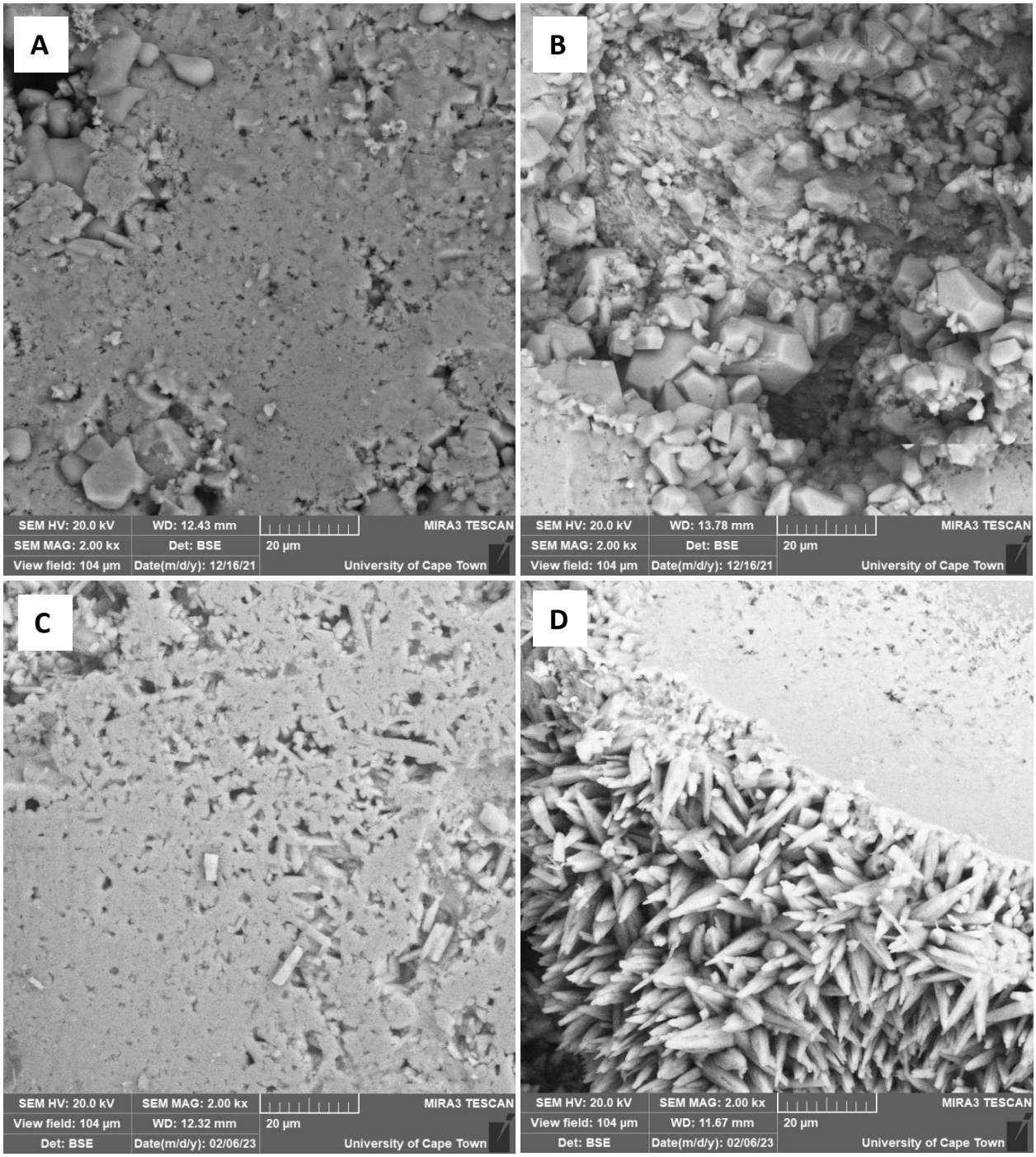

Figure A.6: SEM images of bio-tiles without magnesium, edge (A) and middle (B) and in the presence of 0.3 M magnesium, edge (C) and middle (D).

9.2.5 *Rate constants of calcium carbonate precipitation for different parameters*

The rate constants of calcium carbonate precipitation were calculated using the natural logarithm and then gradient of the linear relationship taken as the rate constant and the Nash-Sutcliffe Efficiency (NSE) calculated. The relationship of the rate constant to the breaking strength for each parameter is shown in Figure A.7A through Figure A.7D and these graphs are summarised in Table A.3.

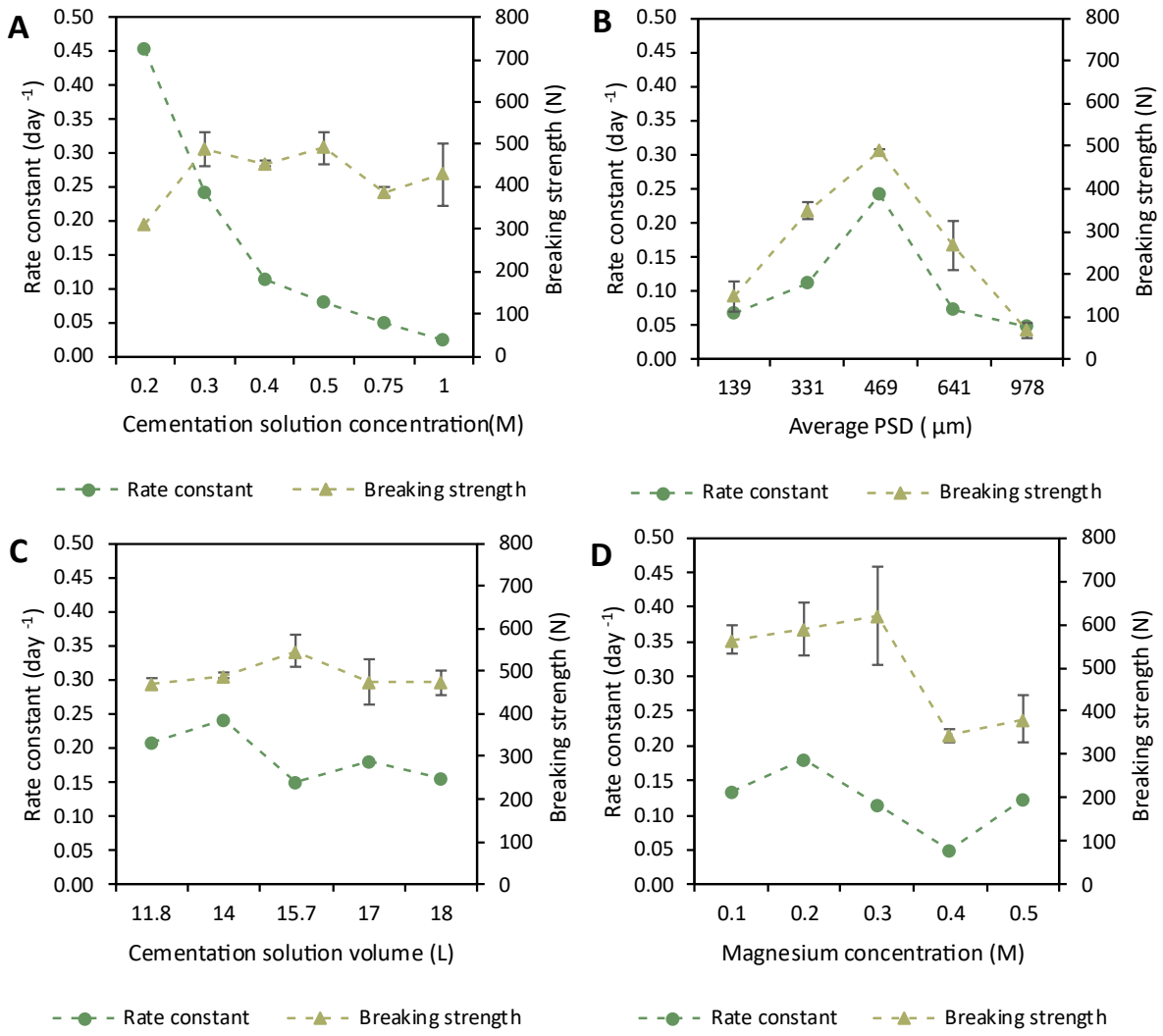

Figure A.7: Change in the $CaCO_3$ precipitation rate constant and breaking strength (error bars represent standard deviation, n = 3 or 4) with cementation solution concentration (A), volume at a cementation solution concentration of 0.3 M (B) and magnesium concentration (C).

Table A.3: Rate constants and NSE for the cementation solution concentration, PSD, cementation solution volume and magnesium concentration parameters investigated. Concentration refers to the cementation solution concentration, volume to the volume of cementation solution and magnesium to the concentration of supplemental magnesium added.

Concentration (M)	**0.2**	**0.3**	**0.4**	**0.5**	**0.75**	**1**
Rate constant (day^{-1})	0.452	0.241	0.114	0.080	0.050	0.026
NSE	0.935	0.860	0.829	0.934	0.746	0.725
D_{50} (µm)	469	469	469	469	469	469
Volume (L)	14	14	14	14	14	14
PSD, D_{50} (µm)	139	331	469	641	978	
Rate constant (day^{-1})	0.066	0.112	0.241	0.073	0.049	
NSE	0.794	0.847	0.860	0.953	0.794	
Concentration (M)	0.3	0.3	0.3	0.3	0.3	
Volume (L)	14	14	14	14	14	
Volume (L)	**11.8**	**14**	**15.7**	**17**	**18**	
Rate constant (day^{-1})	0.208	0.241	0.150	0.179	0.155	
NSE	0.900	0.860	0.966	0.953	0.794	
Concentration (M)	0.3	0.3	0.3	0.3	0.3	
D_{50} (µm)	469	469	469	469	469	
Magnesium (M)	**0.1**	**0.2**	**0.3**	**0.4**	**0.5**	
Rate constant (day^{-1})	0.135	0.181	0.116	0.049	0.124	
NSE	0.951	0.981	0.993	0.970	0.995	
Concentration (M)	0.3	0.3	0.3	0.3	0.3	
D_{50} (µm)	469	469	469	469	469	
Volume (L)	14	14	14	14	14	

NSE = Nash-Sutcliffe Efficiency, PSD = particle size distribution

The optimised experiment with a volume of 15.7 L and a magnesium concentration of 0.3 M had a rate constant of 0.112 day^{-1} and an NSE of 0.912.

9.2.6 *Finished bio-tile product*

The bio-tiles produced take on the colour of the aggregate used. For example, the bio-tiles grown from sand (Figure A.8) are characterised by their beige-sand colour.

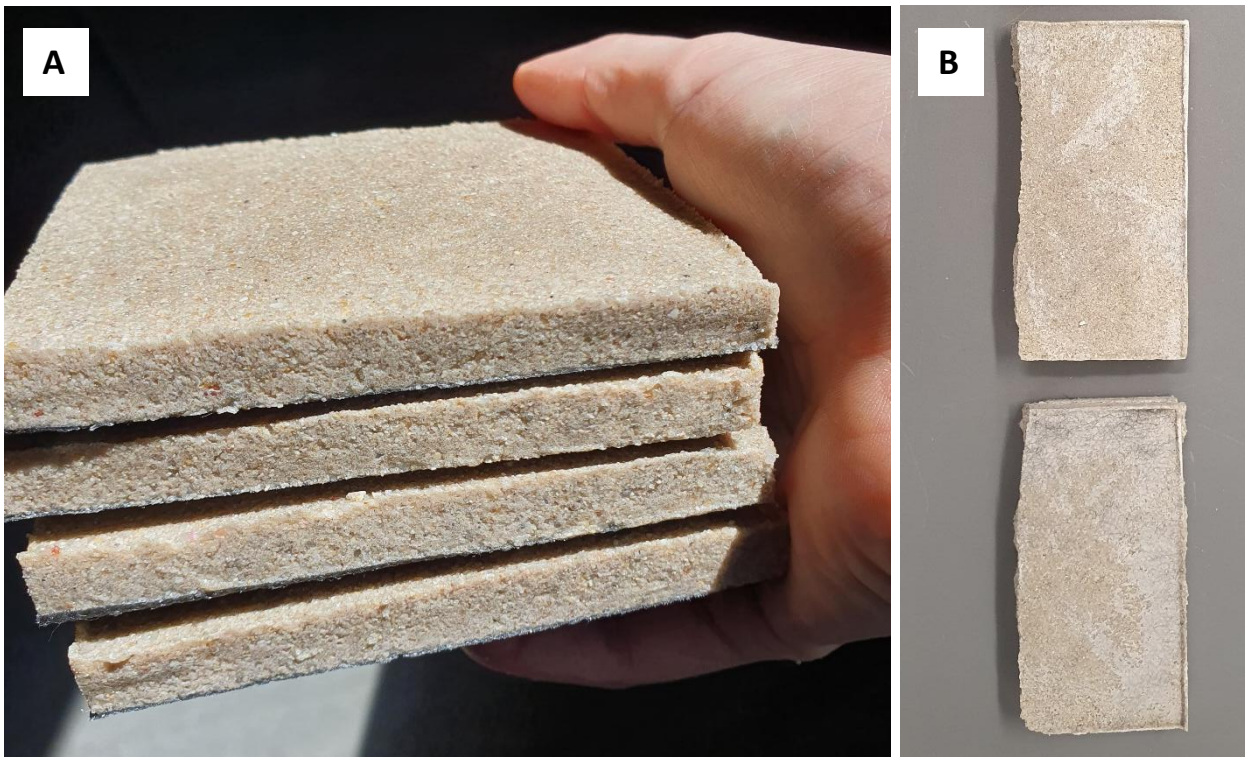

Figure A.8: Examples of the bio-tiles, whole (A) and after breaking strength test (B), grown with the submersion technique using sand as an aggregate.

9.3 Pumping technique

9.3.1 *Utilisation of calcium depending on retention time and inversion*

As expected, it was found that when the retention time was longer, the utilisation of calcium was greater (Figure A.9). Unfortunately, this higher utilisation per treatment did not result in a higher breaking strength compared to lower retention times. What is of particular interest with regards to Figure A.9, is when the moulds were inverted on day 2, both the two hour and four hour treatment cycle length groups showed an almost complete halt in the utilisation of calcium (2% and 5%, respectively). This minimal utilisation continued until they were inverted once more, at which point the trend in utilisation continued as if the un-inverted state had never happened. Additionally, the bacteria undergo a continual loss in activity, regardless of the inversion condition and the retention time. However, the loss in activity was slower for longer retention times. This is another reason why inversion at the end of the first retention time was beneficial, because the bacteria were at their most active.

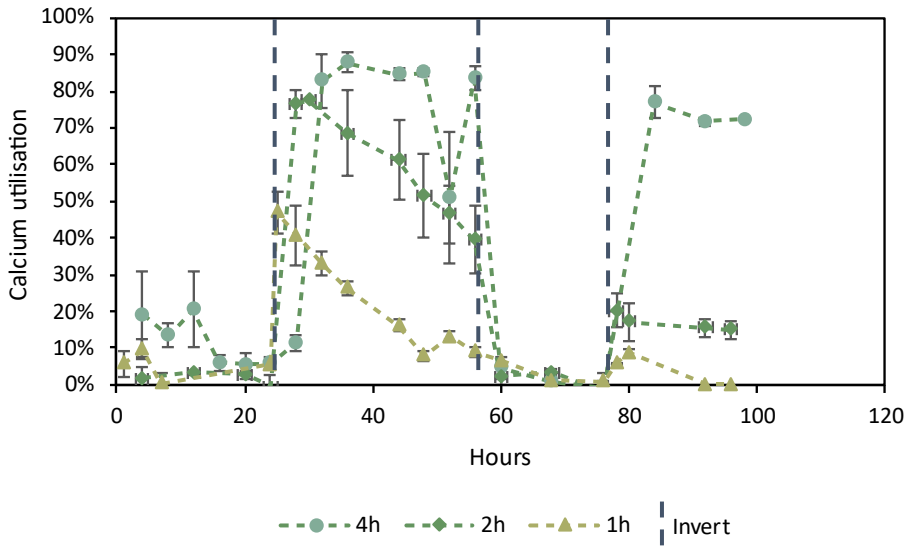

Figure A.9: The calcium utilisation of the tested treatment cycles over time for 1, 2, and 4 h retention time experiments. Error bars indicate standard deviation of number of samples, n = 3.

9.3.2 *Utilisation of calcium for different inversion times, seeded materials and seed loadings*

Unseeded foam and geotextile were compared to seeded counterparts over the short term (Figure A.10). Based on the utilisation of calcium either remaining minimal (in the case of seeded foam) or only reaching 54% for seeded geotextile, it was concluded that inverting the mould as soon as possible was still beneficial to the MICP process efficiency.

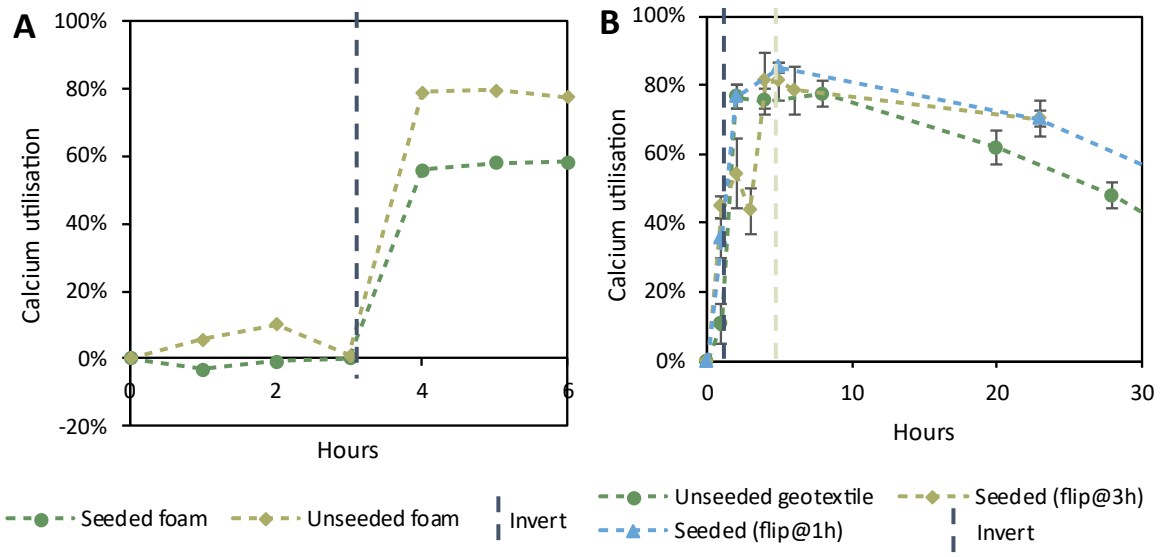

Figure A.10: The influence of (A) unseeded and seeded foam on the utilisation of calcium before and after inverting at 3 h, and of (B) unseeded geotextile inverted at 1 h and seeded geotextile when inverting at 3 h and 1 h. Error bars represent the standard deviation of n = 3 bio-tiles.

9.3.3 *Analysis of the mass of calcium carbonate seeds contained in the geotextile and foam*

Based on the benefits of using pre-seeded geotextile over foam, the amounts of seeds in each were quantified. It was identified that the geotextile and foam originally on the top had more seeds than

the geotextile and foam on the bottom (Figure A.11), making the top geotextile more effective at seeding the MICP process when the mould was inverted and the feed passed through the additional seeds. Even though the average mass of geotextile was lower (2.59 ± 0.18 g) than the mass of foam (3.66 ± 0.21 g), the higher seed density shows that the geotextile is more effective at retaining seeds than the foam.

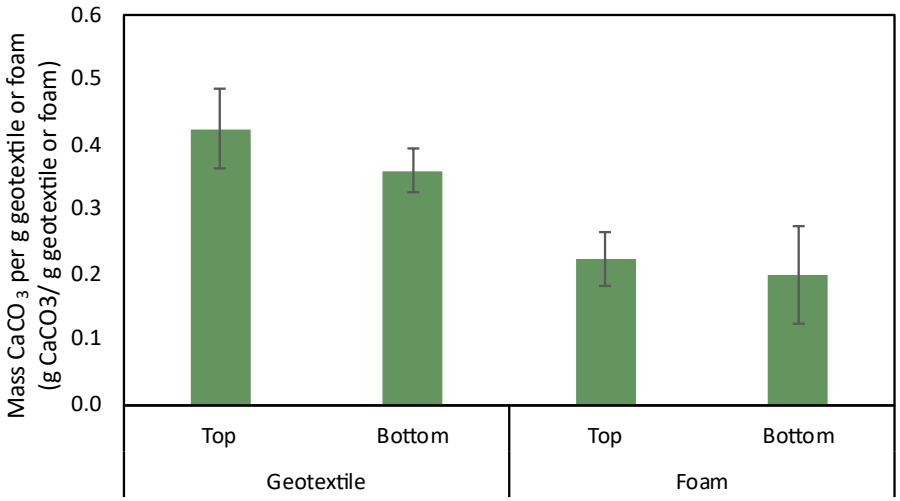

Figure A.11: The mass of $CaCO_3$ seeds generated per mass of geotextile and foam after one treatment cycle. Error bars represent the standard deviation of n = 3 geotextiles or foam pieces.

9.3.4 *Discussion of errors*

Deviation in the seeds compared to the overall error in the breaking strength did not have a strong correlation, even so, the error in the seeds was under 11%. This relationship had a Pearson's correlation coefficient of 0.44, and therefore there was not a significant correlation.

With each bio-tile formed, the error is compounded by variations in initial bacteria activity, the colonisation of the aggregate, deviations in the geotextile and foam size and density, the varying mass and distribution of seeds on the geotextile where seeded geotextiles were used and in how the inoculated sand was packed into the mould. Many of these factors also have an influence on the final thickness of the bio-tile. Table A.4 summarises the errors for each experiment.

Table A.4: Summary of the breaking strength of each bio-tile from each experiment and the percentage the associated standard deviation constitutes. Outlier tiles and errors exceeding 15% are given in red.

Experiment		Sample	Breaking strength (N)	Average (N)	Standard deviation (N)	Error
Activity (mmol/L·min)	8	A	178	150	19	12.9%
		B	134			
		C	140			
	24	A	180	172	23	13.5%
		B	195			
		C	140			
	40	A	338	288	35	12.3%
		B	262			
		C	264			
Treatment cycle length (h)	1	A	326	395	51	12.8%
		B	368			
		C	439			
		D	448			
	2	A	109	140	43	30.9%
		B	70			
		C	165			
		D	172			
		E	300			
		F	183			
	4	A	50	73	15	20.2%
		B	92			
		C	86			
		D	59			
		E	78			
		F	74			
Reactor seeded		A	862	827	98	11.8%
		B	694			
		C	926			
Pre-seeded: seed loading of the geotextiles (g/cm^2)	0	A	551	517	43	8.4%
		B	456			
		C	544			
	0.021	A	634	628	19	2.9%
		B	603			
		C	647			
	0.035	A	696	659	49	7.5%
		B	589			
		C	691			
	0.039	A	999	836	117	13.9%
		B	733			
		C	776			
	0.072	A	1065	940	92	9.8%
		B	906			
		C	847			

9.4 Automated technique

9.4.1 *Diagrams of the prototype*

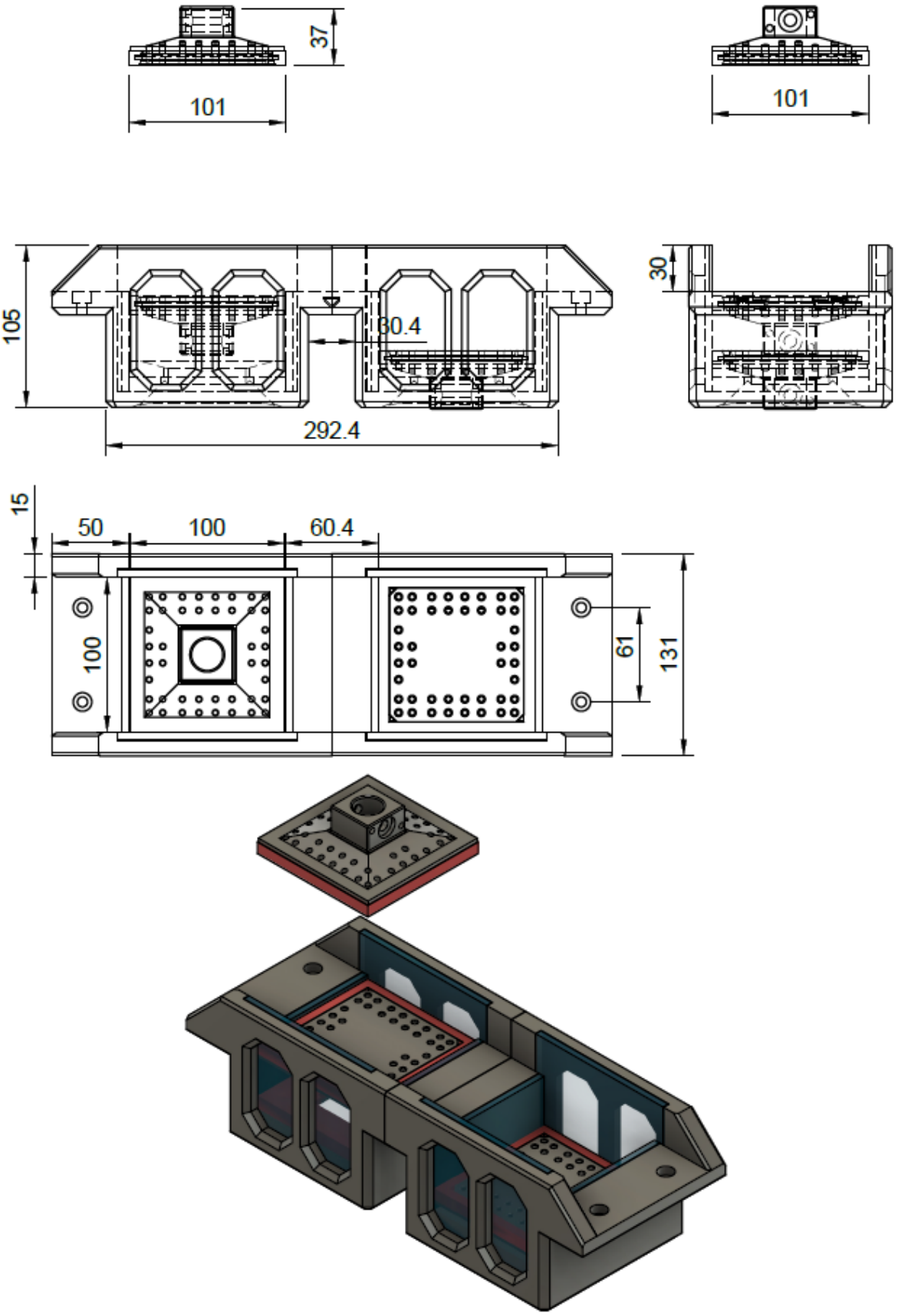

Figure A.12: Diagrams of the prototype reaction chamber from various angles. Dimensions in mm.

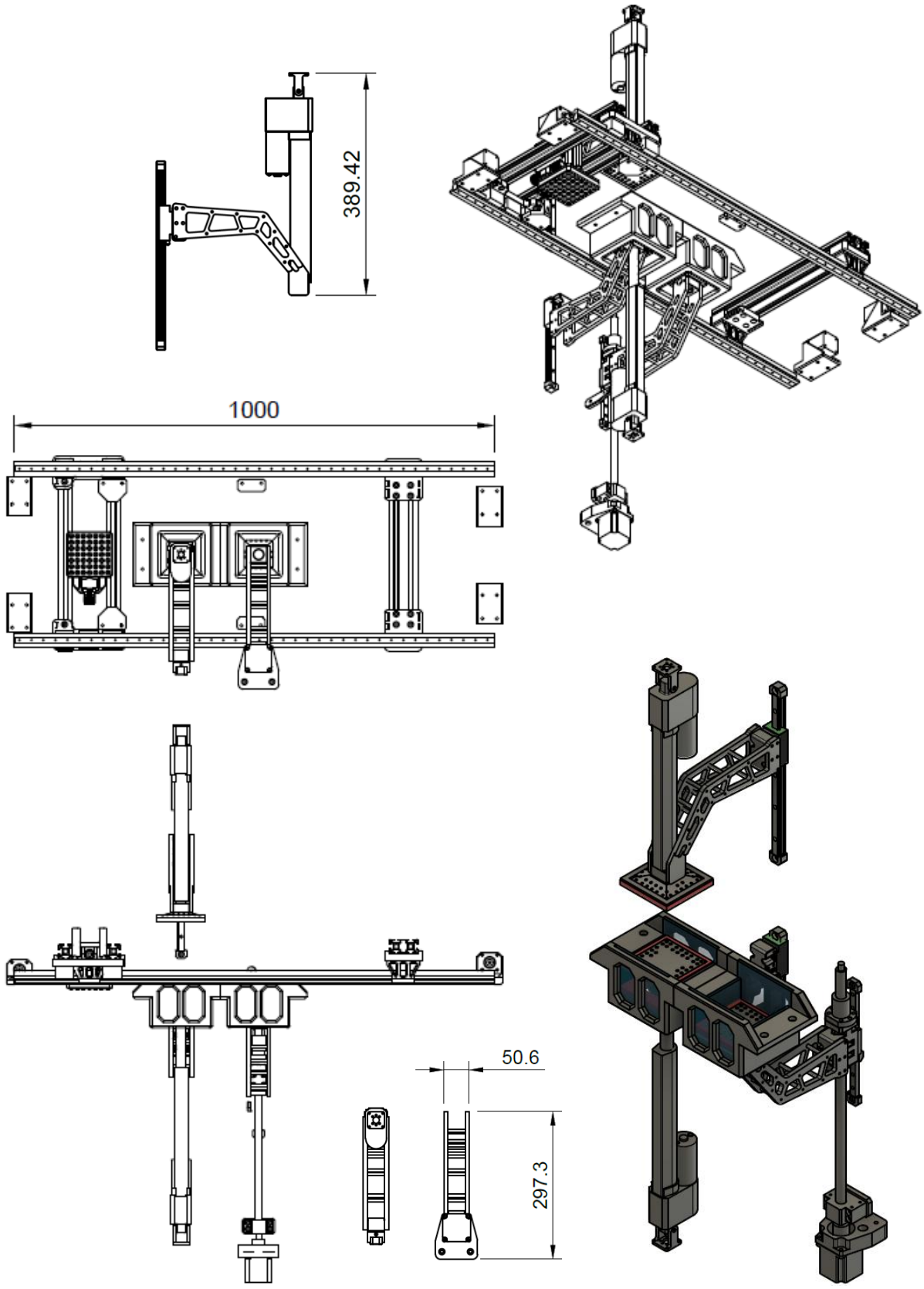

Figure A.13: Diagrams of horizontal and vertical mechanisms from various angles. Horizontal powers the showerhead, vertical top, the compaction arm and vertical bottom, the platform and sealing. Dimensions in mm.

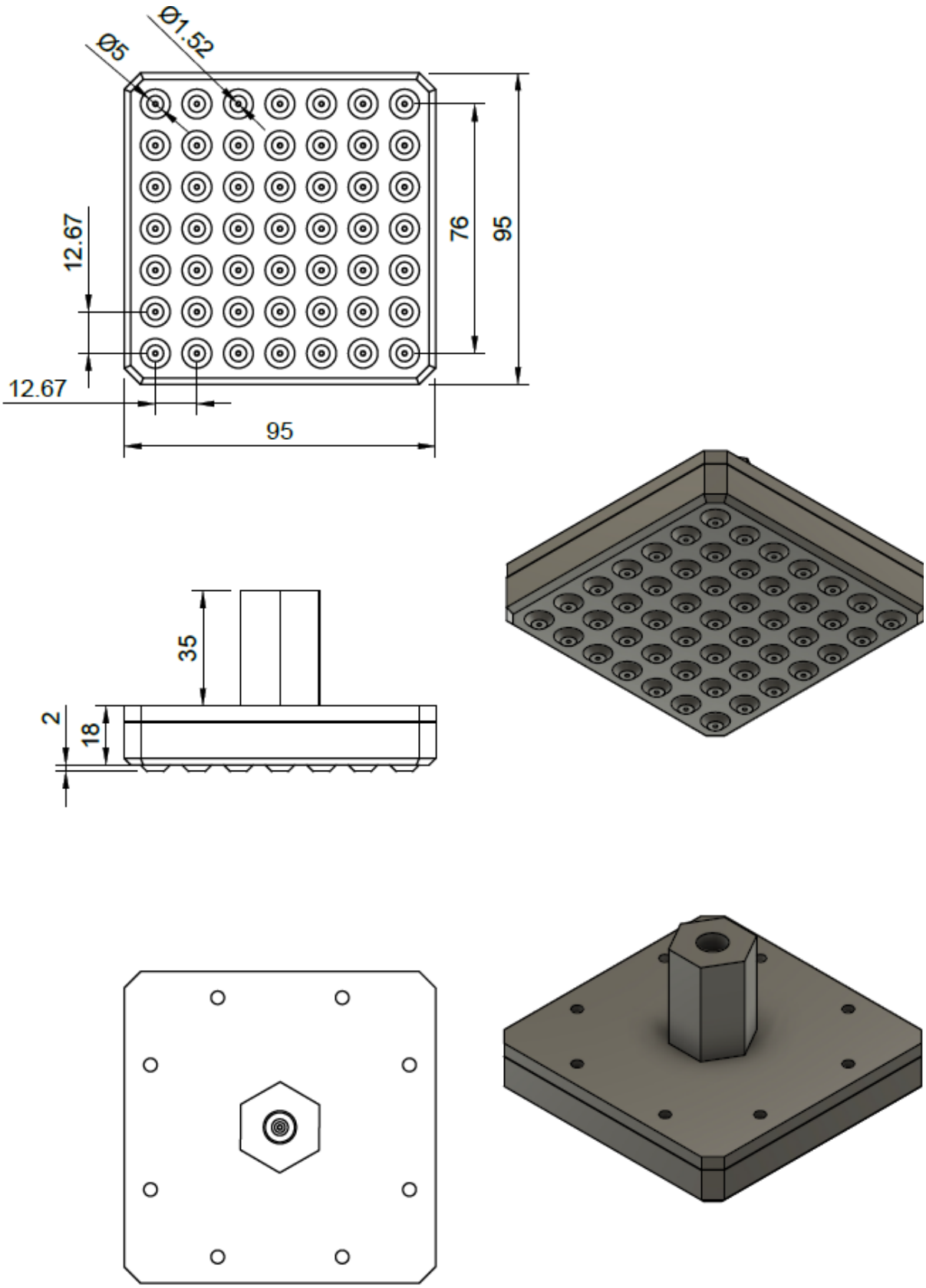

Figure A.14: Diagrams from various angles of the showerhead that deposits cementation solution. Dimensions in mm.

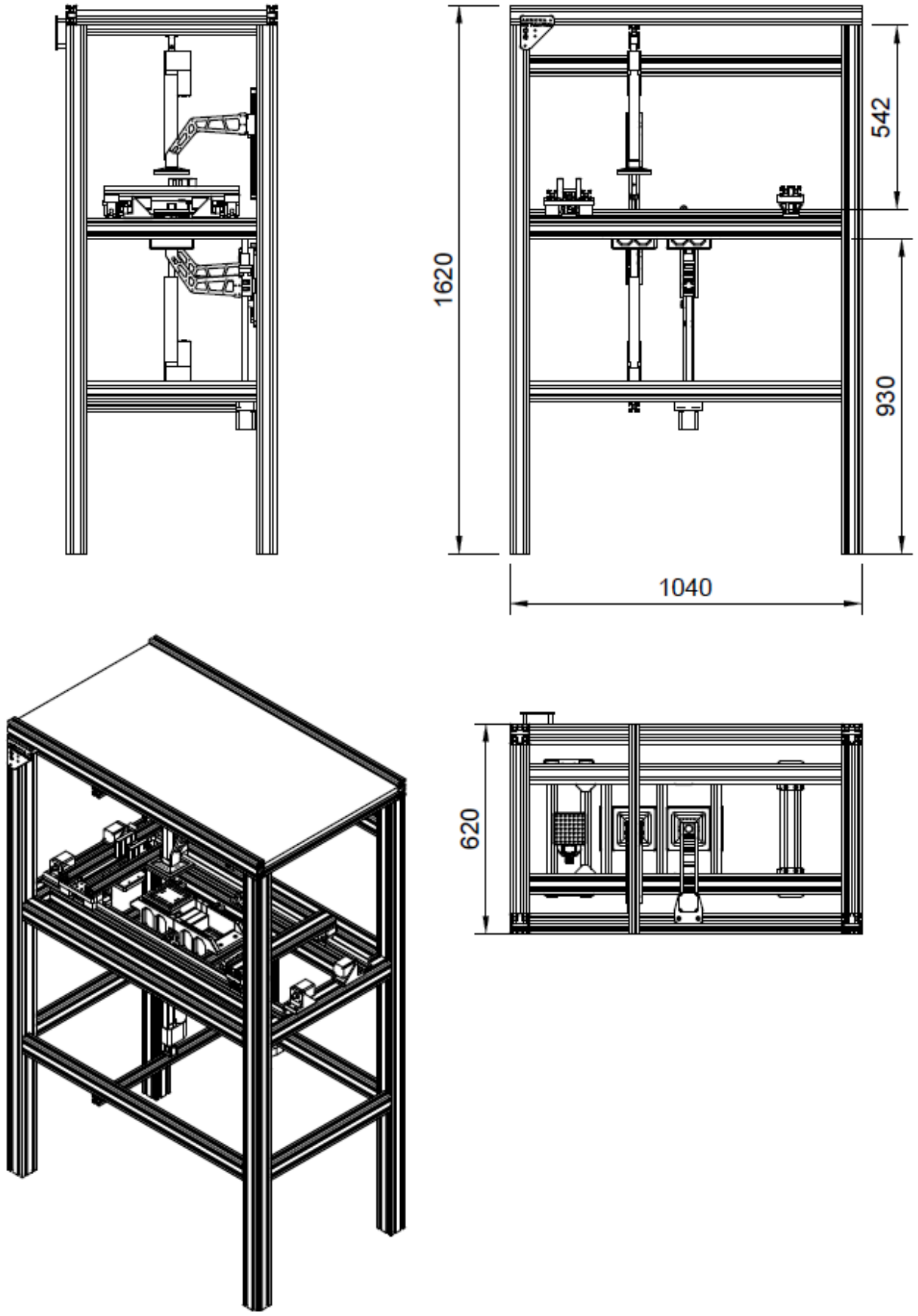

Figure A.15: Diagrams of the entire protype with frame from various angles. Dimensions in mm.

9.4.2 *Calcium carbonate content and water absorption of the best performing bio-tiles produced with the automated technique*

Bio-tiles supplemented with nutrient broth alone were not able to be measured for their water absorption as they crumbled during the boiling process, causing an invalid measurement. This is supported by their relatively lower $CaCO_3$ content compared to bio-tiles supplemented with magnesium as well (Figure A.16).

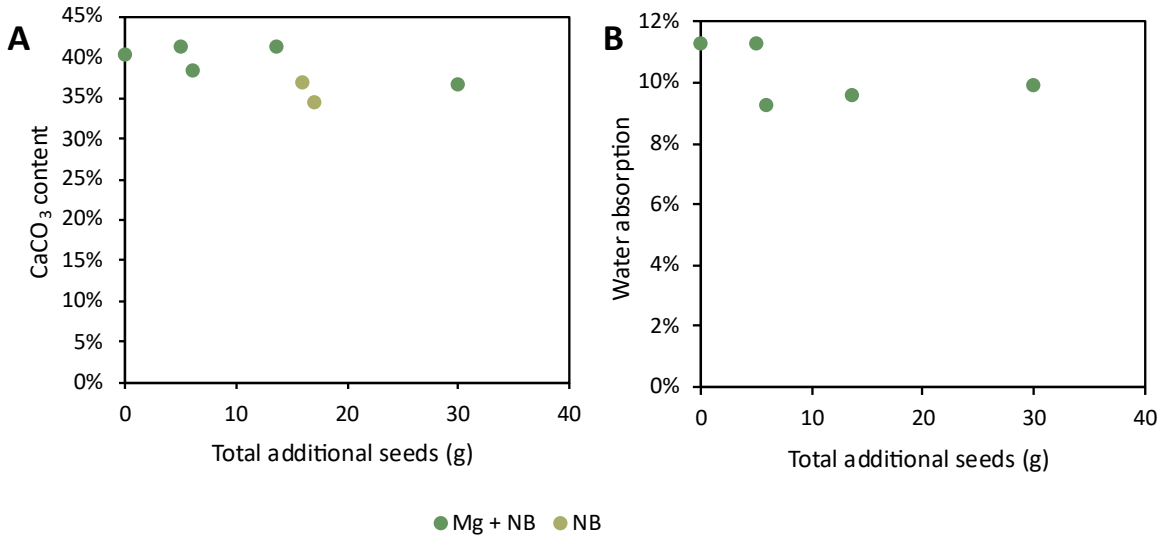

Figure A.16: $CaCO_3$ content (A) and water absorption (B) of bio-tiles supplemented with magnesium and daily nutrient broth treatments or only nutrient broth.

9.4.3 *Effect of nutrient broth prior to methodology finalisation*

Multiple preliminary runs were carried out during the process of finalising the methodology and improving the consistency of bio-tiles formed in the 3D printer. During this process, a daily nutrient broth treatment was utilised and compared to without any nutrient broth. The addition of the nutrient broth treatment was initially identified to be beneficial to the breaking strength of bio-tiles produced with the 3D printer (Figure A.17). However, later experiments found the opposite to be true.

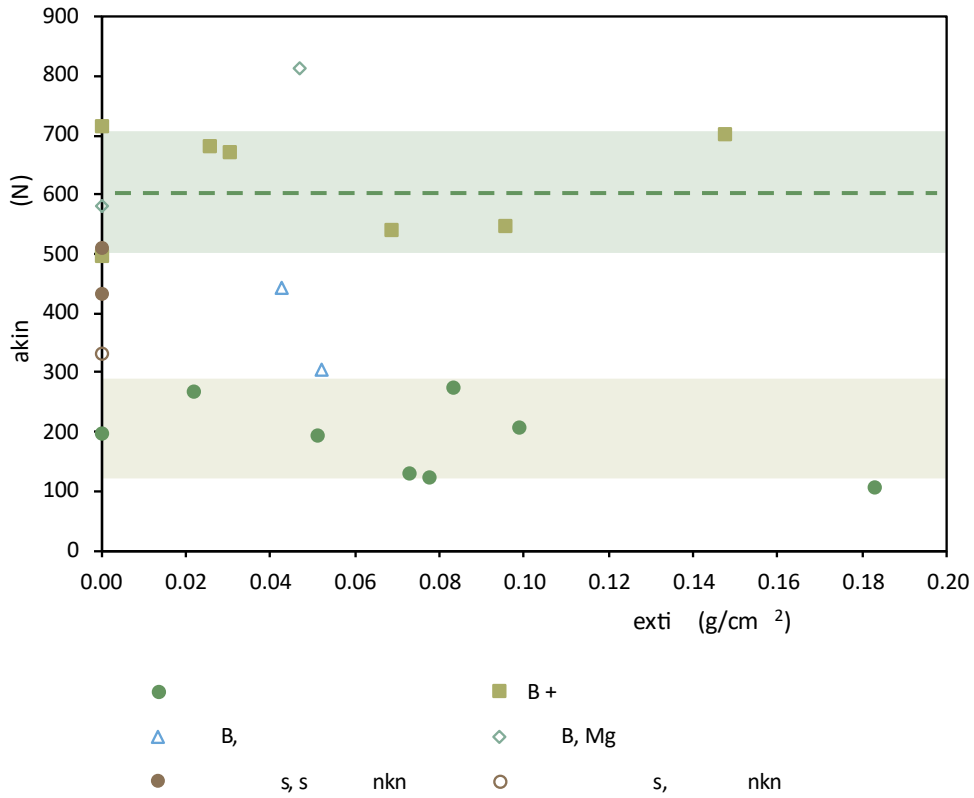

Figure A.17: effect

fin tion.